

**T.C.
REPUBLIC OF TURKEY
HACETTEPE UNIVERSITY
GRADUATE SCHOOL OF HEALTH SCIENCES**

**DISCOVERY OF NEW INDOLEAMINE 2,3-DIOXYGENASE 1
(IDO1) INHIBITORS THROUGH VIRTUAL SCREENING**

Pharm. Naufa HANIF, M.Sc

**Pharmaceutical Chemistry Program
MASTER OF SCIENCE THESIS**

ANKARA

2024

**T.C.
REPUBLIC OF TURKEY
HACETTEPE UNIVERSITY
GRADUATE SCHOOL OF HEALTH SCIENCES**

**DISCOVERY OF NEW INDOLEAMINE 2,3-DIOXYGENASE 1
(IDO1) INHIBITORS THROUGH VIRTUAL SCREENING**

Pharm. Naufa HANIF, M.Sc

**Pharmaceutical Chemistry Program
MASTER OF SCIENCE THESIS**

ADVISOR OF THESIS

Assoc. Prof. Suat SARI

ANKARA

2024

**DISCOVERY OF NEW INDOLEAMINE 2,3-DIOXYGENASE 1 (IDO1)
INHIBITORS THROUGH VIRTUAL SCREENING**

Pharm. Naufa HANIF, M.Sc.

Assoc. Prof. Suat SARI

This thesis study has been approved and accepted as a Master dissertation in “Pharmaceutical Chemistry Program” by the assessment committee, whose members are listed below, on 04.01.2024

Chairman of the Committee : *Prof. Nesrin GÖKHAN KELEKÇİ*

Hacettepe University

Advisor of the Dissertation : *Assoc. Prof. Suat SARI*

Hacettepe University

Member : *Prof. Oya ÜNSAL TAN*

Hacettepe University

Prof. Arzu KARAKURT

Inönü University

Assoc. Prof. Mehmet ABDULLAH ALAGÖZ

Inönü University

This dissertation has been approved by the above committee in conformity to the related issues of Hacettepe University Graduate Education and Examination Regulation.

Prof. Dr. Muge YEMİŞÇİ OZKAN, MD, PhD

Director

YAYIMLAMA VE FİKRİ MÜLKİYET HAKLARI BEYANI

Enstitü tarafından onaylanan lisansüstü tezimin/raporumun tamamını veya herhangi bir kısmını, basılı (kağıt) ve elektronik formatta arşivleme ve aşağıda verilen koşullarla kullanıma açma iznini Hacettepe Üniversitesine verdiğimi bildiririm. Bu izinle Üniversiteye verilen kullanım hakları dışındaki tüm fikri mülkiyet haklarım bende kalacak, tezimin tamamının ya da bir bölümünün gelecekteki çalışmalarda (makale, kitap, lisans ve patent vb.) kullanım hakları bana ait olacaktır.

Tezin kendi orijinal çalışmam olduğunu, başkalarının haklarını ihlal etmediğimi ve tezimin tek yetkili sahibi olduğumu beyan ve taahhüt ederim. Tezimde yer alan telif hakkı bulunan ve sahiplerinden yazılı izin alınarak kullanılması zorunlu metinlerin yazılı izin alınarak kullandığımı ve istenildiğinde suretlerini Üniversiteye teslim etmeyi taahhüt ederim.

Yükseköğretim Kurulu tarafından yayınlanan “*Lisansüstü Tezlerin Elektronik Ortamda Toplanması, Düzenlenmesi ve Erişime Açılmasına İlişkin Yönerge*” kapsamında tezim aşağıda belirtilen koşullar haricince YÖK Ulusal Tez Merkezi / H.Ü. Kütüphaneleri Açık Erişim Sisteminde erişime açılır.

- Enstitü / Fakülte yönetim kurulu kararı ile tezimin erişime açılması mezuniyet tarihimden itibaren 2 yıl ertelenmiştir. (1)
- Enstitü / Fakülte yönetim kurulunun gerekçeli kararı ile tezimin erişime açılması mezuniyet tarihimden itibaren ... ay ertelenmiştir. (2)
- Tezimle ilgili gizlilik kararı verilmiştir. (3)

...../...../.....

(İmza)

Naufa HANIF

i

i “*Lisansüstü Tezlerin Elektronik Ortamda Toplanması, Düzenlenmesi ve Erişime Açılmasına İlişkin Yönerge*”

- (1) *Madde 6. 1. Lisansüstü teze ilgili patent başvurusu yapılması veya patent alma sürecinin devam etmesi durumunda, tez danışmanının önerisi ve enstitü anabilim dalının uygun görüşü üzerine enstitü veya fakülte yönetim kurulu iki yıl süre ile tezin erişime açılmasının ertelenmesine karar verebilir.*
- (2) *Madde 6. 2. Yeni teknik, materyal ve metotların kullanıldığı, henüz makaleye dönüşmemiş veya patent gibi yöntemlerle korunmamış ve internetten paylaşılması durumunda 3. şahıslara veya kurumlara haksız kazanç imkanı oluşturabilecek bilgi ve bulguları içeren tezler hakkında tez danışmanının önerisi ve enstitü anabilim dalının uygun görüşü üzerine enstitü veya fakülte yönetim kurulunun gerekçeli kararı ile altı ayı aşmamak üzere tezin erişime açılması engellenebilir.*
- (3) *Madde 7. 1. Ulusal çıkarları veya güvenliği ilgilendiren, emniyet, istihbarat, savunma ve güvenlik, sağlık vb. konulara ilişkin lisansüstü tezlerle ilgili gizlilik kararı, tezin yapıldığı kurum tarafından verilir *. Kurum ve kuruluşlarla yapılan işbirliği protokolü çerçevesinde hazırlanan lisansüstü tezlere ilişkin gizlilik kararı ise, ilgili kurum ve kuruluşun önerisi ile enstitü veya fakültenin uygun görüşü üzerine üniversite yönetim kurulu tarafından verilir. Gizlilik kararı verilen tezler Yükseköğretim Kuruluna bildirilir. Madde 7.2. Gizlilik kararı verilen tezler gizlilik süresince enstitü veya fakülte tarafından gizlilik kuralları çerçevesinde muhafaza edilir, gizlilik kararının kaldırılması halinde Tez Otomasyon Sistemine yüklenir*

* *Tez danışmanının önerisi ve enstitü anabilim dalının uygun görüşü üzerine enstitü veya fakülte yönetim kurulu tarafından karar verilir.*

ETHICAL DECLARATION

In this thesis study, I declare that all the information and documents have been obtained in the base of the academic rules and all audio-visual and written information and results have been presented according to the rules of scientific ethics. I did not do any distortion in data set. In case of using other works, related studies have been fully cited in accordance with the scientific standards. I also declare that my thesis study is original except cited references. It was produced by myself in consultation with supervisor (Assoc. Prof. Suat SARI) and written according to the rules of thesis writing of Hacettepe University Graduate School of Health Sciences.

(signature)

Naufa HANIF

ACKNOWLEDGEMENTS

I would like to express my gratitude to my supervisor, Assoc. Prof. Suat SARI, for his invaluable guidance and full support throughout my research. His expertise, encouragement, patience, and constructive feedback have played a crucial role in shaping my work.

Special thanks to Prof. Dr. Nesrin GÖKHAN KELEKÇİ, Head of Department of Pharmaceutical Chemistry Hacettepe University, for providing the necessary resources and facilitates for my research.

I would like to express my appreciation to the staffs of the Department of Pharmaceutical Chemistry for their contributions and valuable support during my master study and research journey in department.

I am really grateful to my parents, Ayoeb AMİN and Diah RATNAWIATI, as well as my siblings, Naela NABIELA and Naesrina OKFIANA, for their unwavering loves, unlimited prays, encouragements, and supports throughout my academic journey.

Finally, I want to acknowledge my supportive friends from CCRC Farmasi UGM, Yayasan Bentala Tamaddun Nusantara, PCIM Türkiye, PPI Türkiye, Rumah Cebesi Berkah, and Seduh Çay communities, for their encouragement, support, and willingness to help. Thank you for every party that I cannot mention one by one who have contributed during my academic journey.

ABSTRACT

Hanif, N. Discovery of New Indoleamine 2,3-Dioxygenase 1 (IDO1) Inhibitors Through Virtual Screening, Hacettepe University Graduate School of Health Sciences Program of Pharmaceutical Chemistry Master Thesis, Ankara, 2024.

Cancer, a leading global cause of deaths, utilizes mechanisms and pathways to evade the immune system, one of which is the kynurenine (Kyn) pathway, responsible for degrading amino acid L-tryptophan (Trp). Overexpression of indoleamine 2,3-dioxygenase 1 (IDO1), the rate-limiting enzyme of Kyn pathway, in certain cancers makes it a target of interest. In this study, virtual screening was conducted to discover new apo-IDO1 small molecule inhibitors. In the virtual screening process, encompassing both ligand-based and structure-based approaches, three compounds were successfully identified from a commercial library of 555,557 compounds. The library compounds underwent an initial filtering based on drug-likeness parameters to remove those with potentially undesired pharmacokinetic attributes and reactive functional groups. The refined library then underwent parallel ligand-based virtual screening, employing both shape similarity and pharmacophore modeling screening with the involvement of five different known apo-IDO1 inhibitors. The screened library was subsequently docked to the selected crystallographic human apo-IDO1 structure (PDB ID: 6wjy), which exhibited the best validation results, utilizing standard and then extra precision modes. The top 500 compounds with their three best poses were selected to calculate their MM-GBSA free binding energy (ΔG) values. Fingerprint similarity analysis was performed and similar entities were removed to ensure structural diversity for the selected hits. Among the top scoring 10 compounds regarding MM-GBSA ΔG values, three hits namely STOCK2S-34127, STOCK3S-69016, and STOCK2S-94986, were better than the reference inhibitor. In MD simulations, apo-IDO1 complexes of these hits displayed favorable outcomes, regarding structural conformation and stability, residue fluctuations, compactness, salt bridge formations, and binding free energy. Lastly, the three hits were predicted to show low oral toxicity, moderate toxicity to *Daphnia magna*, low bioaccumulation in aquatic environments, and be inactive in both nuclear receptor signaling and stress response pathways of toxicity. As a result, STOCK2S-34127, STOCK3S-69016, STOCK2S-94986 were predicted as potent, selective, and safe apo-IDO1 inhibitors, which need to be confirmed via *in vitro* and *in vivo* assays.

Keywords : IDO1, virtual screening, shape similarity, pharmacophore modeling, molecular docking, MD simulations

ÖZET

Hanif, N. Virtual Tarama Yoluyla Yeni İndolamin 2,3-Dioksijenaz 1 (IDO1) İnhibitörlerinin Keşfi, Hacettepe Üniversitesi Sağlık Bilimleri Enstitüsü, Eczacılık Kimyası Ana Bilim Dalı Yüksek Lisans Tezi, Ankara, 2024. Kanser, dünya genelinde ölümlerin önde gelen nedenlerinden biri olarak, bağışıklık sistemini atlatmak için çeşitli mekanizma ve yollar kullanır. Bunlardan biri de amino asit L-triptofan'ın (Trp) parçalandığı kinürenin (Kyn) yoludur. Belirli kanser tiplerinde kinürenin yolunun hız sınırlayıcı basamağını katalize eden indolamin 2,3-dioksiyoksijenaz 1'in (IDO1) aşırı ifadesi, bu enzimi ilgi odağı haline getirmiştir. Bu çalışmada, apo-IDO1'in küçük molekül inhibitörlerinin keşfi için sanal tarama gerçekleştirildi. Hem ligand- hem de yapı-temelli yaklaşımları içeren sanal tarama sürecinde, ticari bir kütüphanede yer alan 555,557 bileşik arasından üçü aday bileşikler olarak başarıyla tanımlanmıştır. Kütüphane bileşikleri potansiyel olarak istenmeyen farmakokinetik özelliklere ve reaktif gruplara sahip olan moleküllerin elenmesi amacıyla ilaç benzerlik parametrelerine dayalı olarak filtreleme işlemine tabi tutuldu. Daha sonra, fitrelenmiş bileşik kütüphanesi, beş farklı apo-IDO1 inhibitörünün referans bileşik olarak dahil olduğu, hem şekil benzerliği hem de farmakofor modelleme taramasının kullanıldığı paralel ligand-temelli sanal taramaya tabi tutulmuştur. Seçilen kütüphane bileşikleri daha sonra, validasyon çalışmalarında en iyi sonucu veren 6wjy PDB kodlu insan apo-IDO1 kristal yapısına önce standart ve ardından ekstra kesinlik kipleri kullanılarak kenetlenmiştir. En iyi üç bağlanma pozunu ile birlikte en yüksek skorlu 500 bileşik, MM-GBSA serbest bağlanma enerjisi (ΔG) hesaplamaları için seçilmiştir. Seçilen bileşiklerin yapısal çeşitlilik gösterdiğinden emin olmak için parmak izi benzerlik analizi gerçekleştirilerek benzer bileşikler elenmiştir. MM-GBSA ΔG değerleri açısından en iyi 10 bileşik arasından STOCK2S-34127, STOCK3S-69016 ve STOCK2S-94986 olmak üzere üçü, referans inhibitörden daha iyi bulunmuştur. Bu üç bileşiğin apo-IDO1 kompleksleri MD simülasyonlarında yapısal konformasyon ve stabilite, aminoasit dalgalanmaları, bütünlük, tuz köprüsü oluşturma ve ligand-reseptör serbest bağlanma enerjileri açısından olumlu sonuçlar göstermiştir. Son olarak, bu üç bileşik için düşük oral toksisite, *Daphnia magna*'ya karşı orta düzeyde toksisite gösterdiler, ve sucul ortamlarda düşük biyobirikim öngörülmüş, toksisite yollarından hem nükleer reseptör sinyalizasyonunda hem de stres yanıt yollarında etkisiz oldukları tahmin edilmiştir. Sonuç olarak, STOCK2S-34127, STOCK3S-69016 ve STOCK2S-94986, güçlü, spesifik, ve güvenli apo-IDO1 inhibitörleri olarak öngörülmüştür; bu öngörülerin *in vitro* ve *in vivo* deneyler ile teyit edilmesi gerekmektedir.

Anahtar kelimeler: IDO1, sanal tarama, şekil benzerliği, farmakofor modelleme, moleküler kenetleme, MD simülasyonları

TABLE OF CONTENT

APPROVAL PAGE	iii
YAYIMLAMA VE FİKRİ MÜLKİYET HAKLARI BEYANI	iv
ETHICAL DECLARATION	v
ACKNOWLEDGEMENTS	vi
ABSTRACT	vii
ÖZET	viii
TABLE OF CONTENT	ix
ABBREVIATIONS	xi
LIST OF FIGURES	xvi
LIST OF TABLES	xviii
1. INTRODUCTION	1
2. LITERATURE REVIEW	6
2.1. Cancer Immunotherapy	6
2.1.1. The History and Development of Cancer Immunotherapy	6
2.1.2. The Cancer Immunity Cycle	7
2.1.3. How Tumor Cells Evade the Immune System	9
2.2. Mechanism of Kynurenine Pathway	11
2.3. Indoleamine 2,3-dioxygenase 1	12
2.3.1. Structure of Indoleamine 2,3-dioxygenase 1	12
2.3.2. Holo- and Apo-Form IDO1, Their Inhibition and Clinically Tested IDO1 Inhibitors	14
2.4. Virtual Screening for Drug Design	19
2.4.1. Ligand-Based Virtual Screening	20
2.4.2. Structure-Based Virtual Screening	24
2.4.3. Combination Approach of Ligand- and Structure-Based Virtual Screening	29
2.5. Previous Studies on IDO1 Inhibitor Through Virtual Screening	30
3. MATERIALS AND METHODS	32
3.1. Ligand preparation	32
3.2. Ligand-Based Virtual Screening	33
3.2.1. Shape Screening	33

3.2.2. Pharmacophore Screening	34
3.3. Structure-Based Virtual Screening	35
3.3.1. Protein Preparation	35
3.3.2. Molecular Docking	35
3.3.3. Validation Studies	36
3.3.4. Molecular Dynamics Simulations	40
3.3.5. Binding Free Energy Calculations using MM-GBSA	41
3.4. Fingerprint Similarity	42
3.5. Toxicity Prediction	43
4. RESULTS	44
4.1. Calculation of Molecular Descriptors and Drug-likeness Filtering	45
4.2. Ligand-Based Virtual Screening	46
4.2.1. Shape Screening	46
4.2.2. Pharmacophore Screening	48
4.3. Structure-based virtual screening	51
4.3.1. Validation Studies	51
4.3.2. Molecular Docking	54
4.3.3. Binding Free Energy Calculations and Fingerprint Similarity	55
4.3.4. Molecular Dynamics Simulations	58
4.4. Toxicity Prediction	63
5. DISCUSSION	65
6. CONCLUSION AND RECOMMENDATION	79
6.1. Conclusion	79
6.2. Recommendation	80
7. REFERENCES	81
8. APPENDIX	103
9. CURRICULUM VITAE	109

ABBREVIATIONS

4PI	: 4-Phenylimidazole
ADMET	: Absorption, Distribution, Metabolism, Excretion, and Toxicity
AFE	: Alchemical free energy
AhR	: Aryl hydrocarbon receptor
ALA	: Alanine
AMBER	: Assisted Model Building with Energy Refinement
AndR	: Androgen receptor
APCs	: Antigen-presenting cells
AR	: Aromatic ring
ARG	: Arginine
AR-LBD	: Androgen receptor ligand binding domain
ASN	: Asparagine
ASP	: Aspartic acid
ATAD5	: ATPase family AAA domain-containing protein 5
AUC-ROC	: Area under the receiver operating characteristic curve
BALB/c mice	: Bagg Albino c mice
BCG	: Bacillus Calmette-Guérin
CAR-T	: Chimeric antigen receptor T
CCL2	: Chemokines C–C motif chemokine ligand 2
CCL22	: Chemokines C–C motif chemokine ligand 22
CCL5	: Chemokines C–C motif chemokine ligand 5
CD19	: Clusters of differentiation 19
CD20	: Clusters of differentiation 20
CD3	: Clusters of differentiation 3
CD4	: Clusters of differentiation 4
CD8	: Clusters of differentiation 8
CGenFF	: CHARMM general forcefield
CHARMM	: Chemistry at HARvard Molecular Mechanics
ClogP	: Calculated octanol/water partition coefficient
CSF1	: Colony stimulating factor 1
CTD	: C-terminus domain

CTLA-4	: Cytotoxic T lymphocyte-associated protein 4
CTLs	: Cytotoxic T lymphocytes
CXCL12	: Cxc chemokine ligand 12
CXCL5	: Cxc chemokine ligand 5
CXCL8	: Cxc chemokine ligand 8
CYS	: Cysteine
D-1MT	: D-1-methyl-tryptophan
DCs	: Dendritic cells
DUD-E	: Directory of Useful Decoys, Enhanced
EC ₅₀	: Half maximal effective concentration
EF	: Enrichment factor
ER	: Estrogen receptor alpha
ER-LBD	: Estrogen receptor ligand binding domain
FaSSIF	: Fasted stated stimulated intestinal fluid
FDA	: Food and Drug Administration
FEP	: Free energy perturbation
Foxp3	: Forkhead box p3+
FRED	: Fast Exhaustive Docking
GA	: Genetic algorithm
GAFF	: General Amber Force Field
GB/SA	: Generalised Born and surface area solvation
GCN2	: General control nonderepressible 2
GI	: Gastrointestinal
GLIDE	: Grid-based Ligand Docking from Energetics
GLN	: Glutamine
GLU	: Glutamic acid
GLY	: Glycine
HAD	: 3-Hydroxyanthranilic acid dioxygenase
HBA	: Hydrogen bond acceptors
HBD	: Hydrogen bond donors
HER2	: Human epidermal growth factor receptor 2
HIS	: Histidine
HSE	: Heat shock factor response element
IBS	: InterBioScreen
IC ₅₀	: Half maximal inhibitory concentration

ICIs	: Immune checkpoint inhibitors
IDO1	: Indoleamine 2,3-dioxygenase 1
IDO2	: Indoleamine 2,3-dioxygenase 2
IFN- α	: Interferon α
IFN- γ	: Interferon γ
IL-1	: Interleukin 1
IL-10	: Interleukin 10
IL-2	: Interleukin 2
ILE	: Isoleucine
IRAEs	: Immune-related adverse events
IUPAC	: International Union of Pure and Applied Chemistry
KYAT	: Kynurenine-oxoglutarate transaminase
Kyn	: Kynurenine
LBVS	: Ligand-based virtual screening
LEU	: Leucine
LPS	: Lipopolysaccharide
LSQA	: Ligand Structure Quality Assessment
LYS	: Lysine
MD	: Molecular dynamics
MDSCs	: Myeloid-derived suppressor cells
MET	: Methionine
MHC I	: Major histocompatibility complex I
MHC II	: Major histocompatibility complex II
MM-GBSA	: Molecular mechanics with generalised Born surface area solvation
MMP	: Mitochondrial membrane potential
MM-PBSA	: Molecular mechanics with Poisson–Boltzmann surface area solvation
MOE	: Molecular Operating Environment
mTOR	: Mammalian target of rapamycin
MW	: Molecular weight
NAMD	: Nanoscale Molecular Dynamics
NC	: Natural compound
NFK	: <i>N</i> -formyl kynurenine
NI	: Negatively ionizable

NK	: Natural killer
NMIBC	: Non-muscle invasive bladder cancer
NMR	: Nuclear magnetic resonance
NN	: Neural networks
NPT	: Isothermal–isobaric ensemble, amount of substance (N), pressure (P) and temperature (T) are conserved
NSCLC	: Non-small cell lung cancer
NTD	: N-terminus domain
NVT	: Canonical ensemble, amount of substance (N), volume (V) and temperature (T) are conserved
OPLS	: Optimized Potentials for Liquid Simulations
OPLS-AA	: Optimized Potentials for Liquid Simulations All Atom
PD-1	: Programmed cell death receptor 1
PDB	: Protein Data Bank
PD-L1	: Programmed cell death ligand 1
PHE	: Phenylalanine
PI	: Positively ionizable
PLANTS	: Protein-Ligand ANTSsystem
PPAR-Gamma	: Peroxisome proliferator activated receptor gamma
PPIs	: Protein-protein interactions
PRO	: Proline
QPRT	: Quinolate phosphoribosyl transferase
QSAR	: Quantitative structure-activity relationship
RB	: Rotatable bond
RCC	: Renal cell carcinoma
RIE	: Robust Initial Enhancement
RMSD	: Root-mean-square deviation
RMSF	: Root-mean-square fluctuation
ROCS	: Rapid overlay of chemical structures
RoG	: Radius of gyration
RP	: Recursive partitioning
rtvFG	: Reactive functional group
SAR	: Structure-activity relationship
SBVS	: Structure-based virtual screening
SC	: Synthetic compound

SER	: Serine
SP	: Standard precision
SVM	: Support vector machine
TAAAs	: Tumor-associated antigens
TAMs	: Tumor-associated macrophages
TANs	: Tumor-associated neutrophils
TCR	: T cell receptor
TDO2	: Tryptophan 2,3-dioxygenase 2
Teffs	: Effector T cells
TEST	: Toxicity Estimation Software Tool
TGF- β	: Transforming growth factor β
Th17	: T helper cells
THR	: Threonine
TI	: Thermodynamic integration
TME	: Tumor microenvironment
TNF- α	: Tumor necrosis factor α
Tox21	: 21st Century toxicology
tPSA	: Topological polar surface area
Tregs	: Regulatory T cells
Trp	: Tryptophan
TYR	: Tyrosine
VAL	: Valine
VEGF	: Vascular endothelial growth factor
VISTA	: V domain immunoglobulin suppressor of T cell activation
VMD	: Visual Molecular Dynamics
WEGA	: Weighted Gaussian algorithm
WHO	: World Health Organization
XP	: Extra precision
XVOL	: Exclusion volume

LIST OF FIGURES

Figure	Page
2.1 The concept of the cancer-immunity cycle (adapted from the work by Chen and Mellman (55))	8
2.2 Kynurenine pathway	12
2.3 The 3D-structure of IDO1 and its pocket (76)	13
2.4 The structures of five IDO1 inhibitors that have entered clinical trials	15
2.5 A diagrammatic representation of the process for calculating similarity between a query molecule and molecules within a database (119)	21
2.6 Pharmacophoric features (136)	23
2.7 The flowchart of molecular dynamics simulation (181)	28
4.1 Workflow of this study	44
4.2 The alignment of the docked poses and the original co-crystallized poses of (A) QPV, (B) U41, (C) U6G, (D) SLW, and (E) 6RI in the active site of apo-IDO1 structures with PDB IDs 6v52, 6wjy, 6wpe, 7b1o, and 7rrc, respectively.	52
4.3 ROC curves for (a) 6v52, (b) 7b1o, (c) 6wpe, (d) 6wjy, and (e) 7rrc	54
4.4 Apo-IDO1 structure complexed with small-molecule inhibitor U41 (PDB ID 6wjy)	55
4.5 Fingerprint similarity prediction for the top 500 compounds. After the evaluation, there were 54 clusters with a clustering strain of 1.083	57
4.6 The MD simulations trajectories for the ligand-free and ligand-bound IDO1 structures with a duration of 100 ns depicting (A) RMSD values, (B) average RMSF values for each amino acid residue, and (C) RoG values over time	60
4.7 Salt bridges formed in each system throughout the MD simulations and their % distribution according to the types	61

	indicated as ASP-/ARG+ (blue bar), ASP-/LYS+ (orange bar), GLU-/ARG+ (gray bar), and GLU-/LYS+ (yellow bar)	
4.8	ΔG variation over time for ligand-bound IDO1 structures	62
5.1	The selected hits from virtual screening along with U41, and their three moieties concerning apo-IDO1 are illustrated.	70
5.2	The 3D and 2D interaction visualizations of (A) STOCK2S- 34127, (B) STOCK3S-69016, (C) STOCK2S-94986, and (D) U41 were presented.	72
5.3	Total energy plots of the protein complexes with ligand-bound states and the ligand-free state during 100 ns of MD simulations	73
5.4	The four regions that experienced the most fluctuation according to RMSF values are highlighted.	74

LIST OF TABLES

Table		Page
2.1	Examples of selective apo-IDO1 inhibitors from the literature	18
2.2	Here are the following examples of molecular docking programs with their scoring functions	26
3.1	The central coordinates of the grid box for each protein	36
3.2	Active apo-IDO1 inhibitors used to generate decoys	39
4.1	Molecular descriptors and drug-likeness filtering of the IBS libraries	46
4.2	Query structures as references for shape screening	47
4.3	Number of selected compounds ^a from each query of each method from each library and the score ranges ^b obtained through shape similarity screening	48
4.4	Pharmacophore models of the study and their features	49
4.5	Number of selected compounds ^a from each pharmacophore model of each method from each library and the score ranges ^b obtained through pharmacophore screening	50
4.6	Number of total selected compounds from each library obtained through both shape similarity and pharmacophore screening	51
4.7	The enrichment study for five different complexes	53
4.8	Selected 10 compounds with best MM-GBSA ΔG values and structural diversity and U41	56
4.9	Amino acids interactions of the top three compounds predicted by molecular docking and those of U41 identified experimentally	58
4.10	Minimum, maximum, average binding free energy values of the top three ligands, and U41	62
4.11	Toxicity Prediction of top three candidate compounds	64

1. INTRODUCTION

According to World Health Organization (WHO), cancer is one of the leading causes of death, responsible for approximately 9.9 million deaths, with 19.3 million new cases in 2020 alone. Among all cancers, breast cancer ranked at the top with 2.2 million new cases (11.7%), while lung cancer, held the top position as the leading cause of death among all cancers accounting for 1.8 million deaths (18%). There have been several therapeutic approaches to cure this deadly disease, such as chemotherapy, radiotherapy, immunotherapy, and cancer surgery. The primary method of treating cancer to far has been chemotherapy; however, the majority of chemotherapeutic medications have severe side effects. These medications also impact proliferative non-cancerous cells like stem cells, hair follicle cells, and gastrointestinal (GI) epithelial cells (1) and develop resistance rapidly (2). Additionally, many chemotherapeutic medications lack an oral form and have sensitive pharmacokinetics, making them challenging to administer (1,3). In contrast to chemotherapy, which eradicates cancer through cytotoxic qualities, immunotherapy uses the host immune system to target tumor cells in general (4).

Cancer immunotherapies aim to utilize the immune system to eliminate cancerous cells and halt the growth of tumors. The success of these therapies, exemplified by immune checkpoint inhibitors (ICIs), is demonstrated by the US FDA-approved biologic medicines targeting the programmed death receptor/ligand 1 (PD-1/PD-L1) and cytotoxic T lymphocyte-associated protein 4 (CTLA-4) antibodies (5). Examples of PD-1 inhibitors, such as pembrolizumab and nivolumab, have shown promising results in numerous cancer types, including non-small-cell lung cancer (NSCLC), Hodgkin lymphoma, and melanoma. Similarly, ipilimumab, a CTLA-4 inhibitor, has also demonstrated efficacy in melanoma (6). However, ICIs are also responsible for triggering autoimmunity. Combining ipilimumab with nivolumab, for instance, has shown a marginal improvement in survival but with a more than twofold increase in the incidence of serious immune-related adverse events (IRAEs) (7). To enhance the outcome while minimizing the risk of autoimmunity, it is necessary to identify a partner for ICIs that can enhance the immune system's recognition of the tumor prior to treatment.

Focusing on the modified metabolism of tumors is a newly developing approach in the field of cancer therapy. Cancer cells exhibit significant differences compared to normal cells. The primary metabolic dependence of cancer cells is known as the “Warburg effect”, which distinguishes cancer cell metabolism from that of normal cells. It is characterized by their tendency to consume glucose and produce lactate even in the presence of oxygen (8,9). For instance, binding to PD-L1 can trigger glycolysis in cancer cells, facilitating tumor growth and metastasis (10). Consequently, this phenomenon can significantly influence the metabolic balance within the tumor microenvironment (TME). In addition to glycolysis, amino acid catabolism plays a significant role in regulating immune function within the TME (11). Thus, directing attention towards these specific amino acids and their associated metabolic pathways in cancer treatment emerges as a promising approach in the development of novel therapeutic agents.

One such example of an amino acid is tryptophan, which plays essential roles in both tumor progression and immune responses. Its metabolic pathway, the kynurenine (Kyn) pathway, is responsible for the degradation of L-tryptophan amino acid (Trp) (12). The first and rate-limiting stage of the Kyn metabolic pathway, which generates the endogenous aryl hydrocarbon receptor (AhR) agonist Kyn, is catalyzed by indoleamine 2,3-dioxygenase 1 and 2 (IDO1 and IDO2), and tryptophan 2,3-dioxygenase 2 (TDO2). The degradation of tryptophan by IDO1, IDO2, and TDO2 can produce several tryptophan metabolites, such as kynurenic acid, 3-hydroxykynurenine, and 3-hydroxyanthranilic acid, which are then transformed into quinolinic acid and picolinic acid by non-enzymatic process. Quinolinic acid is further metabolized to nicotinamide by quinolinate phosphoribosyl transferase (13).

The degradation of tryptophan has two main impacts: (i) induction of the general control nonderepressible 2 (GCN2), causing the inhibition of CD4⁺ T cells differentiation into T helper cells (14), as well as cell cycle arrest in CD8⁺ T cells (15), and (ii) suppression of the mammalian target of rapamycin (mTOR) (16), which results in immunosuppression by regulating regulatory T cells (Tregs) and effector T cells (Teffs) (17). Furthermore, accumulation of tryptophan metabolites, like Kyn, can stimulate the AhR. The presence of AhR has effects similar to the suppression of

mTOR, leading to immunosuppression. This activity encourages the differentiation of forkhead box p3+ (Foxp3) T regulatory cells (18).

T cells play an essential role in the immune response as protectors and fighters against xenobiotics, including cancer cells. Failure of T cells to carry out their functions is one of the triggers for the development of cancer. In this case, IDO1 behaves as the frontliner against the attacks of T cells (19).

Numerous inhibitors that specifically target IDO1 have been developed in the last decade. Some of the IDO1 inhibitors that have entered clinical trials include indoximod, epacadostat, navoximod, PF-06840003, and BMS-986205. Indoximod belongs to type I inhibitors, which selectively focus on the holo-IDO1 form bound to molecular oxygen. Its mechanism of action involves stimulating mTOR kinase to decrease T cell autophagy (16). On the other hand, epacadostat belongs to type II inhibitor and its mechanism of action is competitive inhibition of IDO1 (20,21), along with β -carboline (22). In contrast to epacadostat, navoximod is a noncompetitive inhibitor of IDO1 (type III inhibitor) (23). PF-06840003 exhibits a different binding type without relying on coordination with the heme iron and demonstrates a novel binding mode (24). Lastly, BMS-986205 belongs to type IV inhibitors, which have an irreversible inhibition mechanism of IDO1, which means that it binds covalently to the enzyme (25,26) and permanently inactivates the apo-IDO1 form (27).

The last-mentioned approach demonstrated remarkable potency and a suicidal mechanism. According to Pham and Yeh's report (2018), BMS-986205 does not exclusively target the apo-form of IDO1. Initially, it binds to a solvent-exposed surface cleft near the active site of holo-IDO1, leading to partial heme release and inducing various conformational changes that ultimately result in the formation of an apo-IDO1 inhibitor complex. They suggested that this unique interaction presents an innovative approach that can be utilized in drug development targeting IDO1 (25). Due to the limited number of inhibitors that have entered clinical trials, such as BMS-986205, efforts are needed to increase the number of candidate compounds with similar activity. One approach to achieve this is virtual screening.

Finding appropriate small compounds that exhibit specific biological effects is a significant challenge in the field of Pharmaceutical Chemistry. Over the past three

decades, computational methods, particularly molecular modeling techniques, have increasingly been employed as a logical solution to this issue. Among these techniques, virtual screening is the most widely utilized approach, enabling prediction or identification of entities with desired properties within a set of potential molecules through diverse molecular modeling methods (28). In the context of virtual screening, molecular modeling techniques can be categorized into two main groups: ligand-based and structure-based methods. Ligand-based virtual screening (LBVS) depends solely on ligand data and aims to identify molecules that resemble known active compounds. This approach operates on the assumption that similar molecules are likely to exhibit similar biological effects (29). In LBVS, several techniques are employed, including Quantitative Structure-Activity Relationship (QSAR), which utilizes physicochemical parameters and descriptors of molecules; fingerprint methods, which encode two-dimensional structures; shape similarity analysis, which is based on three-dimensional structures; and pharmacophore modeling, which involves identifying common pharmacophore groups and their spatial orientations (30). Additionally, scaffold hopping is commonly used strategy in drug discovery, specifically in virtual screening, to enhance the diversity of the compounds considered when searching for new lead compounds or optimizing existing ones (31,32).

The advancements in structural biology and structure elucidation techniques have significantly expedited studies on the structure elucidation of biological macromolecules targeted by drugs. As a result, the development of structure-based virtual screening (SBVS) has emerged, utilizing structural data of target receptors. Molecular docking has emerged as the predominant approach for investigating the interactions between small organic molecules and biological macromolecules. This method facilitates prediction of the optimal positioning of a ligand within a receptor binding site (33). Aside from molecular docking, continuous solvation models, such as molecular mechanics with Generalised Born surface area solvation (MM-GBSA) and molecular mechanics with Poisson–Boltzmann surface area solvation (MM-PBSA) offer more precise prediction of ligand-receptor affinity. Additionally, the free energy perturbation (FEP) technique, involving molecular chelation simulations for predicting ligand-receptor interactions and affinities, as well as molecular dynamics (MD) simulations for modeling dynamic changes in ligand-receptor complexes, is

employed in this context. These methods enable accurate evaluation of ligand-receptor affinity, exploration of structural modifications, and analysis of the dynamic behavior of ligand-receptor complexes (29,34–36).

There are only a few studies in the literature where IDO1 inhibitors were discovered through virtual screening methods. Thus, this study aimed to identify structurally diverse potential IDO1 inhibitor compounds that are commercially available, theoretically drug-like, safe, and selective to the apo form of IDO1. In order to achieve this aim, a comprehensive virtual screening process using both ligand-based and structure-based approaches was applied. The ligand-based methods included shape similarity screening and pharmacophore modeling, while the structure-based methods included molecular docking, MD simulations, and MM-GBSA binding free energy analysis. To enhance the screening process, sequential, parallel, and hybrid approaches were utilized. The compound search was conducted within a ligand library comprising more than 550,000 small molecules. MD simulations were performed to predict the conformational changes, compactness, and stability of the selected ligand-IDO1 complexes over the timeframe. Additionally, binding free energy analysis was conducted using the MD simulations trajectories. In the final section, toxicity was assessed for all the selected compounds to predict the safety and toxicity class of each compound.

2. LITERATURE REVIEW

2.1. Cancer Immunotherapy

2.1.1. The History and Development of Cancer Immunotherapy

- In 1777, the initial approach involved introduction of various pathogens to stimulate an immune response against cancerous growth (37).
- In 1891, William "Father of Immunotherapy" Coley conducted studies in which he administered streptococcal species to individuals with metastatic soft tissue sarcomas. He observed tumor regression following these injections, leading to the term "Coley's toxins". His hypothesis suggested that a robust infection could trigger the immune system to combat malignancies (38,39).
- During 1950s, the concept of immunosurveillance, initially proposed by Burnet and Thomas, emphasized that the immune system actively identifies and eliminates neoplasms by recognizing tumor-associated antigens (TAAs) (40).
- In the 1970s, Bacillus Calmette-Guérin (BCG) was approved as a therapeutic vaccine for the treatment of non-muscle invasive bladder cancer (NMIBC) and has remained the standard approach to prevent the progression or recurrence of high-risk disease (41,42).
- In 1974, the understanding of cytokines' role in cancer immunotherapy commenced with the identification of IL-2, a substance produced by various cells, including CD4+ and CD8+ T cells. IL-2 plays a vital role in the differentiation and proliferation of T cells, the formation of immune memory, and the regulation of Tregs to prevent autoimmune reactions (43). In 1992, the FDA granted approval for the use of IL-2 in the treatment of metastatic renal cell carcinoma, marking it as the pioneering cancer immunotherapeutic administered to humans (44).
- In 1992, Ishida and colleagues made the discovery of both programmed death-1 and programmed death ligand-1 (PD-1/PDL-1) (45).
- In 1997, rituximab, originally approved for CD20+ Non Hodgkin's lymphoma, achieved the distinction by being the first monoclonal antibody included in its composition. Subsequently, it obtained additional approvals for chronic

lymphocytic leukemia, rheumatoid arthritis, and specific autoimmune conditions like pemphigus vulgaris (46,47).

- In 1998, the monoclonal antibody trastuzumab was developed to specifically target breast cancer with human epidermal growth factor receptor 2 (HER2) overexpression. HER2 is characterized as a transmembrane receptor tyrosine kinase and is classified as a proto-oncogene (48,49).
- In the early 2000s, two oncolytic viruses, ECHO-7 (from Latvia, 2004) and H101 (from China, 2005), received initial approvals. However, both of these treatments had negative effects on healthy tissues. It wasn't until 2015 that talimogene laherparepvec became the first oncolytic virus to gain approval in the United States (50).
- In 2011, ipilimumab, which directly binds to CTLA-4, was approved as the first checkpoint inhibitor for cancer treatment, specifically metastatic melanoma. This discovery was made by James Allison. The blockade of CTLA-4 stimulates T cell activation, proliferation, and ultimately results in the destruction of tumor (51,52).
- In 2014, blinatumomab was initially developed as a bispecific antibody, notable for having two distinct antigen-binding sites. One of these binding sites is designed to activate T cells (CD3), while the other binds to a tumor-specific antigen (CD19 found in B cells). This therapy has been employed in the treatment of relapsed or refractory B cell acute lymphoblastic leukemia in patients without the Philadelphia chromosome (Ph-negative) (53).
- In 2017, the first CD-19-directed CAR-T (chimeric antigen receptor T) cells, known as tisagenlecleucel, received approval for treating relapsed and refractory acute lymphoblastic leukemia (54).

2.1.2. The Cancer Immunity Cycle

Chen and Mellman presented the concepts of the cancer-immunity cycle in their review, which consists of seven stages as depicted in Figure 2.1 below.

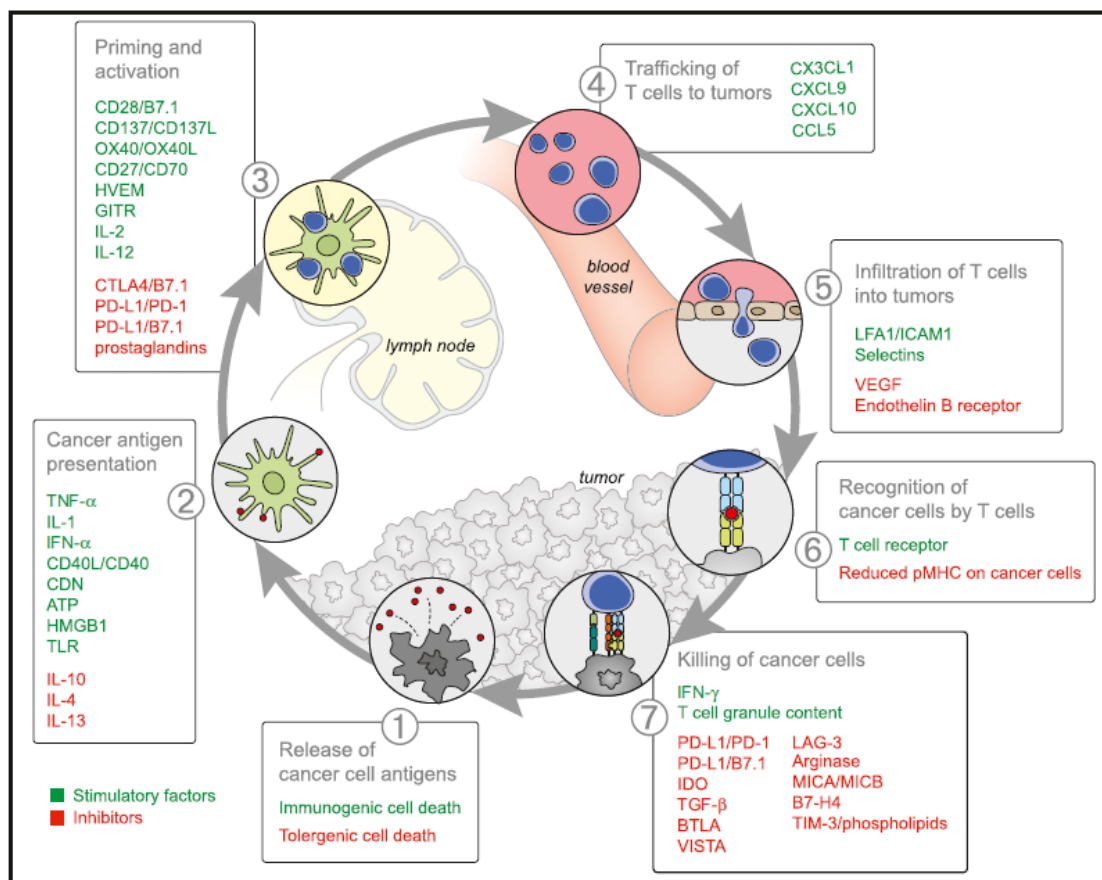


Figure 2.1. The concept of the cancer-immunity cycle (adapted from the work by Chen and Mellman (55))

The initial phase involves the release of neoantigens generated by oncogenesis, which are then captured by dendritic cells (DCs). For an effective anticancer T cell response to occur, this stage must be followed by the provision of immune-activating signals. Without these signals, there is a risk of developing peripheral tolerance to tumor antigens. Examples of such immunogenic signals include proinflammatory cytokines (e.g., TNF- α , IL-1, IFN- α) and substances produced by either tumor cells or the gut microbiota.

In the second stage, T cells are presented with the antigens on MHC I and MHC II molecules by DCs. The third phase involves initiating and activating T cells to mount an immune response against cancer-specific antigens that are recognized as foreign or not effectively controlled by central tolerance mechanisms. The nature of the immune

response is determined during this step, with a crucial factor being the balance between Teffs and Tregs, which significantly influences the ultimate outcome.

In the fourth stage, the activated Teffs travel through the bloodstream within the body. In the fifth stage, they infiltrate the tissue where the tumor cells are located. In the sixth stage, these T cells identify and bind to cancerous cells through the interaction between their T cell receptor (TCR) and the specific antigen presented by MHC I molecules. In the final stage, the Teffs carry out the critical task of killing and eliminating the targeted cancer cells (55).

For the final stage, additional cancer antigens are released, initiating a self-sustaining cycle. It is important to note that within the cancer-immunity cycle, there are checkpoints that can either stimulate or hinder various processes. Cancer cells may exploit these checkpoints to evade immune surveillance. Furthermore, there are instances where tumor antigens might not be accurately recognized, causing DCs and T cells to perceive these antigens as part of the body's own rather than foreign entities. Consequently, this can lead to the development of Tregs responses instead of Teffs responses. As a result, an imbalance where Tregs significantly outnumber Teffs lead to immunosuppression, impeding the immune system's ability to mount robust and efficient immune responses (56).

2.1.3. How Tumor Cells Evade the Immune System

In the outline context, tumor cells employ two primary strategies to evade immune responses, namely (a) avoiding the immune recognition, and (b) creating an immunosuppressive environment within the tumor. To execute the first strategy, cancer cells employ various tactics to escape immune detection. One of these tactics involves mimicking peripheral tolerance, where cancer cells develop mechanisms that imitate peripheral immune tolerance. This enables them to evade immune responses and prevent local cytotoxic response from Teffs such as tumor-associated macrophages (TAMs), natural killer (NK) cells, and tumor-associated neutrophils (TANs) (57,58). Immune tolerance mechanisms encompass pro-tumoral macrophages, Tregs, immature dendritic cells, and pro-metastatic neutrophils (57). In various cancer

types, including breast cancer, Tregs play a role in suppressing the activation of cytotoxic T lymphocytes (CTLs). Recent observations indicate that the presence of Tregs within breast cancer is associated with a poorer prognosis for patient.

Another tactic involves manipulating the presence of immunogenic antigens. As previously discussed in the context of the cancer-immunity cycle, under normal circumstances, CD8⁺ T cells differentiate into CTLs after being primed and activated by antigen-presenting cells (APCs). CTLs then mount an effective anti-tumor response, leading to the destruction of target cells. This scenario remains valid as long as neoplastic cells express highly immunogenic antigens, which are recognized and eliminated during the early stages of tumor development (Matsushita et al., 2012). However, when less immunogenic antigens are expressed, cancer cells can evade T cell-mediated immune control, giving rise to a phenomenon known as cancer immunoediting (59).

The second strategy involves cancer cells releasing factors that promote an immune-tolerant TME. This is achieved through several means: (a) the secretion of suppressive molecules like IL-10, TGF- β , prostaglandin E2, and VEGF (60,61), (b) the expression of inhibitory checkpoint molecules such as PD-L1, CTLA-4 and V domain immunoglobulin suppressor of T cell activation (VISTA) (62–64). The presence of immune checkpoints like CTLA-4 and PD-1 further contributes to immune evasion, as both function as negative regulators of T cell activity. In particular, the interaction of PD-1 with its co-receptor PD-L1 results in the downregulation of T cell activity, leading to the inhibition of T cell migration, proliferation, the release of cytotoxic substances, and the restriction of cell killing (65). Moreover, (c) the recruitment of TAMs, myeloid-derived suppressor cells (MDSCs), and Tregs is induced by tumor-derived chemokines such as CCL2, CSF1, CCL5, CCL22, CXCL5, CXCL8, and CXCL12 also promote immune-tolerant TME (66–68). The induction of MDSCs and Tregs could also be facilitated by IDO1 in the TME (69–71). Hence, inhibition of IDO1 and the potential use of IDO1 inhibitors as adjuvant in cancer immunotherapy are being explored.

2.2. Mechanism of Kynurenine Pathway

Tryptophan is an essential amino acid in our body, and its catabolism follows two distinct pathways: the serotonin and Kyn pathways. The serotonin pathway is responsible for only 5% of tryptophan catabolism and plays a crucial role in regulating mood and gut peristalsis. The majority of tryptophan catabolism occurs through the Kyn pathway (about 95%), which is less well-understood than serotonin pathway (71). In this process, IDO1, along with IDO2 and TDO2, play a significant role in controlling the initial rate-limiting step of tryptophan catabolism by converting L-Trp to *N*-formyl kynurenine (NFK). Subsequently, NFK is transformed into L-Kyn with the assistance of kynurenine formamidase. L-Kyn undergoes further conversions into three different substances, namely, kynurenic acid produced by kynurenine-oxoglutarate transaminase (KYAT), 3-hydroxykynurenine generated by kynurenine 3-monooxygenase, and anthranilic acid formed by kynureninase.

Both 3-hydroxykynurenine and anthranilic acid are combined to create 3-hydroxyanthranilic acid with the help of kynureninase and a non-specific hydroxylase. 3-hydroxyanthranilic acid is then converted into 2-amino-3-carboxy-mucconate-6-semialdehyde by 3-hydroxyanthranilic acid dioxygenase (HAD). This compound can follow two different paths:

- (i) It is converted first to 2-aminomucconate acid semialdehyde through 2-amino-3-carboxymucconate-6-semialdehyde decarboxylase, and then to picolinic acid through non-enzymatic process.
- (ii) It is converted to quinolinic acid through non-enzymatic process and ultimately to nicotinamide via quinolinate phosphoribosyl transferase (QPRT) (Figure 2.2).

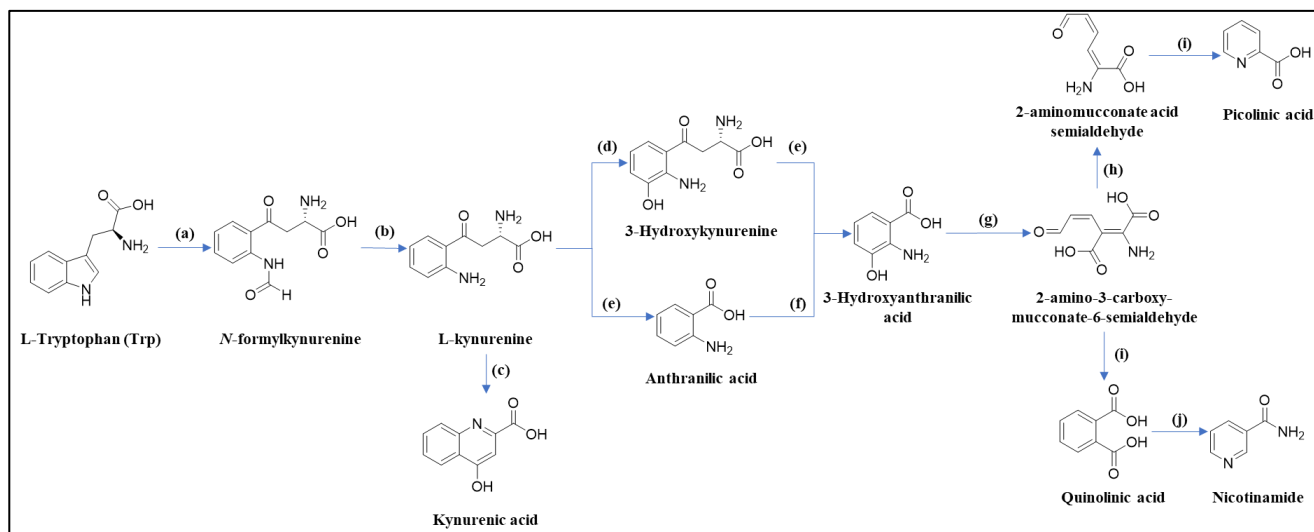


Figure 2.2. Kynurenine Pathway. (a) IDO1, IDO2, TDO2; (b) kynurenine formamidase; (c) kynurenine-oxoglutarate transaminase (KYAT) (d) kynurenine 3-monooxygenase; (e) kynureninase; (f) non-specific hydroxylase; (g) 3-hydroxyanthranilic acid dioxygenase (HAD); (h) 2-amino-3-carboxymuconate-6-semialdehyde decarboxylase; (i) non-enzymatic; (j) quinolinate phosphoribosyl transferase (QPRT).

2.3. Indoleamine 2,3-dioxygenase 1

IDO1 is the heme-containing protein with a pivotal role in catalyzing the conversion of L-Trp into NFK, which is subsequently metabolized into Kyn (26,72). The reduction in tryptophan levels negatively affects the proliferation of Tregs, while, conversely, the accumulation of kynurenine metabolites encourages the differentiation of Tregs. Both of these processes contribute to the suppression of anti-tumor immunity, ultimately facilitating tumor progression (18,73,74). Consequently, the search for IDO1 inhibitors remains critical in restoring the elimination of cancer cells through immune mechanisms.

2.3.1. Structure of Indoleamine 2,3-dioxygenase 1

IDO1, a cytosolic and monomeric enzyme (75), possesses multiple crucial binding pockets that play an important role in establishing interactions with its inhibitors and the heme. According to Röhrig et al., (2021), IDO1 receptor has five distinct pockets, including pocket A, B, C, D, and the heme-binding pocket (Figure 2.3) (76).

1. Pocket A: Located on the opposite side of the heme cofactor and characterized by its hydrophobic nature. Pocket A primarily forms hydrogen bonds via SER167. This pocket is vital for inhibitor binding, as all known inhibitors occupy this space in their binding mode.
2. Pocket B: Positioned at the entrance of the active site, pocket B can only be accessed when the flexible JK-Loop is in an open state. The JK-Loop, composed of two segments known as JK-Loop^C and JK-Loop^N, is situated in proximity to the distal heme pocket of the enzyme. JK-Loop^N is unique to IDO1 and is absent in TDO2 (77). The impact of pocket B on inhibitor binding affinity appears to be less significant compared to that of pocket A.
3. Pocket C (Sa site): This pocket is blocked off by the closure of the JK-loop and has been suggested to interact with specific ligands, such as Trp and epacadostat (77).

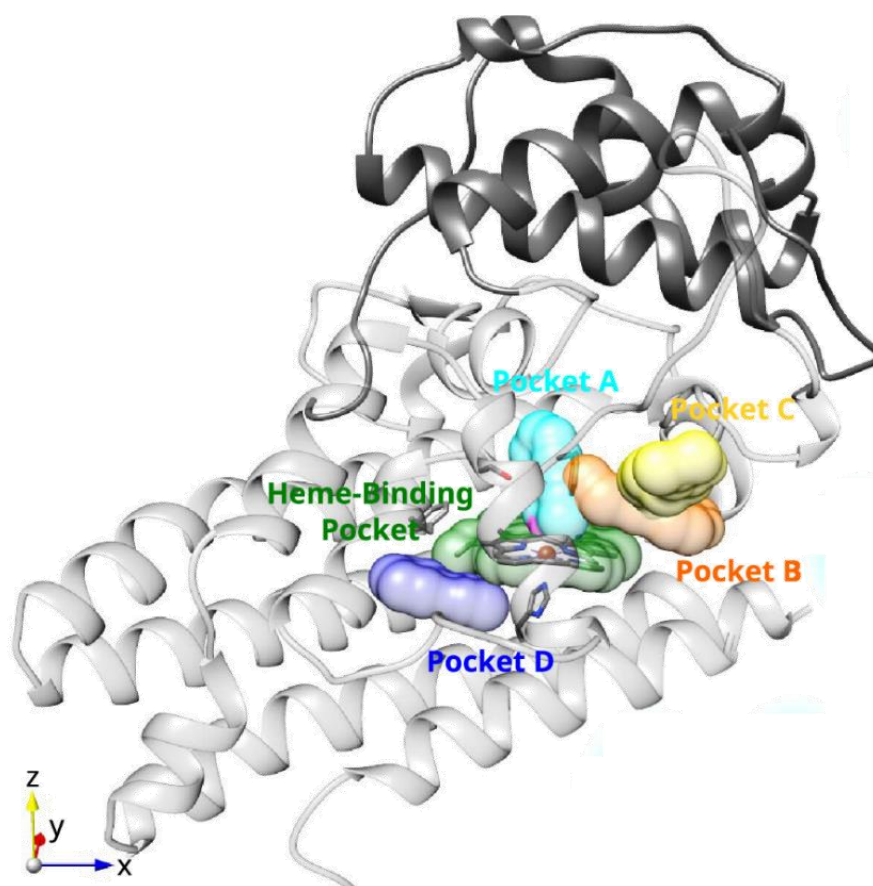


Figure 2.3. The 3D-structure of IDO1 and its pocket (76)

4. Pocket D (Si Site): A compact small binding site located on the side of the heme and close to the active site. It becomes accessible through a structural alteration involving PHE270. In its natural state within holo-IDO1, pocket D is isolated from all the other binding sites due to the presence of the heme cofactor and serves as an additional site for small molecules to bind. In apo-IDO1, it becomes linked to the adjacent pockets due to the absence of heme cofactor and is typically occupied by the majority of type IV inhibitors or apo-IDO1 inhibitors.
5. In addition to pockets A, B, C, and D, there is an additional pocket known as the heme-binding pocket. This pocket comprises several key residues, including VAL170, PHE214, ILE217, and HIS346. In holo-IDO1, these residues interact with the heme cofactor, while in the case of apo-IDO1, they engage with the central components of the apo-IDO1 inhibitors (76).

2.3.2. Holo- and Apo-Form IDO1, Their Inhibition and Clinically Tested IDO1 Inhibitors

A fundamental distinction exists between the holo-form and apo-form of IDO1, hinging on the presence of the heme cofactor within the IDO1 binding site. Holo-IDO1 contains this heme cofactor, which plays a vital role in redox changes, transitioning to the inactive ferric state (Fe^{3+}) during turnover (78). The presence of the heme cofactor significantly impacts the inhibition of this enzyme. According to Röhrig et al., (2019), there are four types of IDO1 inhibitors, specifically: (i) tryptophan-competitive inhibitors binding to oxygen-bound holo-IDO1, (ii) oxygen-competitive inhibitors binding to free ferrous holo-IDO1, (iii) inhibitors binding to free ferric holo-IDO1, and (iv) inhibitors binding to apo-IDO1 (23). It is noteworthy that three of these inhibitor types pertain to holo-IDO1, while only one type of inhibition relates to apo-IDO1.

Until now, eleven IDO1 inhibitors have been clinically tested with different mechanisms, including (a) indoximod (D-1MT), (b) epacadostat (INCB024360), (c) navoximod (NLG-919), (d) PF-06840003 (EOS200271), (e) BMS-986205 (linrodostat), (f) LY3381916, (g) NLG-802, (h) KHK2455, (i) RiMO-301, (j) DN-1406131 and (k) SHR9146 (HTI-1090) (79–81). Additionally, there are IDO1 inhibitors in the form of vaccines, such as IDO1 peptide vaccine (82,83) and the

IO102-IO103 vaccine (84). However, in this literature review, only IDO1 inhibitors (a) to (e) are discussed, representing each inhibitor type (Figure 2.4).

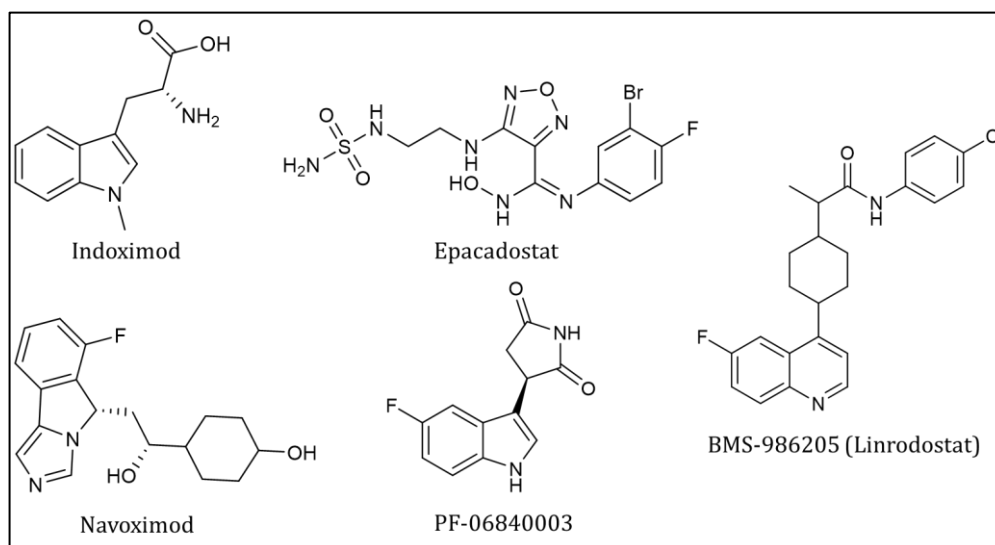


Figure 2.4. The structures of five IDO1 inhibitors that have entered clinical trials

a. Indoximod

1-Methyl-D,L-tryptophan (1MT) consists of two isomers, each displaying different inhibitory effects. The L isomer of 1MT exhibits weak inhibitory activity, while the D isomer, also known as D-1MT or indoximod, demonstrates potent anticancer activity and has the ability to alleviate T cell suppression induced by IDO1-positive dendritic cells from both mouse and human sources (85). Numerous studies have investigated the impact of indoximod, a type I IDO1 inhibitor, on IDO1 through several mechanisms. As outlined by Fox et al., (2018), the cellular mechanisms of action of indoximod have been elucidated. These mechanisms encompass the relief of suppression on T cells in tumors, limitations on the generation of Tregs, and the transformation of Tregs into Th17 helper cells in draining lymph nodes (86–89). In 2021, Zakharia and colleagues conducted a phase II clinical trial involving the combination of indoximod and one immune checkpoint inhibitors, pembrolizumab, for the treatment of advanced melanoma patients. The results from this study indicated that the combination of indoximod and pembrolizumab was well-tolerated and demonstrated antitumor efficacy in specific individuals with advanced melanoma (90).

b. Epacadostat (INCB024360)

Epacadostat functions by binding to the tryptophan binding site and inhibiting IDO1 through its attachment to the heme iron in its ferrous form, also known as ferrous IDO1, via the oxygen atom of the hydroxyamidine moiety. As a result, it is classified as a type II inhibitor (23). Despite facing a significant setback in a phase III trial for melanoma (ECHO-301/KEYNOTE-252), where it failed to demonstrate an improvement in progression-free survival in combination with pembrolizumab compared to pembrolizumab alone (91), epacadostat continues to be a prominent candidate. It is currently the most advanced IDO1 inhibitor in development with ongoing phase III clinical trials enrolling patients with locally advanced or metastatic renal cell carcinoma (RCC) (ClinicalTrials.gov ID: NCT03260894). Additionally, research has shown that epacadostat can hinder the growth of Tregs induced by human DCs when these cells are exposed to IFN- γ and lipopolysaccharide (LPS), both of which trigger IDO1 expression. T cells stimulated with DCs treated with epacadostat exhibit notably increased levels of IFN- γ and display enhanced effectiveness in *in vitro* assays for lysing tumor cells (92).

c. Navoximod (NLG-919)

Navoximod, also recognized as NLG-919, functions as an inhibitor of IDO1. Its mode of action is noncompetitive inhibition and it demonstrates a preference for binding to the ferric oxidative state (Fe^{3+}) of heme iron, categorizing it as a type III inhibitor. In the structure of navoximod, a 4-phenylimidazole (4PI) structural moiety is present (93). Although 4PI alone is a relatively weak inhibitor of active IDO1, when incorporated into navoximod's fused tricyclic ring system, it adopts a conformation that optimizes its binding to the IDO1 receptor. Navoximod also demonstrates substantial potency as a dual inhibitor of both IDO1 and TDO2 and has undergone clinical trials for the treatment of recurrent advanced solid tumors (94,95). It has been shown that navoximod is a potent dual inhibitor of IDO1 and TDO2 with an IC_{50} value of 79 nM and 247 nM, respectively (96). In A172 cells derived from the brain tissue of a 53-year-old male patient with glioblastoma, it exerted inhibitory effects with an IC_{50} of 0.45 μM for IDO1 and 2 μM for TDO2 (97).

d. PF-06840003 (EOS200271)

PF-06840003, also known as EOS200271, has been observed to interact with the IDO1 enzyme without directly binding to the heme iron (24). This highly selective IDO1 inhibitor, which distinguishes itself from TDO2 and IDO2, has advanced to phase I clinical trials for brain tumors (98,99). According to the review from Gomes et al., (2018), PF-06840003 effectively inhibits IDO1 and hinders the production of L-kynurenine, both *in vitro* and *in vivo*. In *in vitro* studies, PF-06840003 promotes T cell proliferation when co-cultured with immunosuppressive tumor cells, exhibiting EC₅₀ values ranging from 60 to 74 nmol/L at serum concentrations between 10% and 50%. In *in vivo* studies, PF-06840003 treatment significantly reduces plasma L-kynurenine levels in non-tumor-bearing BALB/c mice. Furthermore, when combined with an anti PD-L1 antibody, PF-06840003 enhances the proportion of IFN γ -secreting T cells, correlating with improved treatment efficacy (99). Given that PF-06840003 has entered a phase I clinical trial for brain tumors, its physicochemical properties suggest its potential for brain penetration. These properties include a low molecular weight, moderate polar surface area, and a low number of hydrogen bond donors or acceptors (98).

e. BMS-986205

BMS-986205 (27) competes effectively with iron by binding to the apo-form of the enzyme, especially when the heme cofactor is unstable (100). As indicated by Nelp's findings, BMS-986205 initially binds to a solvent-exposed surface cleft located near the active site of holo-IDO1. This interaction leads to the release of heme and the formation of an apo-IDO1-inhibitor complex, which involves a series of conformational changes. On the other hand, within cells, in the apo-IDO1 form, compounds like BMS-986205, which compete with the heme, hinder the enzyme's ability to bind to heme, effectively preventing the formation of holo-IDO1 and the execution of IDO1 activity. However, it is essential to recognize that these heme-competitive inhibitors are less effective at lower temperatures in suppressing IDO1 activity. Even under optimal conditions, the dissociation of heme and the subsequent generation of apo-IDO1 *in vitro* are gradual and reversible processes (27,101). Apo-IDO1 inhibitors have demonstrated encouraging results in early clinical studies.

However, the future of this type of inhibitors largely depends on the outcomes of phase III clinical trials for BMS-986205 (102). While BMS-986205 has made progress in clinical trials, there is an ongoing quest to identify an alternative apo-IDO1 inhibitor. In fact, there are several compounds that hold promises as potential apo-IDO1 inhibitors, including those listed in Table 2.1.

Table 2.1. Examples of selective apo-IDO1 inhibitors from the literature

No	Structure	Effect	Ref.
1.		The newly developed GSK5628, which targets apo-IDO1 is potent with a biochemical efficacy of 39 nM and a cellular potency of 5.9 nM. Due to its unique mechanism and high performance, further <i>in vivo</i> profiling is warranted.	(101)
2.		Compound A shows robust binding to apo-IDO1 and displays substantial effectiveness in HeLa cells, with an IC ₅₀ of 9 nM.	(103)
3.		Adding a fluorophenyl group to compound A boosts IDO1 potency in compound B. Incorporating a polar 2-pyridyl oxetane component notably improves its pharmacokinetic profile. As a result, compound B shows an IDO1 IC ₅₀ of 3.2 nM in HeLa cells.	(103)
4.		By substituting the carbamate segment from t-Bu to ethyl, compound C, a Spirochromane derivative, exhibited a substantial enhancement in potency as an apo-IDO1 inhibitor.	(104)
5.		Compound D, with an (<i>S</i>)-configuration, shows a significant IC ₅₀ of 5.4 nM. It interacts with apo-IDO1 but not ferrous IDO1. However, it has limited bioavailability	(104)
6.		A prodrug of compound E, designed to improve solubility, achieved over 1 mg/mL solubility in fasted stated stimulated intestinal fluid (FaSSIF). In initial human pharmacokinetic studies, administering this compound at 60 mg twice daily (equivalent to 35 mg of the parent compound twice daily) resulted in an average of 90% IDO1 inhibition over 24 hours.	(104)

2.4. Virtual Screening for Drug Design

Virtual screening plays a pivotal role in drug discovery pipeline. It circumvents the challenges associated with extensive searches in chemical space by focusing on libraries containing specific and readily available compounds, often those that are easily procurable. This approach helps avoid expensive syntheses, decreases the number of *in vitro* or *in vivo* assays, and narrows the search to compounds with established biological interest. Even if initially synthesized for a different purpose, this strategy thereby reduces time and enhances cost-effectiveness in the development of novel drugs. Filters can be applied to ensure that the library aligns with predefined standards of biological relevance or “drug-likeness” (28,105–107).

A widely used and straightforward method for assessing drug-likeness involves property-based filters or rules, which set acceptable limits on specific molecular physicochemical properties or molecular descriptors for drugs or drug candidates. One of the most well-known rules in this regard is the “Rule of Five” introduced by Lipinski et al. This rule establishes thresholds for four basic molecular descriptors deemed suitable for orally active compounds. These molecular descriptors include a molecular weight (MW) of ≤ 500 , an octanol/water partition coefficient (logP) of ≤ 5 , a maximum of 5 hydrogen bond donors (HBD), and a maximum of 10 hydrogen bond acceptors (HBA). If a compound violates two or more of these rules, it may exhibit unfavorable ADMET (absorption, distribution, metabolism, excretion, and toxicity) profiles (106).

In addition to these rules, a multitude of molecular descriptors and various machine learning techniques have been applied, such as support vector machine (SVM) (108), neural networks (NN) (109), genetic algorithm (GA) (110), recursive partitioning (RP) (111), and others. Importantly, many prediction models for drug-likeness developed using machine learning approaches demonstrate effective capabilities in distinguishing between molecules with drug-like and non-drug-like characteristics (112).

Principally, there are two main approaches in virtual screening. First if the macromolecule target is unknown, LBVS should be used. Second, on the other hand, if the information of the structural target is known and available on protein database, then SBVS can be employed.

2.4.1. Ligand-Based Virtual Screening

LBVS relies on the structural information and physicochemical characteristics of the chemical scaffold found in known active and inactive molecules. This screening method operates on the principle of molecular similarity, where relationships between compounds in a given library and one or more known active compounds are assessed through similarity measurements using appropriate molecular descriptors. These measurements typically involve 1D and 2D descriptors, which encode information about the chemical nature and topological features of compounds (113,114). Additionally, 3D descriptors related to molecular fields (115), shape and volume (116,117), and pharmacophores (118) can be utilized.

a. Shape Similarity

Molecular shape similarity holds significant importance within drug discovery, particularly in the context of virtual screening. A prevailing assumption suggests that molecules exhibiting structural resemblance are likely to share similarities in both physical attributes and biological functionalities. Concerning shape similarity, it involves the utilization of structural representations and quantitative measurements to gauge the similarity between two structural representations (119). There exist various techniques for quantifying the similarity between two structural representations, which encompass metrics like the Tanimoto coefficient, cosine coefficient, Euclidean distance, Tversky index, and others. Among these, the Tanimoto coefficient, established by Rogers and Tanimoto in 1960, stands out as the most commonly used and popular method for measuring similarity (120).

Molecular similarity can be categorized into two main groups: 2D and 3D similarity approaches. The 2D similarity approach exclusively relies on 2D information, encompassing methods like substructure search, fingerprint similarity search and 2D descriptor-based techniques. While 2D information can capture the connectivity of atoms and allow for scaffold hopping, it still lacks the spatial orientation details provided by 3D structures. The limitation lies in the inability of fully represent the three-dimensional arrangement of atoms in space. In recent times, researchers have increasingly adopted the 3D approach for various applications, such as pharmacophore modelling, shape similarity, molecular field-based methods, and 3D fingerprinting.

Notably, the use of 3D shape-based similarity has gained prominence in virtual screening, demonstrating numerous successful instances (121–125). There are three different types of 3D shape similarity methods, namely atomic-distance based method, Gaussian overlay-based method, and surface-based methods (Figure 2.5). In this study, we used Gaussian overlay-based methods.

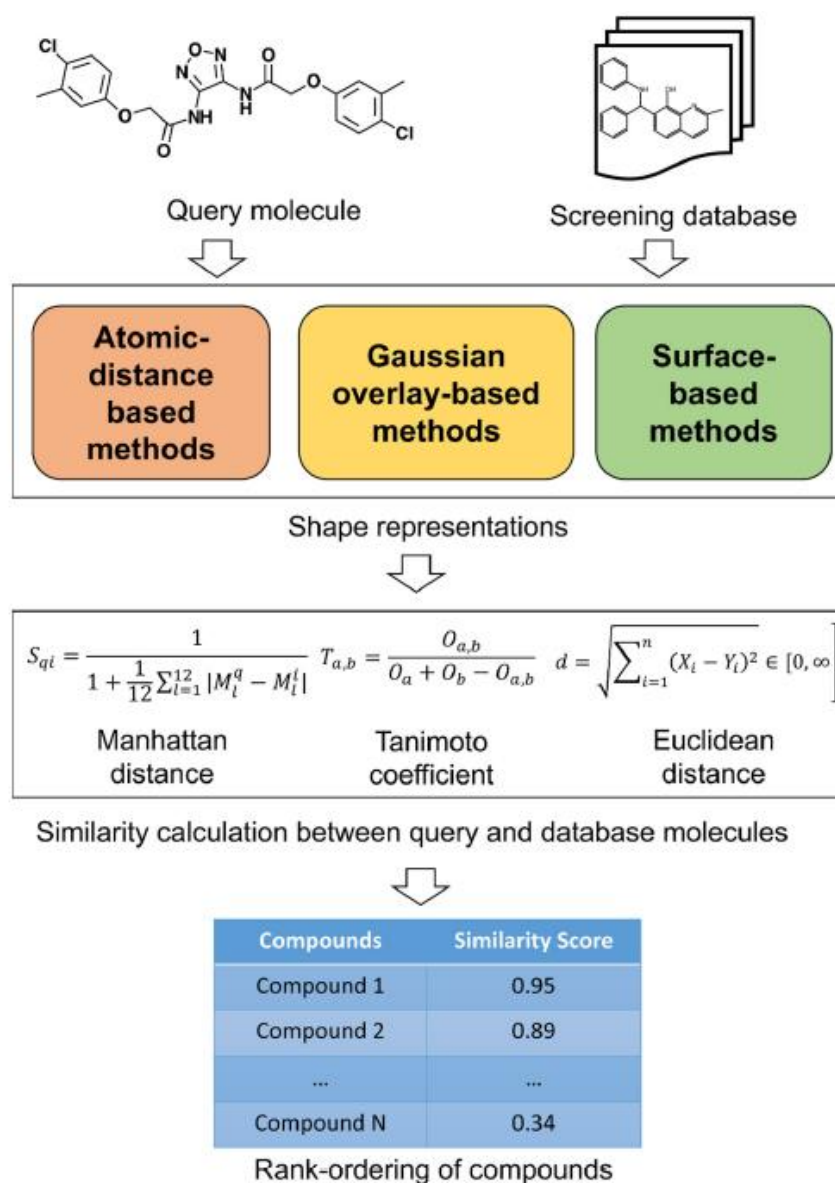


Figure 2.5. A diagrammatic representation of the process for calculating similarity between a query molecule and molecules within a database (119).

Gaussian sphere and hard sphere are the most widely adopted models among many methods of describing the molecular shape of a molecule. Both of these models

describe the shape in terms of the volume of a molecule. Two molecules will possess similar shape if they have similar volume. Gaussian sphere model represents a molecule using a set of overlapping Gaussian spheres and measures the integral volume of overall overlapping Gaussians. In this model, each intersection is expressed as the integral of a set of overlapping atom-centered Gaussian spheres and the volume of a molecule is described based on the inclusion-exclusion principle (126).

Several methods based on Gaussian overlays were developed to measure the shape similarity between two molecules, such as ROCS developed by OpenEye Scientific Software (116,127), PAPER developed by Stanford University (128), MolShaCS developed by University of Sao Paulo (129), Phase Shape developed by Schrödinger LLC (117), and WEGA developed by Research Center for Drug Discovery, Sun Yat-sen University, China (130).

b. Pharmacophore Modelling

In addition to shape similarity, another method for conducting virtual screening is pharmacophore modeling. While shape similarity focuses on the structural likeness between a known active ligand and the screened library, pharmacophore modeling focuses on crucial chemical features that are pivotal in demonstrating a specific biological activity.

The concept of “pharmacophore” was introduced by Ehrlich in 1909. It was defined as a molecular framework that carries (phoros) the essential features responsible for a drug’s (pharmakon) biological activity (131). Günd later refined this definition by stating that pharmacophore is a set of structural features within a molecule that is recognized at a receptor site and is responsible for that molecule’s biological activity (132). According to the International Union of Pure and Applied Chemistry (IUPAC), a pharmacophore is described as “the ensemble of steric and electronic features necessary to ensure optimal supramolecular interactions with a specific biological target structure and to trigger (or block) its biological response” (133–135). Therefore, the molecular features responsible for a particular biological effect play a crucial role in pharmacophore modeling. These pharmacophoric features include various types such as HBA, HBD, hydrophobic areas (H), positively and negatively ionizable groups (PI/NI), aromatic groups (AR), and metal coordinating areas. Moreover, the exclusion

volume corresponds to restricted regions that define the size and the shape of binding pocket (Figure 2.6).

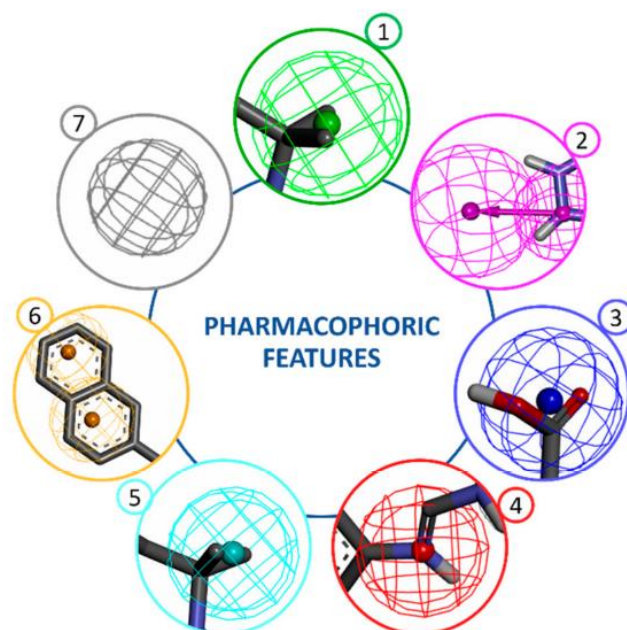


Figure 2.6. Pharmacophoric features. The primary types of pharmacophoric features are depicted using geometric shapes and encompass the following categories: (1) HBA, (2) HBD, (3) negatively ionizable (NI), (4) positively ionizable (PI), (5) hydrophobic (H), (6) aromatic (AR), and (7) exclusion volume (XVOL) (136).

In fact, there are two distinct approaches to pharmacophore modeling, comprising ligand-based and structure-based approaches. The choice of which approach to employ depends on the availability of data and information about the target receptor. When structural details of the target proteins, such as enzymes or receptors, are accessible, applying structure-based pharmacophore modeling, which is based on ligand-receptor interactions is possible. Conversely, when there is no information about the structural features of the target, opting for the alternative approach named ligand-based pharmacophore modeling is preferable. This approach relies on the common physicochemical properties of known ligand molecules (136).

2.4.2. Structure-Based Virtual Screening

The term “structure-based” pertains to virtual screening that concentrates on the structural information of target receptors. In this method, compound databases are subjected to docking with the chosen target binding site (137). The predominant approach in SBVS is molecular docking, which exploits the structural and chemical complementarity arising from the interaction between drug-like compounds and their targets. This method predicts the preferred orientation of ligands in the binding site by employing scoring functions (138,139). Other SBVS techniques frequently involve examining the stability and conformational changes at the atomic level of ligand-protein complexes through molecular dynamics (MD) simulations (140). Additionally, binding free energy trajectory analysis is commonly performed using methods such as MM-GBSA or MM-PBSA (34).

a. Molecular Docking

The molecular docking scoring is employed to rank these compounds in the database. Researchers can then use this ranking as a foundation for selecting potential hit compounds. Additionally, visual inspection is utilized to assess the intermolecular interactions within the ligand-receptor complex (141). Hit compounds are typically subjected to *in vitro* evaluation to validate and determine their biological activity against the molecular target being investigated (142).

To carry out the SBVS method, there are primarily four essential steps involved. These steps encompass (i) preparing the target protein, (ii) selecting and preparing the compound database, (iii) conducting molecular docking and scoring, and (iv) analyzing the docking results. It is crucial to consider the selection of both the conformational search algorithm and scoring function. These two elements are of significant importance in molecular docking as they serve separate but interrelated roles.

Conformational search algorithms are responsible for exploring the numerous potential orientations and conformations of a ligand within the binding site of a receptor. They can be approached in two different ways, namely systematic and stochastic search methods (143,144). Systematic search methods entail making

incremental adjustments to the structural characteristics, gradually modifying the ligand's conformation (145). During the conformational search, systematic search methods may converge towards a local minimum instead of the global minimum (146). Examples of systematic search methods include DOCK (147), GLIDE (148), FRED (149), and FlexX (150).

In contrast, stochastic search methods perform the conformational search by randomly altering the structural parameters of the ligands. Consequently, the algorithm generates sets of molecular conformations and explores a broad range of the energy landscape, increasing the likelihood of discovering a global minimum rather than getting trapped in a local minimum (151). Examples of stochastic search methods include AutoDock (152), PLANTS (153), MOE_Dock (154), and LigandFit (155).

Regardless of the particularities of each method, every conformational search algorithm should possess the ability to efficiently explore a wide range of the energy landscape within a reasonable time frame. Ideally, the assessment of a small set of molecules should be completed in just a few minutes (156).

On the other hand, scoring functions play a pivotal role in estimating the binding affinity of the predicted ligand-receptor complexes. The energy change resulting from the formation of the ligand-receptor structure is described by the binding constant (K_d) and the Gibbs free energy (ΔG). When it comes to predicting and assessing binding energy, the critical physicochemical phenomena include intermolecular interactions, desolvation, and entropic effects. It is worth noting that the more physicochemical parameters are taken into account, the greater the accuracy of the scoring functions (156).

There are three categories of scoring functions, specifically forcefield-based, empirical, and knowledge-based functions (157). The first group, forcefield-based functions, determine the binding energy by combining the impacts of both bonded interactions (like bond stretching, angle bending, and dihedral variations) and non-bonded interactions (including electrostatic and van der Waals (vdW) forces) within a comprehensive equation (158). In contrast, empirical scoring functions focus on individual types of physical events involved in ligand-receptor complex formation, including hydrogen-bonding, ionic interactions, nonpolar interactions, desolvation and

entropic effects (159). Different with the previous two, knowledge-based scoring functions employ pairwise energy potentials derived from known ligand-receptor complexes to create a general function (160). As knowledge-based functions do not rely on replicating binding affinities like empirical methods or *ab initio* calculations as in forcefield methods, they strike a balance between accuracy and swiftness (161). Each scoring function has its strengths and weaknesses. Consequently, the simultaneous use of multiple scoring approaches has become increasingly common as a way to establish a consensus score (162). Detailed examples of these scoring functions in various molecular docking software are provided in Table 2.2.

Table 2.2. Here are the following examples of molecular docking programs with their scoring functions

Forcefield-based	References	Empirical	References	Knowledge-based	References
DOCK	(147)	GlideScore	(148)	SMoG	(163)
AutoDock	(152)	ChemScore	(164)	DrugScore	(161)
LigandFit	(155)	Fresno	(165)	PMF_Score	(166)
ICM	(167)	LUDI	(168)	PoseScore	(169)

b. Molecular Dynamics Simulations

MD simulations, as a structural bioinformatic technique, delves into the behavior of molecules by scrutinizing their dynamic characteristics and movements at the atomic level (170,171). Through this approach, it becomes possible to extract kinetic and thermodynamic information about biomolecular structures. For instance, it enables the (i) evaluation of macromolecular stability, (ii) identification of allosteric sites, (iii) understanding of enzymatic activity mechanisms, (iv) exploration of molecular recognition and properties of complexes involving small molecules, (v) investigation of protein associations, and (vi) scrutiny of protein folding and its hydration (172). Furthermore, MD simulations support a wide range of research endeavors, including molecular design (extensively applied in drug design), as well as determination and refinement of structures using techniques like X-ray, NMR, and protein modeling.

When conducting MD simulations (a flowchart of MD simulations is depicted by Figure 2.7), one crucial aspect that researchers need to take into account is the choice

of forcefield. A forcefield can be defined as the potential energy function employed to calculate the energy associated with each atom based on its coordinates and structural data (173). There exist several forcefields suitable for describing both proteins and ligands or candidate compounds. For proteins, available options include the AMBER forcefield (174), CHARMM forcefield (175,176), and the OPLS forcefield (177). While for ligands, researchers can select one of the available forcefield, such as the GAFF forcefield (178), CHARMM general forcefield (CGenFF) (179), and OPLS-AA which is designed for all atom simulations including ligand parameters (180).

The choice of forcefield is of paramount importance because the influence of each forcefield varies depending on the specific system or molecules under investigation. Selecting the appropriate forcefield and ensuring that it is well-parameterized for the specific application is a critical consideration in MD simulations. It is also essential to understand the advantages and limitations of each forcefield. For instance, CGenFF has demonstrated relatively good performance in modeling ligands containing halogen atoms (179).

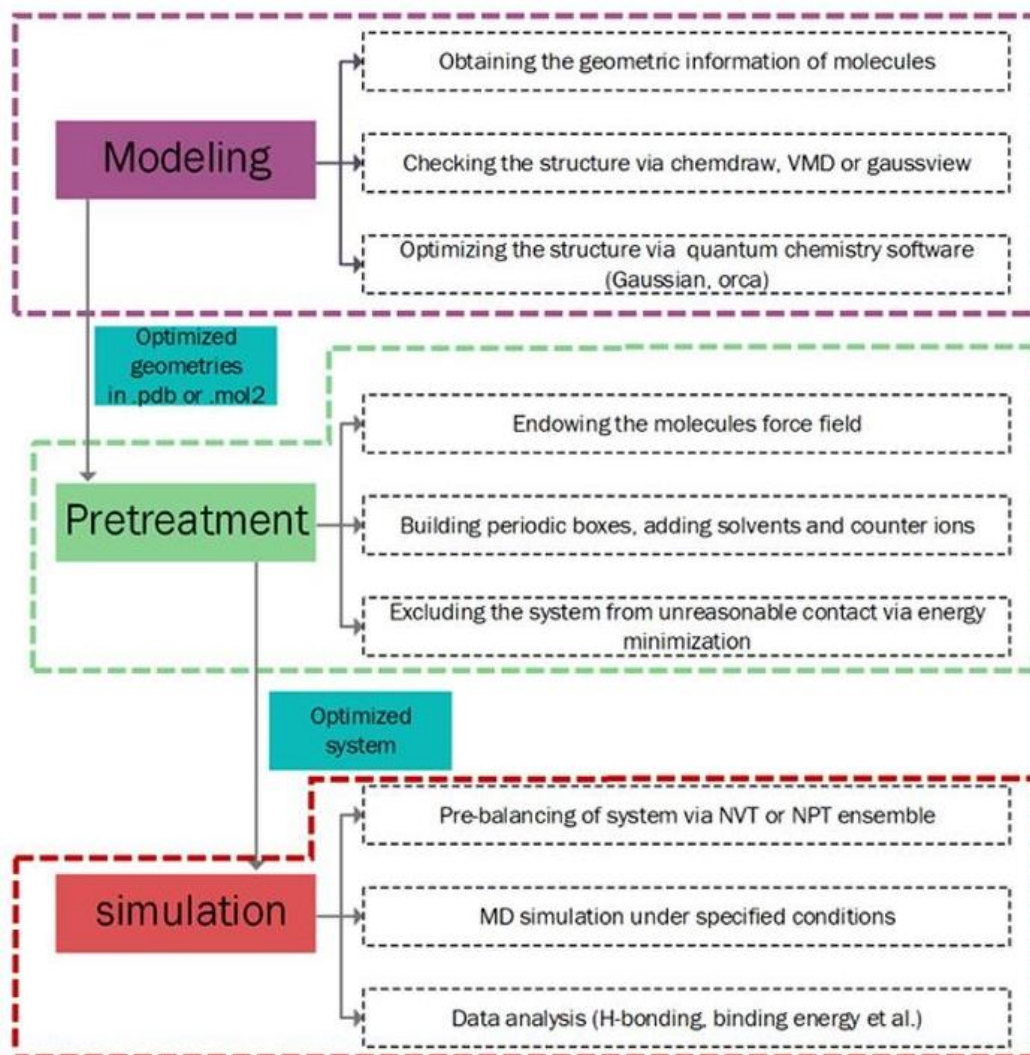


Figure 2.7. The flowchart of molecular dynamics simulation (181)

c. MM-GBSA

Determination of ligand binding free energy is accomplished by employing molecular mechanics in conjunction with the Generalized Born surface area method, commonly known as MM-GBSA. In the MM-GBSA calculations, implicit solvation models offer a computationally efficient means of describing the solvation free energy of protein-ligand complexes (182). These models are utilized to calculate the free energy of binding for ligands to proteins, involving MD simulations with an explicit solvent for the protein-ligand complex to generate a set of snapshots. Subsequently, energies are

calculated using an implicit solvent for these snapshots (183). Implicit solvation methods are widely accepted for assessing protein-ligand binding free energy, especially in the context of relative binding free energy calculations (184).

2.4.3. Combination Approach of Ligand- and Structure-Based Virtual Screening

In recent years, it has become a common practice to integrate ligand-based and structure-based methods in various ways, leveraging available data to the fullest extent (185). This approach harnesses the strengths of both structural and chemical data from ligand-receptor complexes and bioactive precursor compounds, aiming to enhance the success rate and mitigate the drawbacks associated with these two fundamental approaches. For instance, in ligand-based methods, there can be an excessive emphasis on the reference molecule's template, or the chemical properties of compounds forming the pharmacophore model may dominate the selection. Conversely, the molecular docking utilized in structure-based methods often overlooks receptor flexibility (186). Typically, there are three primary strategies for combining ligand and structure-based methods: sequential approaches, parallel approaches, and hybrid approaches (187).

In sequential approaches, ligand-based and structure-based methods are typically employed in a step-by-step manner with the ligand library being refined and reduced at each stage. This strategy is commonly favored, particularly when dealing with extensive ligand libraries, as it permits utilization of techniques that demand fewer resources and a shorter time frame to initially shrink the library size. Subsequently, more advanced and computationally intensive methods can be used to further refine the selection (186). For instance, Khan and colleagues (2019) successfully identified active and selective G protein-coupled estrogen receptor-1 antagonists at the micromolar level through a multi-step sequential screening approach that integrated ligand- and structure-based methods (188). Likewise, Dawood et al. (2018) discovered human aromatase inhibitors by conducting a virtual screening study on an in-house natural compound library, with ligand-based approaches following structure-based approaches (189).

In parallel approaches, the same library or multiple libraries are simultaneously screened using different methods. Each method assigns different scores to the molecules within the library. This approach offers the advantage of not relying solely on a single method, allowing for the identification of a more diverse set of candidate molecules (190). Additionally, in parallel strategies that involve structure-based methods, consensus scoring techniques can be employed to amalgamate the strengths of various scoring algorithms or protein structures (191). Over the recent years, parallel methods have been utilized in numerous research studies (192,193).

The hybrid approach involves the simultaneous utilization of structural data from reference ligands and data from ligand-receptor interactions for virtual screening, both ligand-based and structure-based methods. These approaches can be implemented either through interaction-based or similarity-docking mechanisms (194). In interaction-based hybrid methods, templates of ligand-receptor interactions are extracted from crystallographic structures and transformed into fingerprint or pharmacophore models. These models are then used to virtually screen ligand libraries against the established interaction patterns. Alternatively, in similarity-docking methods, the measurement of similarity to a reference molecule aids in scoring the molecular binding poses and ranking compounds based on these scores. In similarity screening, binding patterns of active molecules derived from crystallographic structures in target receptors serve as a reference, and higher precision in binding patterns and coupling scores is achieved by docking similar molecules to the receptor (186). Hybrid strategies that combine shape similarity and molecular docking techniques have gained popularity in recent years due to their high accuracy. They have even led to the development of software tools like HomDock (195) and Hybrid (149).

2.5. Previous Studies on IDO1 Inhibitor Through Virtual Screening

There are limited studies in the literature that have utilized virtual screening techniques to discover IDO1 inhibitors. In 2017, Coletti et al. conducted a study in which they screened a library of 30,000 fragments using molecular docking. Subsequently, they tested the identified candidate molecules *in vitro*, successfully identifying several

potent IDO1 inhibitors (196). In 2018, Zhang et al. also employed structure-based virtual screening to identify a series of candidate molecules, which they further confirmed through enzymatic experiments (19). In the same year, another study utilized machine learning to detect 50 potential candidate molecules, and three of them exhibited strong activity against IDO1 *in vitro* (197).

In 2019, Xu et al. conducted a study that combined shape similarity and molecular docking. They not only identified a promising molecule but also improved its effectiveness through a structure-activity relationship (SAR) study (198). In another 2019 study by Zhou et al., a comprehensive approach involving ligand and structure-based methods was employed. They used a sequential process, which included a drug similarity filter, molecular docking, pharmacophore modeling, and 3D-QSAR methods to identify six potential IDO1 inhibitors (199).

Moving on to 2020, Serafini et al. employed a molecular docking method for virtual screening and identified 50 molecules. Subsequent *in vitro* testing revealed the activity of some of these molecules. They then conducted a study, the SAR study, to develop selective and anticancer derivatives based on the most active molecule (200).

3. MATERIALS AND METHODS

All the molecular modelling studies, calculations, and analyses in this study were performed on a Windows machine with an Intel(R) Core(TM) i7-9700K CPU @3.60GHz (8 CPUs), ~3.6GHz with 64GB RAM and a NVIDIA GeForce RTX 2070 GPU.

3.1. Ligand preparation

Ligand databases from InterBioScreen (IBS) (<https://www.ibscreen.com/>) were retrieved as of March 7th, 2023. These databases consist of four distinct files: (i) natural compounds (NC) (69,064 compounds), (ii) synthetic compounds 1 (SC1) (192,714 compounds), (iii) synthetic compounds 2 (SC2) (118,512 compounds), and (iv) synthetic compounds 3 (SC3) (170,267 compounds).

All ligands, including library ligands, query molecules, and active and decoy compounds for the enrichment study, were prepared using LigPrep (2023-1, Schrödinger LLC, New York, NY, USA). Subsequently, energy minimization for all ligands was performed according to the OPLS_2005 forcefield and default parameters using MacroModel (2023-1, Schrödinger LLC, New York, NY, USA). The library ligands were modeled while maintaining ionization states, desalting, avoiding generation of tautomers, and determining chiralities from 3D structures. Only one ligand per compound was generated. On the other hand, the selected IBS compounds for molecular docking as well as the active and decoy compounds modelled for enrichment studies, were prepared to generate stereoisomers and tautomers. Additionally, Epik (2023-1, Schrödinger LLC, New York, NY, USA) was employed to generate protonation states of the ligands at pH 7.0 ± 2.0 (201).

Molecular descriptors were calculated using QikProp (2023-1, Schrödinger LLC, New York, NY, USA). The followings descriptors were used to apply drug-likeness filter to the database: molecular weight (MW) (reference values: 130.0 – 725.0 Da), HBD count (reference values: ≤ 6.0), HBA count (reference values: 2.0 – 20.0), predicted octanol/water partition coefficient (logP) (reference values between -2.0 – 6.5), number of rotatable bonds (RB) (reference values: ≤ 15), topological polar surface area

(tPSA) (reference values: 7.0 – 200.0 Å²), and the number of reactive functional groups (rtvFG) (reference value: 0).

3.2. Ligand-Based Virtual Screening

3.2.1. Shape Screening

In this study, Phase (2023-1, Schrödinger LLC, New York, NY, USA) was utilized for shape similarity screening by the help of Shape Screening panel of Maestro. Phase Shape utilizes sets of three atoms (atom triplets), and the process generates initial alignments, which are further improved through Gaussian overlay techniques (117). In the first step, query models were constructed using various compounds, namely 3-chloro-N-{4-[1-(propylcarbamoyl)cyclobutyl]phenyl}benzamide (QPV), 3-chloro-N-(3-{(2S)-1-[(4-fluorophenyl)amino]-1-oxopropan-2-yl}bicyclo[1.1.1]pentan-1-yl)benzamide (U41), 4-chloro-N-[[1-(3-chlorobenzene-1-carbonyl)-1,2,3,4-tetrahydroquinolin-6-yl]methyl]benzamide (U6G), 4-chloranyl-N-[(1R)-1-[(1S,5R)-3-quinolin-4-yloxy-6-bicyclo[3.1.0]hexanyl]propyl]benzamide (SLW), and N-(4-fluorophenyl)-3-{4-[4-(hydroxymethyl)-6-(trifluoromethyl)pyridin-3-yl]phenyl}oxetane-3-carboxamide (6RI), which were proven to be apo-IDO1 inhibitors through X-ray crystallography found co-crystallized with apo-IDO1 structure in the protein data bank (PDB ID: 6v52 (103), 6wjy (202), 6wpe (203), 7b1o (204), and 7rrc (205), respectively).

In this research, the 3D perspective was employed for shape screening. The fundamental principle of this method is that molecules with comparable volumes may possess the ability to efficiently bind to spaces of comparable or identical size within the active pockets of proteins (206,207). Within the volume scoring options, typed pharmacophore option was selected to treat each structure as a set of pharmacophoric sites, with their positions determined by applying Phase pharmacophore feature definitions. The calculation of overlapping volume is restricted to sites of the same feature type, with each site being represented by a sphere with a radius of 2 Å. The similarity of the descriptors in 3D methods was assessed using the Tanimoto coefficient, indicating the ratio of the union to the intersection of the shapes of two molecules (208).

3.2.2. Pharmacophore Screening

Pharmacophore modeling involved two main steps: generating pharmacophore models and conducting pharmacophore screening of a ligand database. For this process, Phase (2023-1, Schrödinger LLC, New York, NY, USA) was utilized.

The process of generating pharmacophore models began with the formulation of a pharmacophore hypothesis derived from a protein-ligand complex. For this purpose apo-IDO1 structures with PDB ID 6v52, 6wjy, 6wpe, 7b1o, and 7rrc, and their co-crystallized inhibitors, namely QPV, U41, U6G, SLW, and 6RI, were used, respectively. Upon importing the protein-ligand complex into the Maestro window, the next step involved navigating to the “Develop Pharmacophore Hypothesis” panel. Within this panel, the “Create pharmacophore model using” menu was accessed, and the option was switched to “Receptor-ligand complex”, initiating the automatic progression through the receptor ligand complex workflow. This method was executed manually, involving manual selection and adjustment of features. Prior to feature selection, the interactions pane was activated to identify which features held significance for binding. Subsequently, each feature deemed critical for binding was carefully chosen in the process.

Then the “Hypothesis Settings” menu was opened, which included two submenus: Features and Excluded Volumes. In the Features submenu, the settings were kept the same as the default, maintaining a minimum feature-feature distance of 2.0 Å and a minimum feature-feature distance for features of the same type of 4.0 Å. Meanwhile, in the Excluded Volumes submenu, the option to create receptor-based excluded volume shell was activated to confine regions that define and mimic the size and shape of the binding pocket. The radii sizes, radii scaling factors, and other options were left as default settings. The hypothesis was then ready to be used in screening.

Each pharmacophore model was represented by one pharmacophore hypothesis. Thus, five models were generated, each originating from a distinct complex, namely 6v52-QPV, 6wjy-U41, 6wpe-U6G, 7b1o-SLW, and 7rrc-6RI, involving the apo-IDO1 inhibitors used in the shape screening study above. These models were employed to calculate the Phase screen score for filtered databases, covering both natural and synthetic compounds.

3.3. Structure-Based Virtual Screening

3.3.1. Protein Preparation

From the Protein Data Bank (PDB) (<https://www.rcsb.org/>) (209), selected five apo-IDO1 enzyme structures with co-crystallized ligands were retrieved (PDB ID: 6wjy, resolution: 1.91 Å; PDB ID: 6wpe, resolution: 2.43 Å; PDB ID: 6v52, resolution: 1.78 Å; PDB ID: 7b1o, resolution: 2.58 Å; and PDB ID: 7rrc, resolution: 2.18 Å). Protein complexes were prepared using the Protein Preparation Wizard (2023-1, Schrödinger LLC, New York, NY, USA). Utilizing the pre-process feature involved several steps: assigning bond orders using the CCD database, adding hydrogen atoms, and creating disulfide bonds. After addressing structural defects, the next stage following the pre-process step entails scrutinizing the structure and making necessary adjustments, which may include the removal of undesirable elements such as the chain, cofactor and co-crystallized ligand. This procedure is carried out within the Review and Modify tab.

Within the Refine tab, three sections are present including H-bond assignment, removal of waters, and restrained minimization. The optimization of H-bonds includes activating the option to sample water orientations and employing PROPKA at pH 7.0. In the subsequent section, waters positioned beyond 3 Å from het groups are eliminated. In order to realign side-chain hydroxyl groups and avoid steric clashes, a controlled forcefield minimization was conducted on the protein structures. This process utilized restrained minimization option settings with an RMSD cut-off value of 0.30 Å.

3.3.2. Molecular Docking

Receptor grids were generated using Glide (2023-1, Schrödinger LLC, New York, NY, USA), specifically in the Receptor Grid Generation panel for molecular docking. There are five tabs available for the receptor grid generation process: receptor, site, constraints, rotatable groups, and excluded volumes. In the receptor settings, the co-crystallized ligand of each protein structure was identified to be excluded from the grid generation and to define its centroid for docking coordinates. Additionally, the scaling factor and partial charge cutoff for Van der Waals radius scaling remained the same, which were 1.0 and 0.25, respectively. In the Site settings, the enclosing box was set

to the centroid of workspace ligand with the volume of 20x20x20 Å, and the coordinates for each protein was displayed in Table 3.1. The settings for constraints, rotatable groups and excluded volumes remained the same as the default settings.

Table 3.1. The central coordinates of the grid box for each protein

PDB ID	Coordinates		
	X	Y	Z
6v52	-14.02	33.29	-29.00
6wjy	62.05	50.18	14.97
6wpe	71.88	13.01	28.32
7b1o	61.96	50.73	15.21
7rrc	61.58	50.46	15.37

Molecular docking was conducted against the apo-IDO1 structures using Glide (2023-1, Schrödinger LLC, New York, NY, USA) in both standard precision (SP) and extra precision (XP) modes. Ligands were allowed flexibility in both modes, and Epik state penalties were factored into the docking scores. Advanced docking settings, including sampling parameters for nitrogen inversions and ring conformation, were enabled. Torsion bias sampling was configured for all predefined functional groups, while docking and scoring for atoms with more than 500 atoms and 100 rotatable bonds were restricted. To mitigate the nonpolar aspects of the ligand, the vdW radius of ligand atoms with less than 0.15 partial charges was scaled by 0.8, maintaining the default scaling parameter. Constraints in the Constraints tab were remained unchanged. In the Output tab, the number of poses per ligand included was set to 50 for SP mode and 100 for XP mode.

3.3.3. Validation Studies

In order to validate the molecular docking method and select the ideal protein structures, validation studies were conducted with two different approaches; i.e., redocking and enrichment analysis, applied to the five apo-IDO1 in Table 3.1.

a. Redocking Study

The redocking study was performed using the molecular docking method at SP mode as described above. The co-crystallized inhibitor in each protein structure was redocked to their respective active site and the binding poses of each inhibitor were

compared with their original conformation by calculating root-mean-square deviation (RMSD) values in formula (3.1).

$$\text{RMSD} = \sqrt{\frac{\sum_{i=1}^N (X_{e,i} - X_{o,i})^2}{N}} \quad (3.1)$$

Where:

$X_{e,i}$ is the coordinates of the i^{th} atom in the reference structure;

$X_{o,i}$ is the coordinates of the i^{th} atom in the predicted structure; and

N is the number of atom pairs (or heavy atoms) in the molecules being compared.

b. Enrichment Study

The active compounds used in the enrichment study were retrieved from the literature (103,202,204). Decoys were generated from these active compounds using DUD-E (<https://dude.docking.org/>) (210). Both the active (Table 3.2) and decoy compounds were prepared as defined above. Subsequently, all the active and decoy compounds were docked to the selected protein structures according to the settings described above at SP mode. To assess the receptor's ability to distinguish between active and inactive compounds, the enrichment factor (EF), the area under the receiver operating characteristic curve (AUC-ROC), and robust initial enhancement (RIE) were calculated using the following formula 3.2, 3.3, and 3.4, respectively:

$$EF = \frac{\frac{\text{Hits}_{set}}{n}}{\frac{\text{Hits}_{all}}{N}} \quad (3.2)$$

Where:

Hits_{set} is the number of actives in the selected subset n of the ranked database and

Hits_{all} is the total number of actives in the database of N compounds.

Formula AUC-ROC

$$AUC - ROC = \frac{1}{M} \sum_{j=1}^M (X_j - X_{j-1}) \times Y_j \quad (3.3)$$

Where:

M is the total number of data points (usually, the number of compounds in the dataset)

X_j is the false positive rate at the j -th data point

X_{j-1} is the false positive rate at the $(j-1)$ -th data point

Y_j is the true positive rate at the j -th data point

Formula of RIE

$$RIE = \frac{\frac{1}{n} \sum_{i=1}^n e^{-ax_i}}{\frac{1}{N} \left(\frac{1-e^{-a}}{e^{a/N}-1} \right)} \quad (3.4)$$

Where:

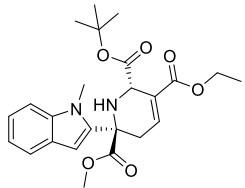
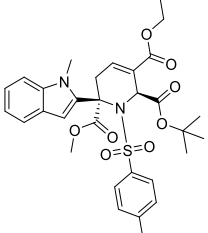
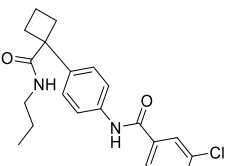
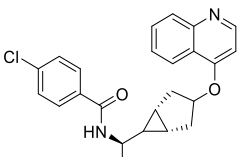
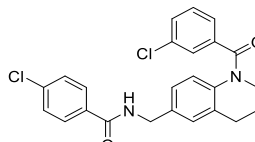
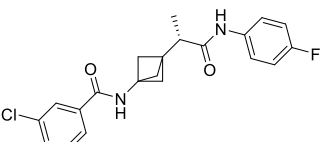
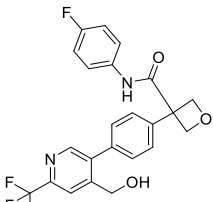
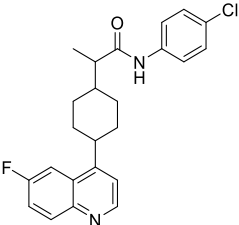
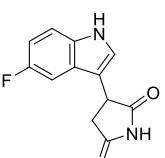
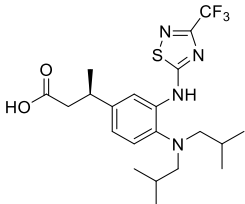
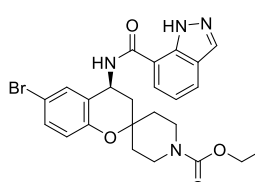
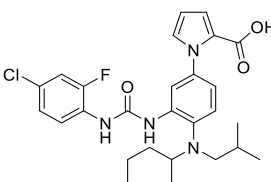
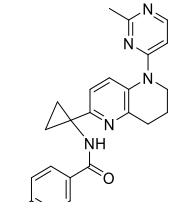
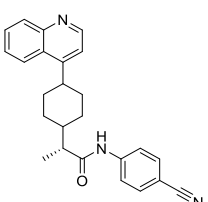
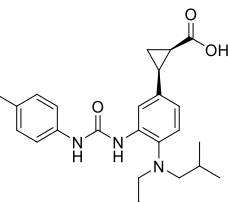
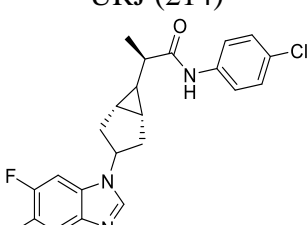
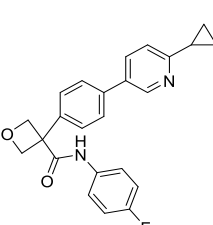
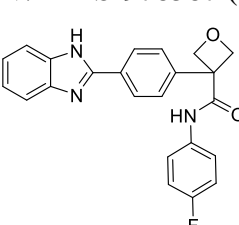
N is the total number of data points (usually, the number of compounds in the dataset)

n is the number of actives

a is an early recognition parameter

x_i is the relative rank where $x_i = r_i/N$ (r_i , represents its ranking position in the full list for i -th active molecule)

Table 3.2. Active apo-IDO1 inhibitors used to generate decoys

No.	Compound	No.	Compound	No.	Compound
1.	 N2U (211)	2.	 N39 (211)	3.	 QPV (103)
4.	 SLW (204)	5.	 U6G (203)	6.	 U41 (202)
7.	 6RI (205)	8.	 BMS-986205 (27)	9.	 PF-06840003 - (24,212)
10.	 GSK5628 (101)	11.	 Compound D (104)	12.	 B37 (213)
13.	 URJ (214)	14.	 C51 (27)	15.	 C4V/ BMS-978587 (27)
16.	 YRP (204)	17.	 6ZI (205)	18.	 6IZ (205)

3.3.4. Molecular Dynamics Simulations

MD simulations were performed using NAMD (2.13, University of Illinois and Beckman Institute, Urbana, USA) (215) and VMD (1.9.3, University of Illinois and Beckman Institute, Urbana, USA) (216). The preparation of the proteins and ligands was carried out using CHARMM36m (Forcefield option) and CGenFF, both accessible through the CHARMM-GUI web server (217). To initiate solvation and neutralization, a rectangular water box with a distance of 10.0 Å was incorporated, K⁺ and Cl⁻ ions were introduced using the Monte-Carlo ion placing method. NAMD was employed for both equilibration and production processes, incorporating a 20 ps minimization step. Equilibration simulations were conducted to achieve a stable state prior to the commencement of data collection. These simulations were executed within the NPT ensemble conditions, with a constant pressure of 1 atm and a temperature of 303 K. Following the successful equilibration, the production phase was simulated for a duration of 100 ns, representing the concluding phases of the MD simulations.

The visualization of MD simulations trajectories involved the use of VMD, assessing the RMSD of the protein backbone atoms for the trajectories, which was measured by formula (3.1), and the root-mean-square fluctuation (RMSF) to evaluate the fluctuations of carbon alpha (C α) atoms measured by formula (3.5). Furthermore, the compactness of the systems was evaluated through the calculation of the radius of gyration (RoG) using formula (3.6). The RoG values refer to the distribution of atoms in the molecular structure with respect to its center of mass.

$$RMSF = \sqrt{\frac{\sum_{j=1}^N \|r_{ij} - \langle r_i \rangle\|^2}{N}} \quad (3.5)$$

Where:

N is the total number of frames or snapshots in the simulation,

r_{ij} is the position vector of atom or residue i in frame j ,

$\langle r_i \rangle$ is the average position of atom or residue i over all frames.

$$RoG = \sqrt{\frac{\sum_{i=1}^N m_i (r_i - r_{CM})^2}{\sum_{i=1}^N m_i}} \quad (3.6)$$

Where :

N is the total number of particles (atoms or mass elements)

m_i is the mass of particle i

r_i is the distance of particle i from the axis of rotation

r_{CM} is the distance of center of mass

The RMSD, RMSF, and RoG values were calculated using the script (see attachment), while the formation of salt bridges was conducted through Salt Bridges panel in VMD, which required importing the psf and dcd trajectory files to the window. The selection column was filled with “protein”, and frames with “all”. The oxygen-nitrogen distance remained the same with a cut-off value of 3.2 Å, while side-chain COM distance had no cut-off. Alternatively, salt bridge formation could be generated using the script (see attachment).

3.3.5. Binding Free Energy Calculations using MM-GBSA

In this study, the free binding energies between the receptor and the selected ligands were analyzed using MM-GBSA twice: first following molecular docking and then after MD simulations. For the first stage, the Prime MM-GBSA (2023-1, Schrödinger LLC, New York, NY, USA) was employed. The free binding energies were calculated using the all-atom optimized potential for liquid simulation (OPLS-AA) and the GB/SA method. The calculation involved the top 500 compounds, with three best poses for each compound. In the solvation model, the VSGB (218) solvation model was employed. Other options, including input ligand partial charges, implicit membrane, and constraints on flexible residues, were not selected. No adjustments were made to protein flexibility, and the distance from the ligand was maintained at 0.0 Å.

For the second analysis, MolAICal, a freely available software at <https://molaical.github.io>, was utilized to analyze binding free energies from the MD simulations trajectories. Through this tool, MM-GBSA values that capture the

variations of ligand-receptor affinity throughout the MD simulations were computed (219). The underlying methodology can be summarized by the following equation:

$$\Delta G = G_{\text{complex}} - G_{\text{protein}} - G_{\text{ligand}} \quad (3.7)$$

$$\Delta G = \Delta H - T\Delta S \approx \Delta E_{\text{MM}} + \Delta G_{\text{sol}} - T\Delta S \quad (3.8)$$

$$\Delta E_{\text{MM}} = \Delta E_{\text{internal}} + \Delta E_{\text{electrostatic}} + \Delta E_{\text{vdw}} \quad (3.9)$$

$$\Delta G_{\text{sol}} = \Delta G_{\text{GB}} + \Delta G_{\text{SA}} \quad (3.10)$$

The binding free energy (ΔG) is defined as the energy of the complex subtracted by the sum of energies of the receptor and the ligand (as expressed in formula 3.7). Each component in formula (3.7) can be computed using the equations presented in formula (3.8). In the formula (3.9), ΔE_{MM} represents the alterations in gas-phase molecular mechanics energy, which encompasses $\Delta E_{\text{internal}}$ (bond, angle, and dihedral energies), $\Delta E_{\text{electrostatic}}$ (electrostatic energy), and ΔE_{vdw} (van der Waals energy). ΔG_{sol} is the summation of the solvation free energy including electronic or polar contribution (ΔG_{GB}) and non-electronic or nonpolar contribution (ΔG_{SA}) as shown in formula (3.10). The term $-T\Delta S$ accounts for the conformational entropy change upon binding. Typically, a series of conformational snapshots obtained from MD simulations were subjected to normal-mode analysis to compute the conformational entropy change ($-T\Delta S$) (219,220).

3.4. Fingerprint Similarity

Fingerprint similarity was conducted using Canvas Similarity and Clustering (2023-1, Schrödinger LLC, New York, NY, USA). In this menu, there were three submenus: Fingerprints, Similarity and Cluster. In the Fingerprint settings, the precision was set to 64-bit, the fingerprint type to linear, and the atom typing scheme to “Daylight invariant atom types; bonds were distinguished by bond order”. In the Similarity submenu, default settings were kept. In the Cluster submenu, the linkage method was set to average for calculating clustering, and duplicate entries were grouped into a new group for each cluster. Each cluster had a different scaffold and was structurally diverse from the others.

3.5. Toxicity Prediction

The toxicity parameters were predicted using the ProTox-II web-server (https://tox-new.charite.de/protox_II/index.php?site=home), and Toxicity Estimation Software Tool (TEST) v.5.1.2. These tools determined potential adverse effects of the compounds by analyzing their molecular structures. The ProTox-II web-server provided several toxicity parameters including predicted toxicity class, organ toxicity, toxicity end points covering carcinogenicity, immunotoxicity, mutagenicity, cytotoxicity, and also 21st Century toxicology (Tox21) which covered two pathways: nuclear receptor signaling pathways and stress response pathways. The TEST software evaluated various factors, including 48-hr *Daphnia magna* LC₅₀, oral rat LD₅₀, and bioconcentration factor. *Daphnia magna*, an aquatic organism, was used to assess the potential toxicity of the candidates in aquatic settings (221,222). The Bioconcentration Factor (BCF), on the other hand, quantifies a substance's capacity to accumulate in an organism's tissues from its external surroundings (223).

4. RESULTS

The workflow of the whole virtual screening study was outlined in Figure 4.1. A total of 550,557 compounds (both natural and synthetic) imported from IBS were virtually screened using a series of methods, including drug-likeness analysis, shape similarity, pharmacophore modeling, molecular docking, MM-GBSA analysis, MD simulations, and toxicity analysis in parallel, sequential, and hybrid fashions.

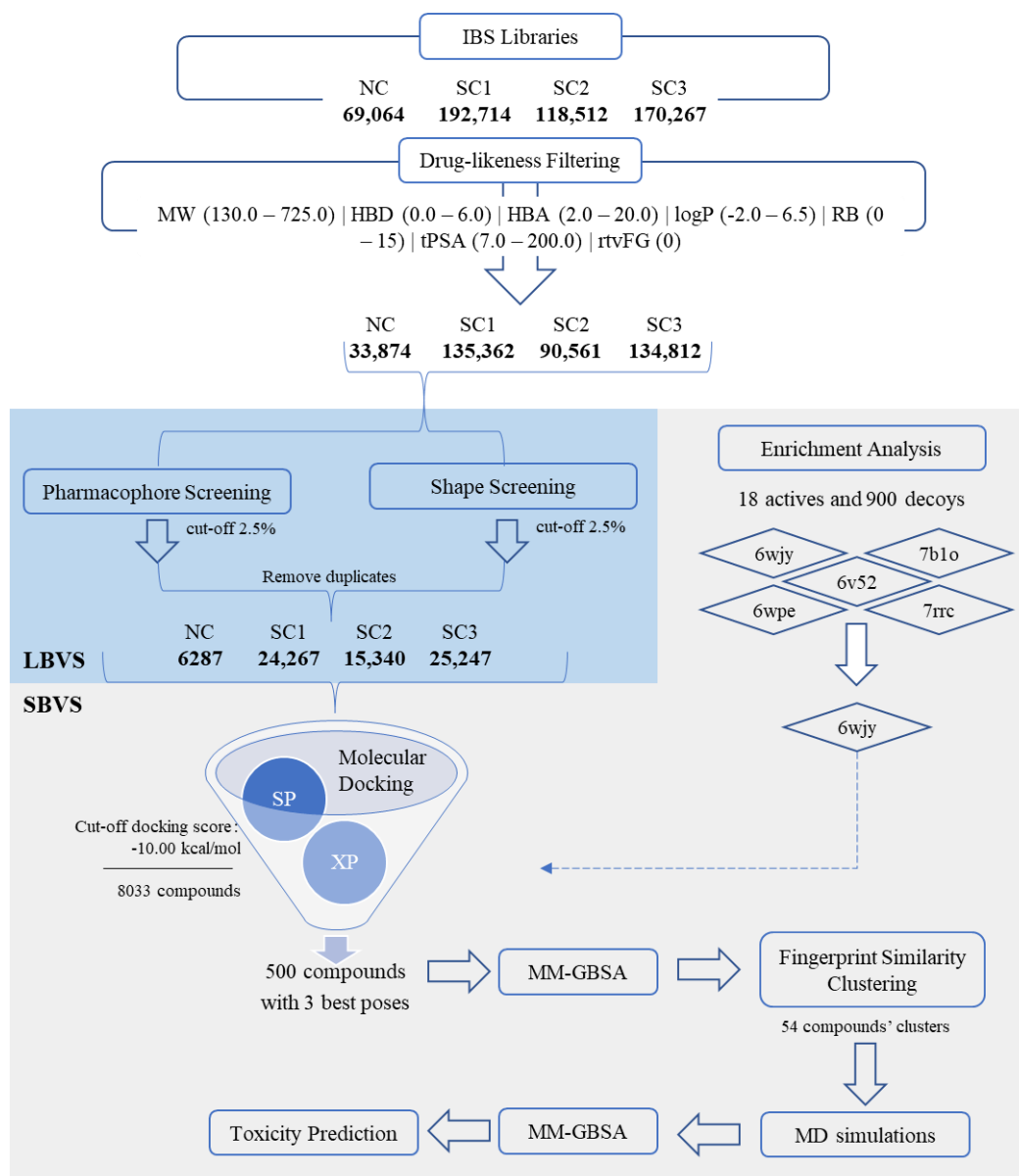


Figure 4.1. Workflow of this study

The ligand library was composed of four databases: natural compounds (NC, 69,064 compounds), synthetic compounds 1 (SC1, 192,714 compounds), synthetic compounds 2 (SC2, 118,512 compounds), and synthetic compounds 3 (SC3, 170,267 compounds). Ligands that met the initial drug-likeness filtration criteria underwent subsequent shape similarity and pharmacophore modeling screening. The query structures employed in this study were derived from previously published molecules known for their potent inhibition of apo-IDO1 and the models used in pharmacophore screening were derived from their receptor interactions. Following LBVS, the top 2.5% of ligands were chosen for further evaluation through SBVS.

Prior to molecular docking, validation studies were conducted, using redocking and enrichment analyses. The protein structure with PDB ID 6wjy was selected upon these validation studies. Compounds selected through LBVS were docked to the apo-IDO1 structure at SP and then XP mode. The top-scoring 500 compounds, with three different conformations each, underwent binding free energy calculations using MM-GBSA. 54 compounds with high free binding energy, ideal receptor interactions and structural diversity were identified. Among them top three compounds were selected for MD simulations. Trajectory analysis for the MD simulations included RMSD, RMSF, RoG, salt bridges formation, and MM-GBSA free binding energy. In the final stage, all the selected compounds were assessed for potential toxicity characteristics using a combination of a free web server and dedicated software.

4.1. Calculation of Molecular Descriptors and Drug-likeness Filtering

A number descriptors relevant to druglike chemical space (106,224–227) were calculated for the IBS library compounds to apply drug-likeness filter. The compounds outside the reference values defined by the software were filtered off (Table 4.1). These values apply for the 95% of the known drug molecules according to the software. The compounds that met these criteria were retained, resulting in a database of 33,874 constituents for natural and 360,735 constituents for synthetic compounds, respectively (Table 4.1).

Table 4.1. Molecular descriptors and drug-likeness filtering of the IBS libraries

Descriptors	Reference Value	NC 69,064^a	SC 1 192,714^a	SC 2 118,512^a	SC 3 170,267^a
MW	130.0 – 725.0	-1,328	-1,959	-704	-725
HBD	0.0 – 6.0	-135	-27	-6	-17
HBA	2.0 – 20.0	-556	-2,546	-398	-659
logP	-2.0 – 6.5	-1,659	-10,390	-4,465	-4,819
RB	0 – 15	-178	-201	-17	-87
tPSA	7.0 – 200.0	-691	-277	-296	-150
rtvFG	0	-30,643	-41,952	-22,065	-28,998
#remaining ligands		33,874^b	135,362^b	90,561^b	134,812^b

^a The initial number for each database

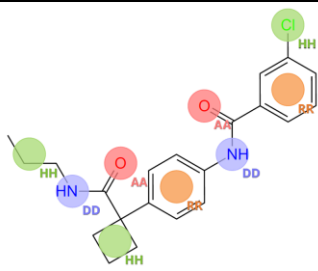
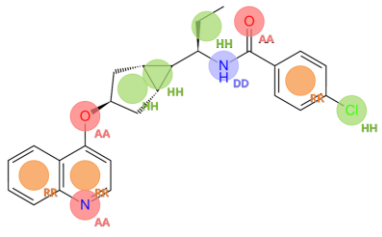
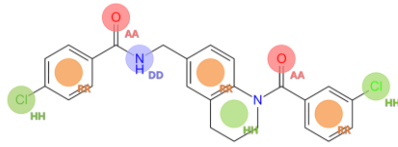
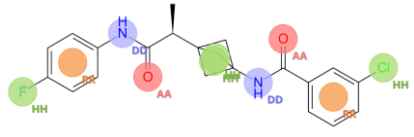
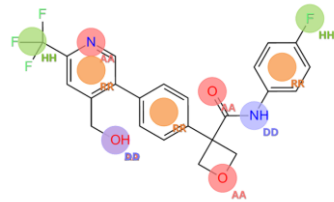
^b The number of remaining ligands after filtering based on the molecular descriptors

4.2. Ligand-Based Virtual Screening

4.2.1. Shape Screening

Shape screening was performed by 3D aligning all the compound in the refined databases with each query compound, known to be potent and selective apo-IDO1 inhibitors. Each alignment was scored accounting for matching of the volumes and pharmacophoric groups, denoted as similarity score, and the database compounds were ranked according to their similarity scores with each query compound (Table 4.2). The top 2.5% of the ligands from each database according to their similarity scores were passed on to the subsequent steps. As shown in Table 4.3, the NC database had a range of similarity scores between 0.41 and 0.66, compiling from five different queries. Similarly, ligands in the SC databases exhibited values ranging from a minimum of 0.42 to a maximum of 0.70. Afterwards, all the selected compounds were aggregated for each database, and duplicate entries within each database were removed. The remaining number of compounds for each database amounted to 3,243; 13,751; 8,740; and 14,364 for NC, SC1, SC2, and SC3, respectively (Table 4.3).

Table 4.2. Query structures as references for shape screening

Query structures	IDO1 HeLa IC ₅₀ (nM)	LSQA ^a	Molecular structure ^b
QPV	9.0	Better	
SLW	9.9	Better	
U6G	9.0	Better	
U41	3.1	Better	
6RI	2.0	Better	

^a LSQA (Ligand Structure Quality Assessment), to evaluate the quality of ligand structures concerning their fit to experimental data for each specific ligand of interest;

^b Hydrogen-bond acceptors were denoted in red (A), hydrogen-bond donors in blue (D), hydrophobic in green (H), negative ionic centers in dark red (N), positive ionic centers in dark blue (P), and aromatic rings in orange (R).

Table 4.3. Number of selected compounds^a from each query of each method from each library and the score ranges^b obtained through shape similarity screening

Query structures	NC		SC1		SC2		SC3	
	#selected compounds	Range	#selected compounds	Range	#selected compounds	Range	#selected compounds	Range
QPV	847	0.45 – 0.66	3384	0.47 – 0.68	2264	0.45 – 0.68	3370	0.49 – 0.66
SLW	847	0.46 – 0.62	3384	0.48 – 0.64	2264	0.48 – 0.65	3370	0.47 – 0.63
U6G	847	0.43 – 0.61	3384	0.45 – 0.63	2264	0.43 – 0.59	3370	0.46 – 0.63
U41	847	0.46 – 0.62	3384	0.47 – 0.70	2264	0.48 – 0.64	3370	0.47 – 0.63
6RI	847	0.41 – 0.53	3384	0.42 – 0.54	2264	0.42 – 0.56	3370	0.44 – 0.59
Total	4235		16,920		11,320		16,850	
Non-duplicate	3243		13,751		8740		14,364	

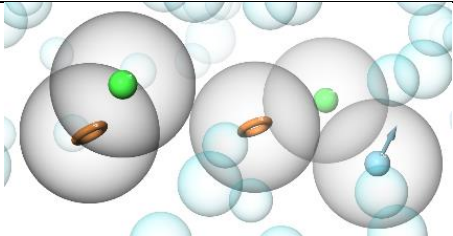
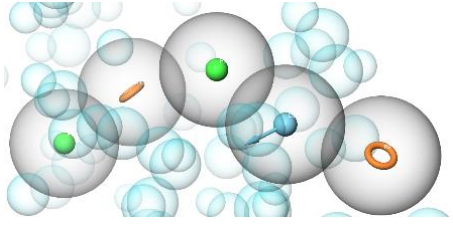
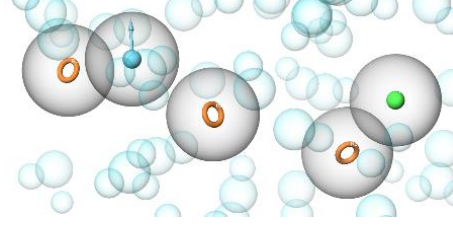
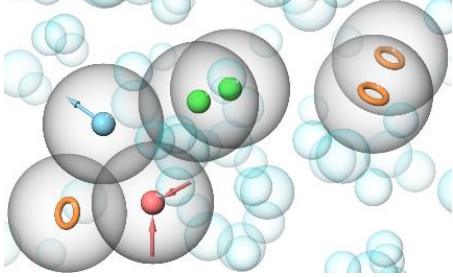
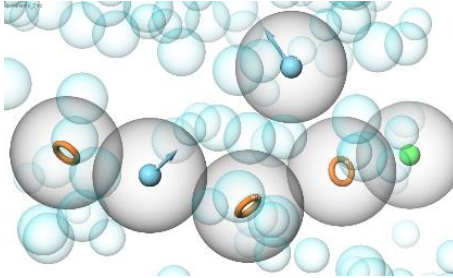
^a #selected compounds refer to the number of selected compounds in each database for every query structure or pharmacophore model with a cut-off 2.5% from the top.

^b The range refers to the Phase score, spanning from the top rank to the lower limit each database.

4.2.2. Pharmacophore Screening

Five inhibitor-apo-IDO1 crystallographic complexes were used to generate pharmacophore hypotheses, as mentioned in the methodology section. Regarding receptor-ligand complexes settings, one pharmacophore hypothesis was generated for each ligand-receptor complex. Each pharmacophore hypothesis comprised of pharmacophores such as hydrophobic regions, hydrogen bond acceptors and donors, aromatic features, positive and negative ionizable regions. Notably, among the selected models, 7b1o-SLW model exhibited the most comprehensive feature set, comprising one hydrogen-bond acceptor (A), one hydrogen-bond donor (D), two hydrophobic regions (H), and three aromatic rings (R), denoted as ADHRRR (Table 4.4).

Table 4.4. Pharmacophore models of the study and their features

Pharmacophore model	No. of Features	Feature Set ^a	Feature Visualization ^b
6v52-QPV	5	DHHRR	
6wjy-U41	5	DHHRR	
6wpe-U6G	5	DHRRR	
7b1o-SLW	7	ADHHRRR	
7rrc-6RI	6	DDHRRR	

^a Feature abbreviation A for hydrogen-bond acceptor, D for hydrogen-bond donor, H for hydrophobic, R for aromatic ring.

^b Feature visualization included the representation of A as red balls, D as blue ball, H as green ball, and R as orange rings. Feature tolerance cut-off represented as gray transparent spheres around the features and excluded volumes as blur transparent spheres.

The refined ligand databases were screened against each pharmacophore model in parallel. As resumed in Table 4.5, top-scoring 2.5% compounds of each library

according to the Phase screen score from each model were selected. When compared with each other, the results from 7b1o-SLW model exhibited low scores in all databases with the lowest Phase screen score of 0.76 in NC, 0.72 in SC1, 0.79 in SC2, and 0.82 in SC3. The remaining compounds were then retrieved from each database and duplicate compounds were removed. The remaining ligands for each database amounted to 3,556; 13,575; 9,079; and 14,152 ligands for NC, SC1, SC2, and SC3, respectively (Table 4.5).

Table 4.5. Number of selected compounds^a from each pharmacophore model of each method from each library and the score ranges^b obtained through pharmacophore screening

Pharmacophore model	NC		SC1		SC2		SC3	
	#selected compounds	Range	#selected compounds	Range	#selected compounds	Range	#selected compounds	Range
6v52-QPV	847	0.93 – 1.16	3384	0.92 – 1.45	2264	0.94 – 1.44	3370	0.95 – 1.24
7b1o-SLW	847	0.76 – 1.14	3384	0.72 – 1.11	2264	0.79 – 1.17	3370	0.82 – 1.17
6wpe-U6G	847	0.88 – 1.24	3384	0.88 – 1.43	2264	0.87 – 1.23	3370	0.92 – 1.36
6wjy-U41	847	0.87 – 1.24	3384	0.89 – 1.25	2264	0.95 – 1.34	3370	0.92 – 1.36
7rrc-6RI	847	0.85 – 1.09	3384	0.87 – 1.20	2264	0.92 – 1.23	3370	0.92 – 1.23
Total	4235		16,920		11,320		16,850	
Non-duplicate	3556		13,575		9079		14,152	

^a #selected compounds refer to the number of selected compounds in each database for every query structure or pharmacophore model with a cut-off 2.5% from the top.

^b The range refers to the Phase score, spanning from the top rank to the lower limit each database.

For the last step in ligand-base virtual screening, the filtered compounds were combined from shape similarity and pharmacophore modelling, then also checked for and cleared from any duplicate compounds. The number of remaining ligands for each database were 6287; 24,267; 15,340; and 25,347 ligands for NC, SC 1, SC 2, and SC 3, respectively (Table 4.6).

Table 4.6. Number of total selected compounds from each library obtained through both shape similarity and pharmacophore screening

LBVS Screening	NC	SC1	SC2	SC3
Shape similarity^a	3243	13,751	8,740	14,364
Pharmacophore^b	3556	13,575	9,079	14,152
Total	6799	27,326	17,819	28,516
#selected compounds^c	6287	24,267	15,340	25,347

^a selected compounds from shape similarity screening

^b selected compounds from pharmacophore screening

^c selected compounds from both screening and after removed the non-duplicate compounds

4.3. Structure-based virtual screening

4.3.1. Validation Studies

a. Redocking Study

In the self-docking process, RMSD values for the five protein complexes yielded good results, specifically 0.26; 0.46; 0.30; 0.39; 0.16 Å for complexes 6v52, 6wjy, 6wpe, 7b1o, and 7rrc, respectively. These results indicated that all the docked pose coincided with the original ligand in the binding site of apo-IDO1 receptor (Figure 4.2), confirming that the molecular docking process can reproduce poses similar to experimental binding modes.

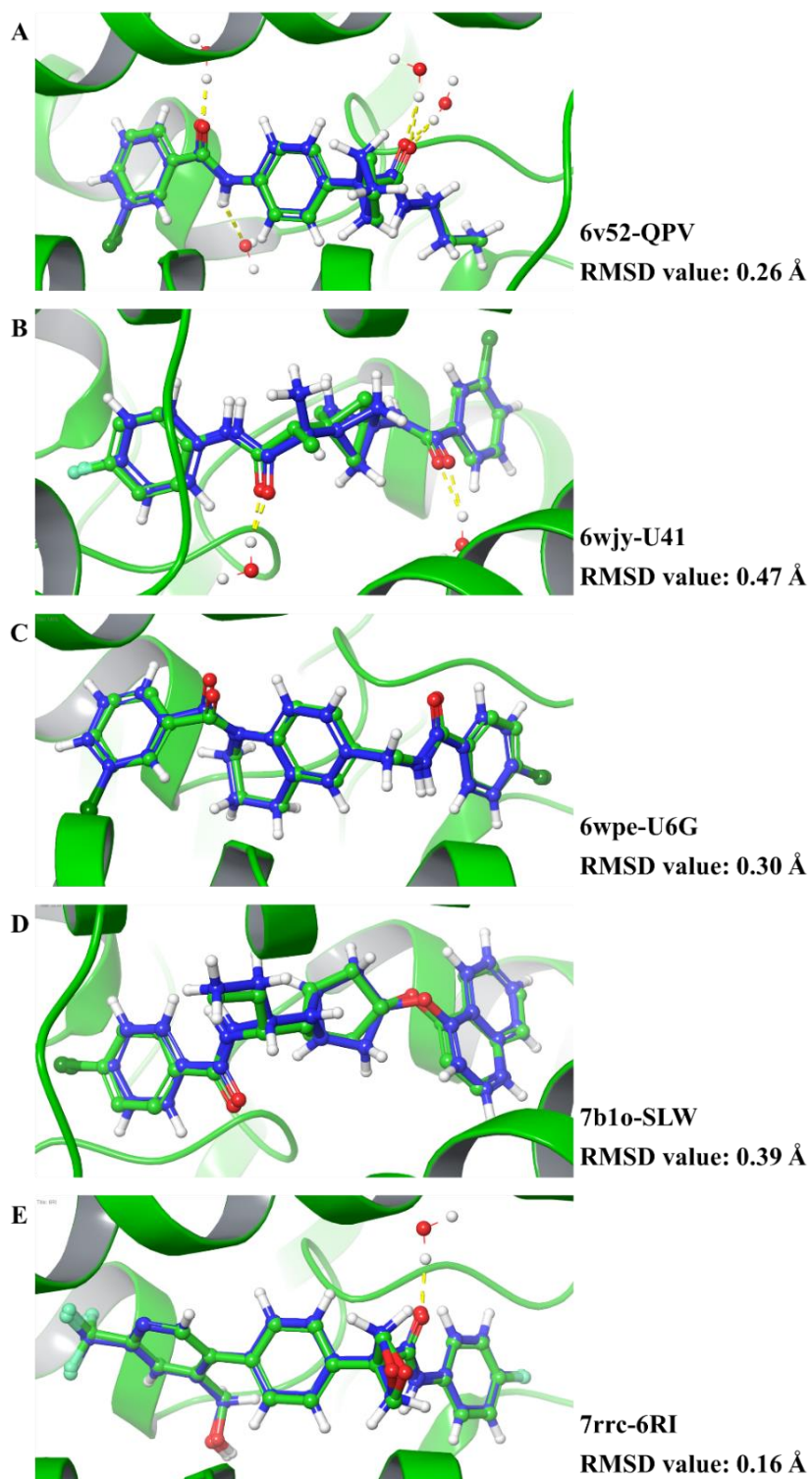


Figure 4.2. The alignment of the docked poses and the original co-crystallized poses of (A) QPV, (B) U41, (C) U6G, (D) SLW, and (E) 6RI in the active site of apo-IDO1 structures with PDB IDs 6v52, 6wjy, 6wpe, 7b1o, and 7rrc, respectively. Ligands are shown in blue stick-and-ball representations for the predicted poses and in green stick-and-ball representations for the co-crystallized poses. The protein backbones are presented in green ribbons.

b. Enrichment Studies

To validate the molecular docking methodology and select an appropriate crystal structure for structure-based virtual screening part of the study, molecular docking of active and decoy molecules to the selected five apo-IDO1 structures was performed. The ability of each protein structure to enrich known active compounds among the top scored compounds was assessed. 18 previously published apo-IDO1 inhibitors were collected from various literature sources (Table 4.7), and 50 decoy compounds for each were generated using DUD-E web server, resulting in a total of 900 decoy compounds. Active and decoy compounds were docked to each apo-IDO1 crystal structure and the enrichment was analysed by calculating EF, AUC-ROC, and RIE (Table 4.7 and Figure 4.3). The apo-IDO1 structure with PDB ID 6wjy exhibited the most promising results achieving an AUC-ROC of 0.90, RIE of 12.73, and an EF 20% of 4.2. Based on these favorable performance metrics, the 6wjy crystal structure was selected for subsequent virtual screening (Figure 4.3).

Table 4.7. The enrichment study for five different complexes

PDB ID	AUC-ROC	RIE	EF ^a	EF ^a	EF ^a	EF ^a	EF ^a
			1%	2%	5%	10%	20%
6v52	0.80	10.59	49.0	27.0	13.0	6.4	3.2
7b1o	0.71	9.01	33.0	21.0	10.0	5.3	2.9
6wpe	0.81	4.39	12.0	6.4	3.7	3.8	2.8
6wjy	0.90	12.73	39.0	35.0	14.0	8.5	4.2
7rrc	0.85	11.48	42.0	29.0	14.0	6.7	3.7

^a Enrichment Factors with respect to the sample size indicated as N% (1, 2, 5, 10, and 20%)

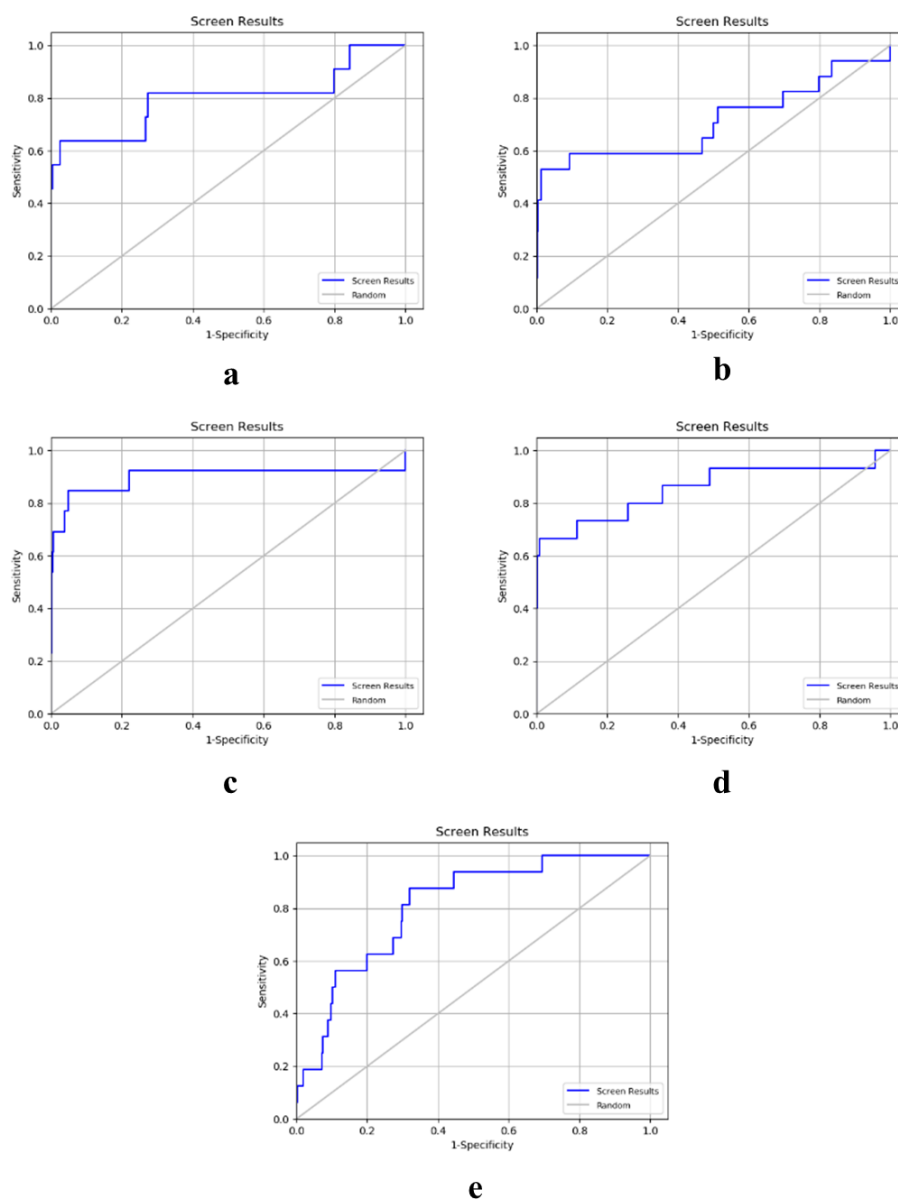


Figure 4.3. ROC curves for (a) 6v52, (b) 7b1o, (c) 6wpe, (d) 6wjy, and (e) 7rrc

4.3.2. Molecular Docking

Molecular docking was performed for the library compounds selected through LBVS. The compounds were docked the selected protein structure, 6wjy (Figure 4.4), at SP mode and subsequently XP mode. In the initial SP run, compounds with docking scores lower than -10.00 kcal/mol were removed. Within the NC database, 387 compounds remained with docking scores ranging from -10.00 to -12.96 kcal/mol, while in the SC database, 7646 compounds remained with docking scores ranging from

-10.00 to -13.28 kcal/mol. Subsequently, the total 8033 compounds from both natural and synthetic compounds were redocked and rescored at the XP mode, which provides higher precision but requires more time to complete compared to the SP mode. Similar to SP, a cut-off docking score value of -10.00 kcal/mol was applied. The top-scoring 500 compounds, each with their three best poses, were selected for MM-GBSA calculations.

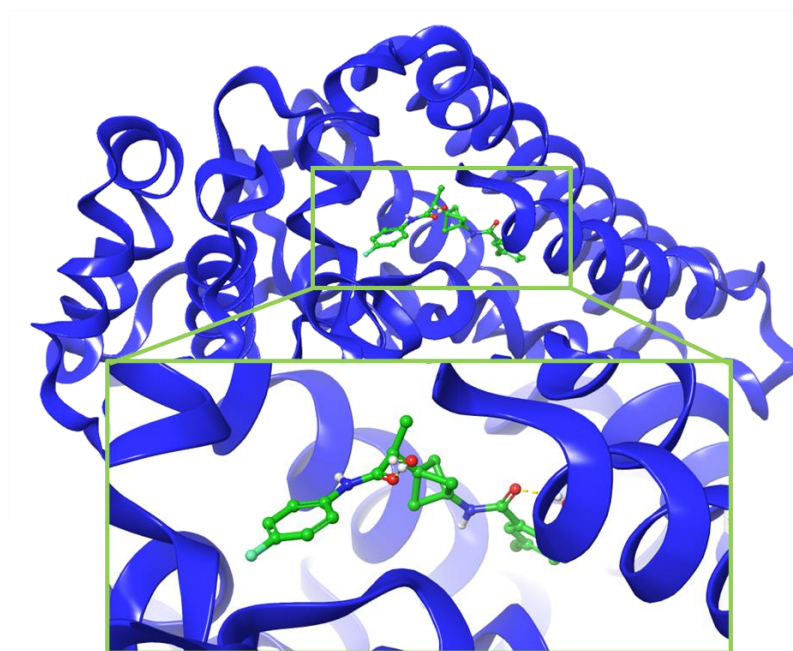


Figure 4.4. Apo-IDO1 structure complexed with small-molecule inhibitor U41 (PDB ID 6wjy)

4.3.3. Binding Free Energy Calculations and Fingerprint Similarity

MM-GBSA method was used to calculate binding free energy (ΔG) values for the top 500 compounds with their three best poses, adding up to 1500 ligand-receptor complexes. In addition, the compounds were clustered according to structural similarity using fingerprint method to eliminate structurally similar compounds and provide structural diversity among the shortlisted compounds. There were 54 clusters with clustering strain of 1.083 from fingerprint similarity evaluation (Figure 4.5). According to the binding free energy calculations, top 10 compounds with structural diversity are provided in Table 4.8.

Table 4.8. Selected 10 compounds with best MM-GBSA ΔG values and structural diversity and U41

No.	Compound	Molecular structure	Docking score (kcal/mol)	MM-GBSA ΔG (kcal/mol)
1.	STOCK2S-34127		-12.223	-128.684
2.	STOCK3S-69016		-11.527	-120.993
3.	STOCK2S-94986		-12.462	-119.968
4.	STOCK7S-27591		-12.037	-119.475
5.	STOCK7S-17282		-12.470	-118.681
6.	STOCK6S-24185		-12.301	-118.109
7.	STOCK3S-41956		-12.417	-116.696
8.	STOCK1N-68588		-12.659	-113.960
9.	STOCK6S-48507		-11.583	-113.392
10.	STOCK6S-09214		-12.361	-111.537
11.	U41		-12.208	-119.780

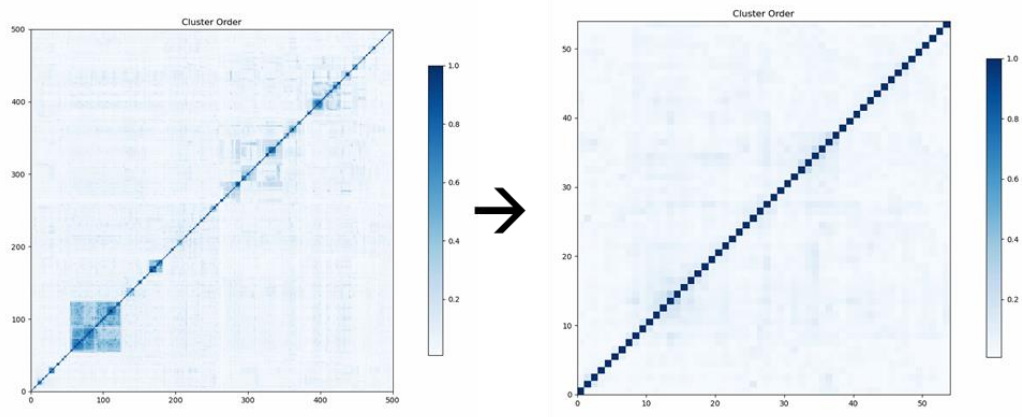


Figure 4.5. Fingerprint similarity prediction for the top 500 compounds. After the evaluation, there were 54 clusters with a clustering strain of 1.083.

Among the top 10 selected compounds, ΔG values of STOCK2S-34127, STOCK3S-69016, and STOCK2S-94986 were -128.684, -120.993, and -119.968 kcal/mol, respectively, better than that of the co-crystallized ligand, U41 (-119.780 kcal/mol) (Table 4.8). These compounds were predicted to bind to the IDO1 active site, forming hydrogen bond interactions with SER167, ARG343, HIS346, and π - π stacking interactions with TYR126, PHE214 (Table 4.9). These compounds were selected for further MD simulations study.

Table 4.9. Amino acids interactions of the top three compounds predicted by molecular docking and those of U41 identified experimentally

No.	Ligand	Amino acid	Type of interaction	Distance (Å)
1.	STOCK2S-34127	SER167	H-bond	1.90
		ARG343	H-bond	2.26
		HIS346	H-bond	2.14
		TYR126	π - π stacking	4.83
2.	STOCK3S-69016	SER167	H-bond	2.03
		PHE214	π - π stacking	4.91
		ARG343	H-bond	2.26
		HIS346	H-bond	2.14
3.	STOCK2S-94986	TYR126	π - π stacking	5.04
		SER167	H-bond	1.97; 2.19
		PHE214	π - π stacking	4.32
		HIS346	π - π stacking	4.48
4.	U41	TYR126	π - π stacking	4.84
		SER167	H-bond	1.93
		ARG343	H-bond	2.26
		HIS346	H-bond	2.14

4.3.4. Molecular Dynamics Simulations

MD simulations were performed for four complexes including the top three selected compounds (STOCK2S-34127, STOCK3S-69016, and STOCK2S-94986) and the co-crystallized ligand (U41), as well as for the ligand-free protein, for 100 ns, to evaluate stability of the predicted binding of the selected compounds to IDO1, as well as structural evolution of IDO1 upon inhibitor binding. The dynamic stability and behavior of each complex were evaluated by analyzing conformational changes, residue fluctuations, and compactness in protein-ligand complexes calculating RMSD, RMSF, and RoG values, respectively. Furthermore, the presence of salt bridges in each of the five complexes was analyzed. The trajectory analyses showed that all of the systems maintained good stability through 100 ns with the average RMSD values of

protein backbone atoms below 2.00 Å (Figure 4.6A). The RMSD value of the ligand-free system was 1.43 Å, followed by IDO1-U41 complex (1.44 Å), IDO1-STOCK2S-94986 complex (1.64 Å), IDO1-STOCK2S-34127 complex (1.68 Å), and IDO1-STOCK3S-69016 complex (1.76 Å).

The RMSF values were analyzed to assess the degree of residue fluctuations of C α atoms in each complex, and four high fluctuating regions were identified: (i) MET10, (ii) the region between GLY284 and ALA288, (iii) the region between SER359 and PRO362 and between GLY380 and THR382, and (iv) the region between LEU400 and LYS401 (Figure 4.6B).

The compactness of the systems was evaluated by analysis of RoG values for the whole protein. As shown in the Figure 4.6C, all the complexes exhibited good compactness from the beginning to the end of the simulation since the differences between the highest and the lowest RoG values were quite low, which were calculated as 0.352 Å (IDO1-STOCK2S-34127 complex); 0.488 Å (IDO1-STOCK3S-69016 complex); 0.386 Å (IDO1-STOCK2S-94986 complex); 0.476 Å (IDO1-U41 complex); and 0.549 Å (ligand-free IDO1).

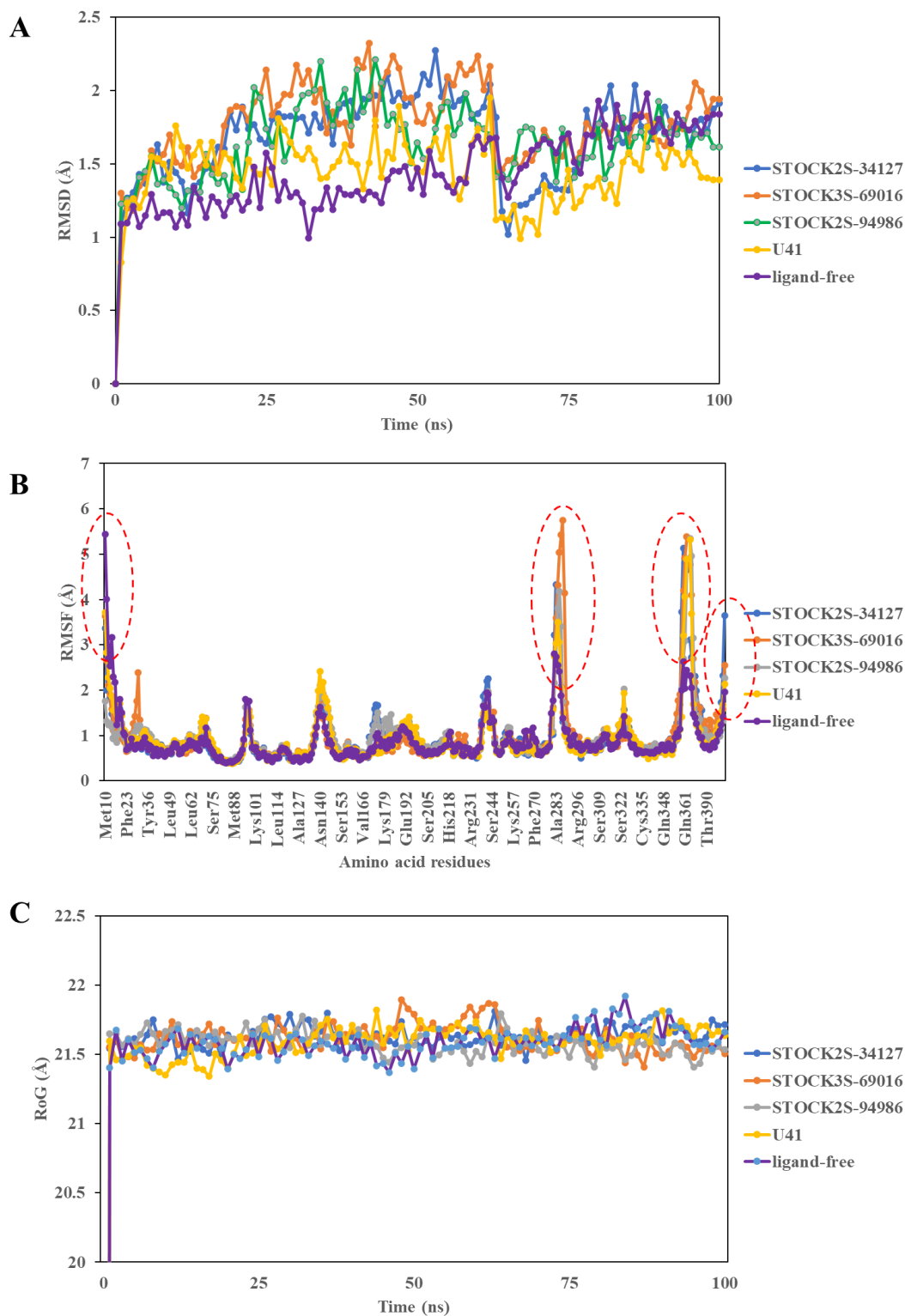


Figure 4.6. The MD simulations trajectories for the ligand-free and ligand-bound IDO1 structures with a duration of 100 ns depicting (A) RMSD values, (B) average RMSF values for each amino acid residue, and (C) RoG values over time.

The complex with co-crystallized ligand (U41) exhibited the highest number of salt bridges, totaling 49 electrostatic interactions. It was followed by the ligand-free IDO1 (47 salt bridges), the IDO1-STOCK2S-34127 complex (45 salt bridges), and both the IDO1-STOCK3S-69016 and IDO1-STOCK2S-94986 complexes (44 salt bridges). All the systems shared the same 33 salt bridges. However, three salt bridges—ASP149-LYS135, GLU119-ARG304, and GLU14-LYS13—were common to all systems except the IDO1-STOCK2S-94986 complex. Additionally, each complex had unique salt bridges exclusive to that complex. For example, in the IDO1-STOCK2S-34127 complex, there were ASP245-LYS238 and ASP98-LYS94 salt bridges. In the IDO1-STOCK3S-69016 complex, there were ASP158-LYS161, ASP383-LYS238, and GLU202-LYS179 salt bridges. In the IDO1-STOCK2S-94986 complex there was the unique GLU396-LYS401 salt bridge. The IDO1-U41 complex exhibited three unique salt bridges (ASP98-LYS101, GLU146-LYS141, and GLU30-LYS136). Lastly, ligand-free IDO1 had two unique salt bridges: ASP18-LYS179 and ASP38-ARG58. All systems exhibited combinations such as ASP-/ARG+, ASP-/LYS+, GLU-/ARG+, and GLU-/LYS+ in their salt bridge interactions. Notably, the number of salt bridges containing LYS+ exceeded those containing ARG+ (Figure 4.7).

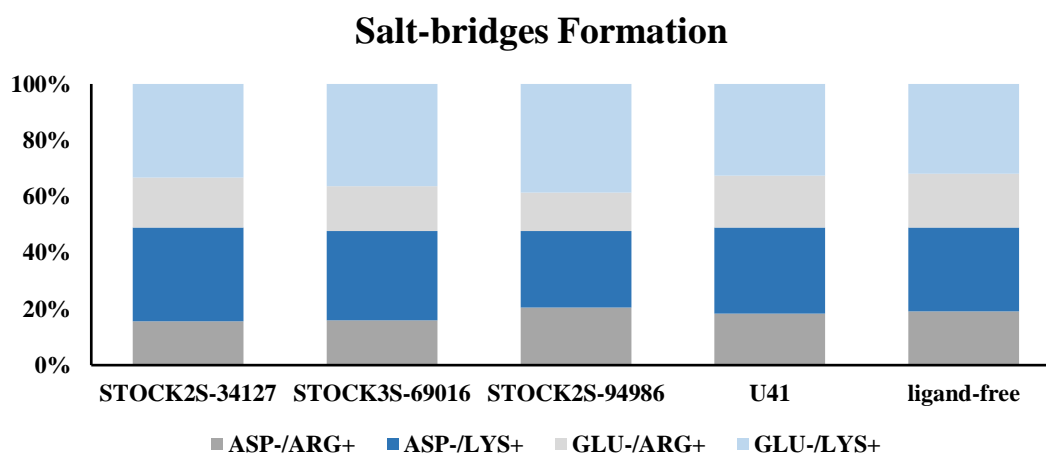


Figure 4.7. Salt bridges formed in each system throughout the MD simulations and their % distribution according to the types indicated as ASP-/ARG+ (dark gray bar), ASP-/LYS+ (dark blue bar), GLU-/ARG+ (light gray bar), and GLU-/LYS+ (light blue bar).

MM-GBSA ΔG was calculated for each frame for the MD simulation trajectories. The average binding free energy impacts of the energy components in protein-ligand interactions were obtained from each calculated trajectory frame for the co-crystallized ligand and top three hit compounds as presented in Table 4.10 and Figure 4.8.

Table 4.10. Minimum, maximum, average binding free energy values of the top three ligands, and U41

	Binding free energy (kcal/mol)			
	STOCK2S-34127	STOCK3S-69016	STOCK2S-94986	U41
Minimum	-56.12	-56.90	-54.75	-47.60
Maximum	-33.28	-45.98	-23.16	-35.10
Average	-47.90	-51.53	-43.37	-42.46
Standard deviation	± 3.55	± 2.51	± 5.16	± 2.64

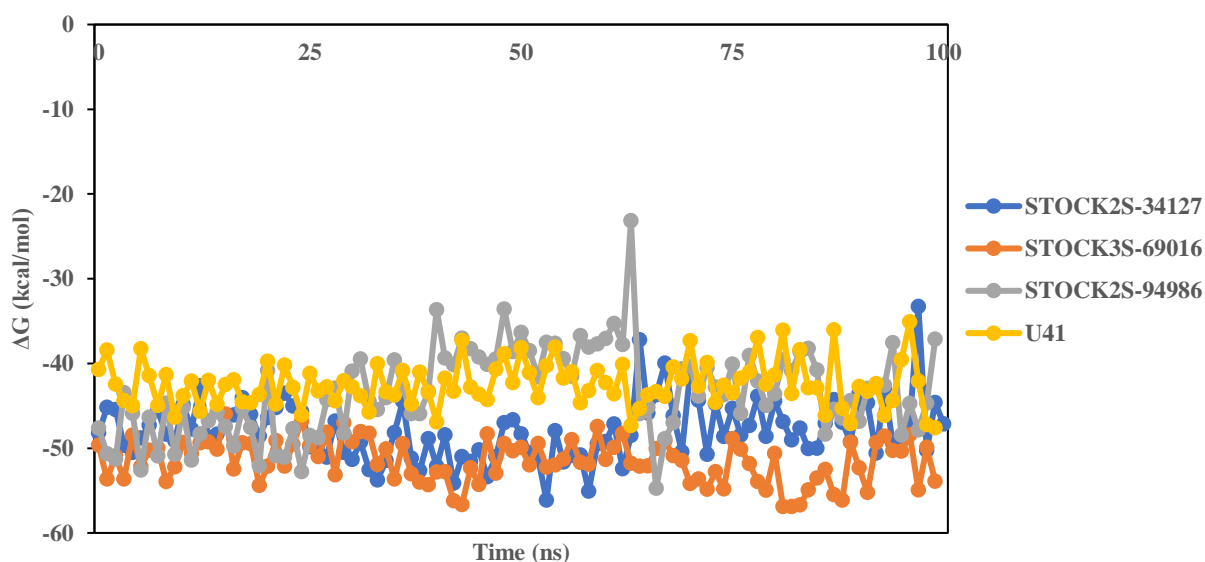


Figure 4.8. ΔG variation over time for ligand-bound IDO1 structures

All complexes showed favorable binding with good binding free energy during the 100 ns MD simulations. Among them, the IDO1- STOCK3S-69016 complex tended to have the highest relative binding affinity (average $\Delta G = -51.55$ kcal/mol), followed by the IDO1-STOCK2S-34127 complex and IDO1-STOCK2S-94986 complex, with average ΔG values of -47.90 and -43.31 kcal/mol, respectively. The IDO1-U41 complex displayed the lowest binding affinity with the average ΔG value of -42.51 kcal/mol. It is worth noting that these total binding free energies were calculated

without considering entropic considerations, as obtaining a converged value for conformational entropy is challenging (219).

4.4. Toxicity Prediction

The findings indicated that all the candidate compounds were categorized into toxicity class 5. This classification aligns with the predicted oral LD₅₀ values, where STOCK2S-34127, STOCK3S-69016, and STOCK2S-94986 had values of 2580, 2500, 2580 mg/kg, respectively. Concerning hepatotoxicity prediction, STOCK3S-69016 and STOCK2S-94986 exhibited a tendency toward hepatotoxicity, while STOCK2S-34127 was considered non-hepatotoxic since the prediction was inactive. Regarding various toxicity endpoints, STOCK2S-34127 was anticipated to be a carcinogen, whereas STOCK2S-94986 was deemed potentially immunotoxic. Additionally, all compounds exhibited 48-hour LC₅₀ values for *Daphnia magna* of 2.43, 2.65, and 0.79 mg/L for STOCK2S-34127, STOCK3S-69016 and STOCK2S-94986, respectively. All compounds also showed very low BCF values, with the values of 4.53, 11.42, 18.16 for STOCK2S-34127, STOCK3S-69016 and STOCK2S-94986, respectively. Moreover, within the realm of 21st Century toxicology, known as Tox21, the two distinct pathways, namely the nuclear receptor signaling pathways and the stress response pathways, were shown inactive in all compounds (Table 4.11).

Table 4.11. Toxicity Prediction of top three candidate compounds

Toxicity Parameters	STOCK2S-34127	STOCK3S-69016	STOCK2S-94986
Predicted Toxicity Class	5	5	5
Organ toxicity			
Hepatotoxicity	Inactive	Active	Active
Toxicity end points			
Carcinogenicity	Active	Inactive	Inactive
Immunotoxicity	Inactive	Inactive	Active
Mutagenicity	Inactive	Inactive	Inactive
Cytotoxicity	Inactive	Inactive	Inactive
<i>Daphnia magna</i> LC ₅₀ (48hr) (mg/L)	2.43	2.65	0.79
Predicted LD ₅₀ (mg/kg)	2580	2500	2580
Bioconcentration factor	4.53	11.42	18.16
Tox21-Nuclear receptor signaling pathways			
Aryl hydrocarbon Receptor (AhR)	Inactive	Inactive	Inactive
Androgen Receptor (AndR)	Inactive	Inactive	Inactive
Androgen Receptor Ligand Binding Domain (AR-LBD)	Inactive	Inactive	Inactive
Aromatase	Inactive	Inactive	Inactive
Estrogen Receptor Alpha (ER)	Inactive	Inactive	Inactive
Estrogen Receptor Ligand Binding Domain (ER-LBD)	Inactive	Inactive	Inactive
Peroxisome Proliferator Activated Receptor Gamma (PPAR-Gamma)	Inactive	Inactive	Inactive
Tox21-Stress response pathways			
Nuclear factor (erythroid-derived 2)-like 2/antioxidant responsive element (nrf2/ARE)	Inactive	Inactive	Inactive
Heat shock factor response element (HSE)	Inactive	Inactive	Inactive
Mitochondrial Membrane Potential (MMP)	Inactive	Inactive	Inactive
Phosphoprotein (Tumor Suppressor) p53	Inactive	Inactive	Inactive
ATPase family AAA domain-containing protein 5 (ATAD5)	Inactive	Inactive	Inactive

5. DISCUSSION

The study aims to propose new small-molecule inhibitors specifically targeting apo-IDO1 through virtual screening, including both ligand- and structure-based approaches. Exploring the inhibition of apo-IDO1, or type IV IDO1 inhibition, offers an alternative strategy to reduce the conversion of tryptophan, specifically targeting the heme-free form of IDO1 enzyme. Heme is included as cofactor in many enzymes prevalent in the body, thus heme-binding inhibitors risk interacting off-targets. According to Nelp et al. (2018), heme cofactor of IDO1 is labile, dynamic, and reversible (27). Additionally, a communication link exists between IDO1 and heme catabolism facilitated by heme oxygenase 1, resulting in reduced IDO1 activity due to heme starvation (228). Heme oxygenase belongs to a group of heme-sparing agents crucial in creating the apo-form of IDO1. Consequently, focusing on the apo-IDO1 provides a unique approach to counteracting immunosuppression.

So far, only BMS-986205, a type IV IDO1 inhibitor, has progressed to phase III clinical trials. On the other hand, several compounds have been identified as inhibitors of apo-IDO1, with GSK5628 being one of them. GSK5628 can effectively compete with the IDO1 heme cofactor, enabling it to bind to apo-IDO1 (101). However, given that only one compound has reached clinical trials, there is a need to explore and identify new compounds that are structurally diverse and have the potential to inhibit the apo-form of IDO1.

This study commenced by obtaining a commercial database of 69,064 natural and 481,493 synthetic compounds from the IBS. Initially, these database compounds were modelled and geometrically optimized. The first filtering step of the database compounds in the virtual screening process involved the calculation of molecular descriptors for drug-likeness. Utilizing drug-likeness filters in drug discovery provides a significant benefit by directing the overall chemical space toward the desired chemical space. Since compounds with similarities tend to share a comparable chemical space, and similar compounds generally exhibit similar activity, narrowing down the chemical space through drug-likeness filtering theoretically enhances the likelihood of identifying potential drugs (229,230).

The criteria for filtering included MW, HBD and HBA counts, and predicted logP. The first four criteria mentioned are commonly associated with the Lipinski's Rule of Five, widely used in medicinal chemistry to assess the likelihood of small molecules in terms of its oral bioavailability and permeability (106). However, for this study, we followed the reference values specified by the utilized software, which provides recommended values based on the properties of 95% of known drugs. Additional criteria included number of rotatable bonds and tPSA (231). Moreover, taking into account the presence of reactive functional groups (rtvFG), as their presence could lead to false positives in high-throughput screening assays (232), thus, compounds containing any rtvFG were excluded from consideration. As a result, a total of 394,609 compounds were selected for LBVS.

The ligands that passed through the drug-likeness filtering process were subsequently subjected to ligand-based virtual screening, which included shape similarity and pharmacophore modeling. In this study, five query structures, namely QPV, U41, U6G, SLW, and 6RI, which have been reported for their potent and selective inhibitory effects on apo-IDO1, were utilized. These structures were elucidated as apo-IDO1 binders within the IDO1 PDB structures, specifically 6v52, 6wjy, 6wpe, 7b1o, and 7rrc, respectively.

During the shape screening step, the five small inhibitors mentioned above served as query compounds. Shape screening was performed via a Gaussian overlay technique which defines a molecule's shape based on its volume, determined using a formula that combines various sets and their intersections. The Gaussian sphere model is used to represent a molecule by utilizing a collection of overlapping Gaussian spheres and computing the integral volume across all these overlapping Gaussians. To represent the molecular shape of a reference molecule, a Gaussian function is utilized. This function is employed to create a 3D volumetric map that characterizes the shape of the molecule. To compare the shape of a group of ligands to the reference molecule, a similar representation based on Gaussian functions is generated for the target molecules. The similarity between the shapes of these two molecules is evaluated by superimposing these Gaussian functions and calculating a similarity score. The greater the resemblance between the shapes of the two molecules, the higher the resulting similarity score (126,233). In this study, the preference was to select the top 2.5% to

pass on to the SBVS step rather than defining a similarity score cut-off since similarity score ranges vary depending on the query structures.

Conversely, in pharmacophore-based virtual screening, the process initiated with the creation of pharmacophore hypotheses, which served as templates or pharmacophore models. Unlike shape similarity, which exclusively employed query ligand structures, the pharmacophore models utilized ligand-enzyme complexes as templates. This approach has the potential to uncover the essential interactions within the binding active site of protein. The primary objective of this screening was to identify molecules that possess chemical features mimicking the ligand-receptor interactions featured by the pharmacophore model. The initial step involved the establishment of pharmacophore sites for each model. Pharmacophore sites represent the shared structural features or specific spatial arrangements of atoms or functional groups within a molecule that are essential for its interaction with a biological target, specifically in the context of apo-IDO1 enzymes. These sites, also referred to as pharmacophoric features, are fundamental elements that contribute to the molecule's capacity to bind to and influence the target or enzyme. These sites encompass characteristics such as hydrogen bond acceptor or donor (A or D), aromatic rings (R), hydrophobic regions (H), negatively charged group (N), and positively charged group (P). Subsequently, the refined ligand library was screened against the five pharmacophore models and the ligands were ranked according to their Phase screen scores.

Similar as shape screening, the preference was to select the top 2.5% of the screened libraries according to Phase screen scores and filter off the rest since for each pharmacophore model the Phase screen score ranges vary like in the case of similarity scores. While some of these hits may resemble known active compounds, others could introduce entirely new structural frameworks (131). The quest for compounds with different structural backbones, while maintaining a shared biological activity, is commonly known as scaffold hopping (31). This aspect represents a fundamental contrast between pharmacophore modeling and shape similarity. While shape similarity focuses on the functional groups present in the screened ligands compared to the reference ligand, pharmacophore screening places significant emphasis on the types of possible interactions, such as hydrogen bonds, charged interaction, metal

interactions, hydrophobic, and aromatic interactions (136). Consequently, the pharmacophore screening has the potential to yield structurally diverse compounds that align with the template in terms of interaction types.

Following the two ligand-based virtual screening approaches, the selection process involved choosing the top 2.5% of the most promising ligands from each approach for further assessment in the context of structure-based virtual screening. Subsequently, all the filtered ligands from each database were combined, eliminating any duplicate entries, adding up to 71,241 compounds.

Before advancing to the structure-based virtual screening phase, validation studies including redocking and enrichment studies were conducted to ensure that the molecular docking protocol works and to determine which PDB structure should be utilized in subsequent steps. First redocking of each co-crystallized inhibitor of the five apo-IDO1 structures to its respective receptor was performed. Typically, the predictive quality of the docking procedure was assessed by comparing the predicted binding poses with the original poses of the co-crystallized inhibitors. This was achieved by measuring the RMSD value which should ideally be lower than 2.0 Å. The outcomes suggest that the docked poses align closely with the original ligand within the binding site of the apo-IDO1 enzyme (Figure 4.2) with RMSD values below 0.5 Å, indicating reliability of the molecular docking process.

Enrichment capacity of a molecular docking model, in this context, serves as a measure of the virtual screening method's performance in distinguishing known active compounds from decoys or inactive compounds. True positives, which are the known active compounds correctly identified by the virtual screening method, play a crucial role in this calculation. The higher the number of true positives identified during the enrichment calculation, the greater the enrichment factor. This, in turn, signifies the effectiveness of the virtual screening method in identifying active compounds within the database and enriching the dataset with such active compounds, surpassing what would be expected by random selection. In this study, PDB ID 6wjy demonstrated the most favorable enrichment factor, as indicated by metrics such as AUC-ROC of 0.90, RIE of 12.73, and EF of 39.0, 35.0, 14.0, 8.5, and 4.2 at 1%, 2%, 5%, 10%, and 20%, respectively.

In the subsequent step, molecular docking studies were conducted for all the filtered ligands using the apo-IDO1 structure with PDB ID 6wjy. Firstly, the ligands were docked at the SP mode and those with docking scores lower than -10.00 kcal/mol were selected, which added up to of 8033 compounds. These compounds were redocked and rescored at XP mode and the top-scoring 500 compounds with three best poses for each were selected. The XP mode involves a more thorough sampling process compared to the SP mode. It initiates with SP sampling before implementing its unique anchor-and-grow procedure. The XP mode also utilizes a more advanced scoring function, which is more stringent than the SP mode. This stricter scoring function places higher demands on the shape compatibility between the ligand and the receptor, effectively eliminating false positives that might be allowed through by SP (148).

For the 500 selected compounds with three poses each, ΔG was calculated using MM-GBSA method. In addition, a fingerprint similarity clustering was performed to ensure structural diversity among the candidate compounds, which resulted a clustering strain of 1.083. The clustering strain expresses the ratio between the total distances of neighboring pairs in the dendrogram and the total distances between the nearest neighbors in all pairs. A lower strain value (minimum 1.0) indicates a more precise alignment of the dendrogram's order with the actual distances between objects. Furthermore, the fingerprint similarity yielded 54 clusters, consisting of eight natural and 46 synthetic compounds.

Compounds with the best MM-GBSA ΔG values, listed sequentially, included STOCK2S-34127, STOCK3S-69016, STOCK2S-94986, STOCK7S-27591, STOCK7S-17282, STOCK6S-24185, STOCK3S-41956, STOCK1N-68588, STOCK6S-48507, and STOCK6S-09214. Within the top 10 chosen compounds, only three (STOCK2S-34127, STOCK3S-69016, and STOCK2S-94986) exhibited better MM-GBSA ΔG values than U41 and demonstrated structural diversity. These three hits, along with U41, were then visually inspected to reveal the involved residues, interaction types, and the binding location of the residues.

According to Röhrig et.al. (2021), the structure of apo-IDO1 inhibitors comprises three different moieties binding to different pockets. The central moiety binds to the heme-binding pocket, while the two side moieties bind to pocket A and D (76). Different

compounds exhibited distinct interaction patterns. As shown in the Figure 5.1, each compound can be divided into three moieties that bind to different pocket. The central moieties for each compound consist of 3-(3-oxobutyl)-2-thioxothiazolidin-4-one, *N*-(5-(methylthio)-1,3,4-thiadiazol-2-yl)acetamide, 1,3,4-thiadiazol, and (*S*)-3-(3-(methylamino)bicyclo[1.1.1]pentan-1-yl)butan-2-one, which occupied the heme-binding pocket for STOCK2S-34127, STOCK3S-69016, STOCK2S-94986, and U41, respectively.

The moieties occupying pocket A include 5-ethyl-*N*-methyl-1,3,4-thiadiazol-2-amine, *N*-(4-chlorophenyl)acetamide, 1-(2-fluorophenyl)-3-methylurea, and 4-fluoro-*N*-methylaniline from STOCK2S-34127, STOCK3S-69016, STOCK2S-94986, and U41, respectively. On the other side, the moieties occupying pocket D consist of 1-bromo-3-vinylbenzene, 1-chloro-2-methylbenzene, (2,4-dichlorobenzyl)(methyl)sulfane, and 1-(3-chlorophenyl)ethan-1-one for STOCK2S-34127, STOCK3S-69016, STOCK2S-94986, and U41, respectively. Each compound was then visually inspected to reveal the interaction type of each moiety for each compound (Figure 5.1).

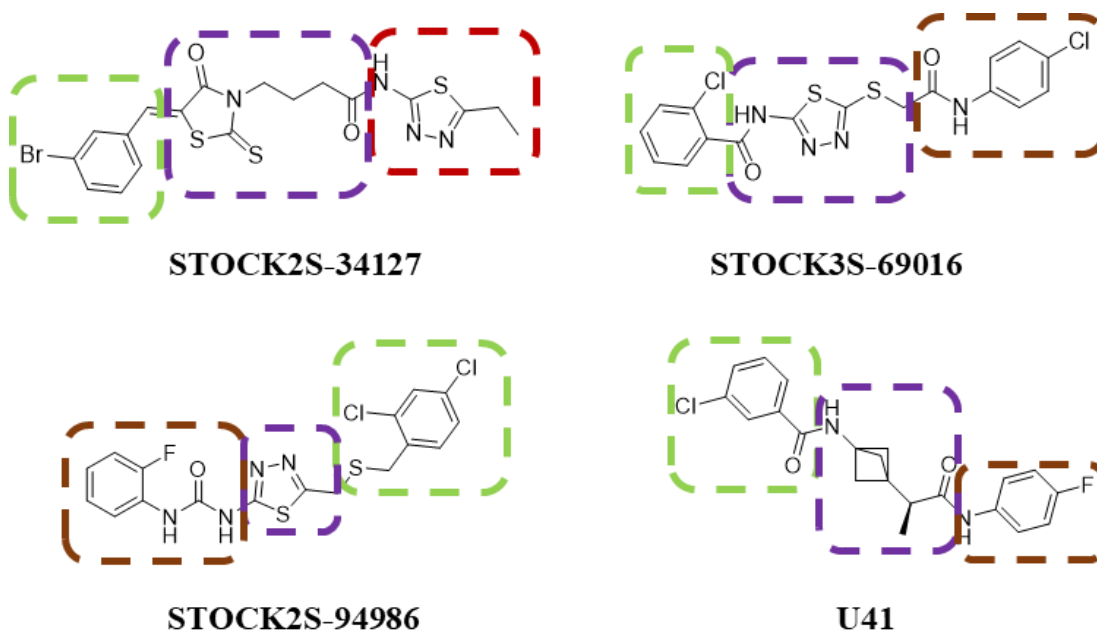


Figure 5.1. The selected hits from virtual screening along with U41, and their three moieties concerning apo-IDO1 are illustrated. The brown-dashed regions fit in pocket A, the purple-dashed regions in heme-binding pocket, and the green-dashed regions in pocket D of the apo-IDO1 active site.

Receptor interactions of the three hits, along with U41, were visually inspected, revealing a common hydrogen bond interaction with SER167 among all compounds. Compound STOCK2S-94986 formed two distinct hydrogen bonds with SER167 at distances of 1.97 Å and 2.19 Å (Table 4.9 and Figure 5.2). These interactions align with the finding by White et al. (2020), indicating that U41 formed a hydrogen bond with the side chain of SER167 in the pocket A region via its amide NH (103).

With the exception of compound STOCK2S-94986, all compounds exhibited water-mediated hydrogen bond interactions with ARG343 and HIS346. The water molecules play as mediator between the amide carbonyl oxygen and the side chain of HIS346. Differently, STOCK2S-94986 exhibited a different type of interaction with HIS346, forming π - π stacking since there was no water molecule. Almost all compounds exhibited π - π stacking interactions with TYR126, except for compound STOCK2S-34127. Furthermore, π - π stacking was also observed with PHE214 in the case of compounds STOCK3S-69016 and STOCK2S-94986 (Figure 5.2).

The following stage was MD simulations of the apo-IDO1 structure in complex with the selected three hits and U41, as well as at ligand-free state. In recent years, there has been a significant increase in research related to MD simulations, as evidenced by the growing number of published papers on the subject (140). This surge in interest is primarily attributed to the valuable insights provided by MD simulations, which offer a detailed understanding of the dynamic evolution of the molecules within complex systems through a limited time scale. These insights are often challenging to obtain through experimental techniques alone. Moreover, MD simulations shed light on the dynamic behavior of water molecules and salt ions within the system. This information is essential for understanding the critical roles these elements play in protein function and ligand binding (234–236). In the context of drug discovery, MD simulations offer several advantages. It is possible to monitor stability of key ligand-receptor interactions at atomic level and predict any structural rearrangements induced by the ligand (237). Importantly, these simulations can provide more accurate estimates of ligand binding affinities compared to traditional molecular docking methods (238).

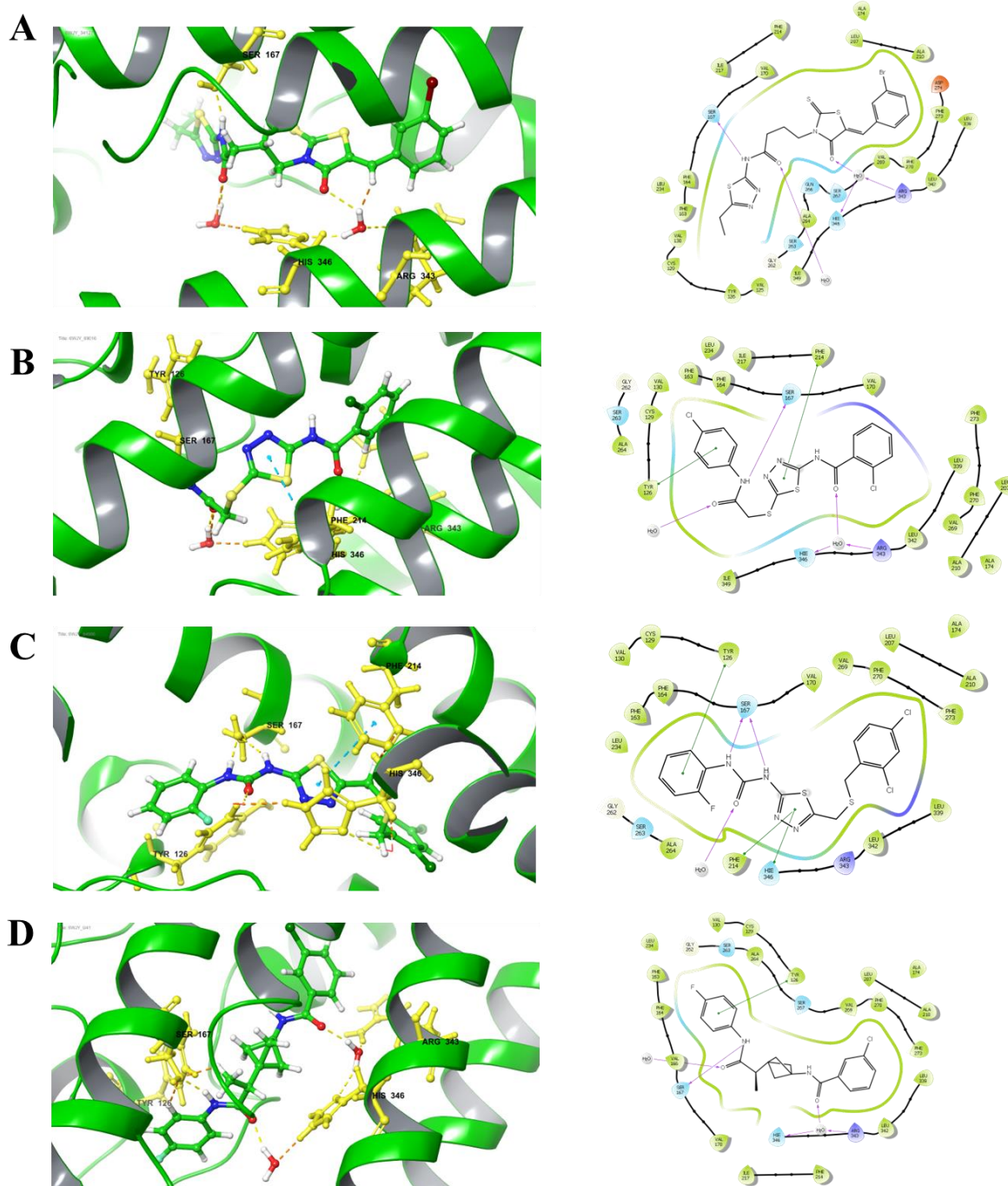


Figure 5.2. The 3D and 2D interaction visualizations of (A) STOCK2S-34127, (B) STOCK3S-69016, (C) STOCK2S-94986, and (D) U41 were presented. The docked ligands were depicted as green stick-and-ball representations, the involved residues shown in yellow stick-and-ball representations, and the protein backbones are presented in green ribbons.

In this study, MD simulations were performed to assess structural/conformational changes and stability (as indicated by RMSD values), residue fluctuations (as indicated by RMSF values), compactness in protein-ligand complexes (as indicated by RoG values), salt bridge formation, and variation of ligand-receptor affinity (as indicated by MM-GBSA ΔG). A set of five IDO1 systems was employed, including the complexes with the three hit compounds and the co-crystallized ligand, U41, and one ligand-free system. The ligand-free system served as a reference state to investigate the response of the biomolecular system to perturbations in the absence of a ligand, a concept supported by prior studies (239,240). The ligand-free system allowed us to detect atomic level conformational changes and compare them to the complex with ligands. The average protein backbone atoms RMSD values of the five systems through 100 ns were very close to each other ranging from 1.44 Å to 1.76 Å, showing that the stability of IDO1 was maintained when bound to the inhibitors. It strengthened with the total energy of each complex basically in a stable state, with average total energies of -209,232, -209,380, -209,297, -209,020, and -209,204 kcal/mol for complexes with STOCK2S-34127, STOCK3S-69016, STOCK2S-94986, U41, and ligand-free, respectively (Figure 5.3).

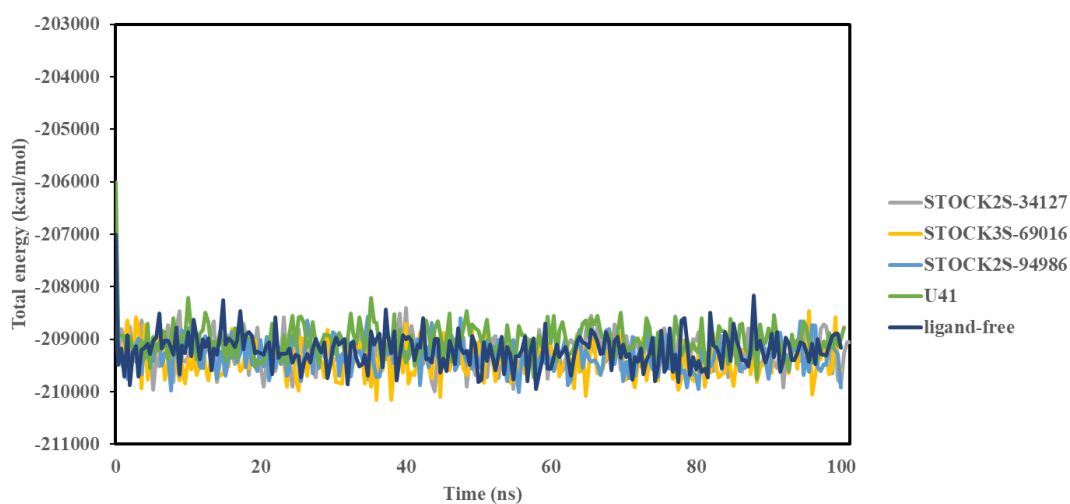


Figure 5.3. Total energy plots of the protein complexes with ligand-bound states and the ligand-free state during 100 ns of MD simulations.

Residue fluctuations were analyzed to discern the flexibility or rigidity of individual residue and pinpoint the significant interactions between the ligand and the protein receptor. In this study, there were four distinct regions that exhibited sharp fluctuations

as indicated by the RMSF values of C α atoms: (i) MET10, the first N terminal residue, (ii) the region between GLY284 and ALA288, (iii) the region between SER359 and PRO362, and (iv) the final region in the terminal sequence between LEU400 and LYS401. The region (i) belongs to the N-terminus domain (NTD), while regions (ii), (iii), and (iv) belong to the C-terminus domain (CTD). Compared to the NTD (residues 1-154), the CTD has larger residues (residues 155-403), and comprises 13 α -helices (G-S) and two 3_{10} helices (81,241). In this RMSF assessment, the marked residues, particularly residues in region (ii) such as HIS287 and ALA288 in the F helix and SER359 in the I helix from region (iii), show fluctuations. The observed fluctuations in these residues suggest reduced stability, leading to their exclusion as key residue interactions in the apo-IDO1 complex. These four regions were far from the active site, as depicted in Figure 5.4.

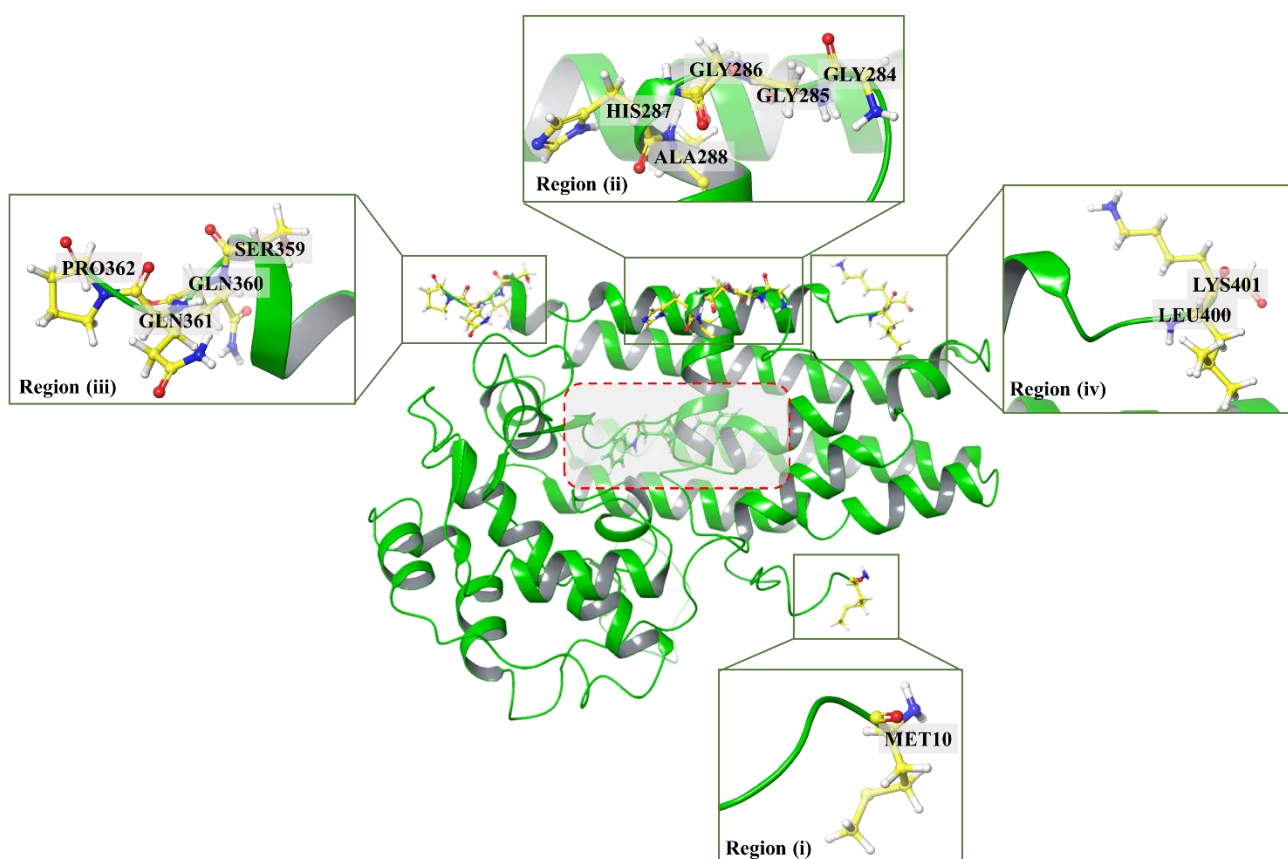


Figure 5.4. The four regions that experienced the most fluctuation according to RMSF values are highlighted. The active site is represented by the red-dashed box, and residues are depicted using yellow stick-and-ball representations.

Another aspect of evaluation is the compactness of the system, which is indicated by the RoG values of all protein atoms. All complexes demonstrated good compactness, with the differences between the maximum and minimum RoG values for each complex remaining below 1.0 Å throughout the simulations. The IDO1-STOCK2S-34127 complex displayed the smallest difference, with the value of 0.352 Å, suggesting that it was the most compact system among all the complexes.

Additionally, the creation of salt bridges in MD simulations is a significant factor in increasing the stability of complex systems at elevated temperatures when contrasted with standard room temperature conditions (242). Salt bridges, in essence, represent the electrostatic interactions occurring between positively charged amino acids like lysine, arginine, and histidine, and negatively charged amino acids such as aspartic acid and glutamic acid within a biomolecular system (243). Several salt bridges were observed to form throughout 100 ns of MD simulations from each complex. Each complex exhibited these salt bridge interactions, and a total of 33 identical salt bridges were formed across all complexes. When considering various combinations of salt bridge interaction, such as ASP-/ARG+, ASP-/LYS+, GLU-/ARG+, and GLU-/LYS+, it was observed that salt bridges containing LYS+ were more prevalent than those containing ARG+. This finding contrasts with the previous research, which suggested that ARG+ containing salt bridges were dominant over LYS+ containing salt bridges due to the guanidinium group's resonance stabilization (244,245). However, this result could be influenced by several factors, including the distance between interacting residues, the presence of other charged residues nearby, and the orientation of each side chain.

Precise theoretical calculations of binding free energies using numerical simulation have gained increasing importance in various research areas, including rational drug design, protein folding, protein-protein interactions (PPIs) and drug design (246). In the context of drug design, binding free energy is frequently employed to assess the strength of interaction between a receptor and a drug molecule, as finding the most potent ligand toward certain receptor is a key objective (247). Several approaches have been successfully employed for theoretical free energy calculations. Molecular docking and alchemical free energy (AFE) techniques play crucial roles in estimating binding free energy affinities for such complexes. Molecular docking offers

advantages in virtual screening by providing efficient and cost-effective predictions of binding affinity. However, it has shortcomings in terms of accuracy (248,249). On the other hand, AFE methods, such as FEP and thermodynamic integration (TI), which are theoretically accurate and rigorous but suffer from slower execution, have substantial environmental reorganization and high computational cost. In the quest for an appropriate binding free energy method that combines accuracy and efficiency, it is recommended to utilize the widely recognized end-point binding free energy method developed by Kollman, known as MM-GBSA (250). The main distinction, beside accuracy and efficiency, lies in its incorporation of implicit solvent and entropic effects in MM-GBSA calculations, which are not included in molecular docking and AFE methods (247).

The stability of five complexes exhibited good results after MD simulations for 100 ns. These results confirmed that the binding of all ligands in the binding site of apo-IDO1 were firm and steady. However, the trajectories of all complexes should be analyzed in terms of changes in ΔG to further measure how stable ligand-receptor complexes were. As explained in the previous section, the formula for calculating ΔG primarily comprises enthalpy energy (ΔH) and conformational entropy associated with ligand binding ($-T\Delta S$). ΔH can be computed by summing the molecular mechanics energy in the gas phase (ΔE_{MM}) and solvation free energy (ΔG_{sol}). ΔE_{MM} encompasses changes in the internal energies (ΔE_{int} , including bond, angle, and dihedral angles), electrostatic energies (ΔE_{ele}), and the van der Waals energies (ΔE_{vdw}). Conversely, ΔG_{sol} consists of the electrostatic polar contribution, including ΔG_{GB} , and the nonpolar contribution, encompassing ΔG_{SA} . It is worth noting that conformational entropy related to ligand binding is often omitted due to its substantial computational demands (247). In this study, all complex systems exhibited favorable outcome, as evidenced by the average ΔG values. The complex involving STOCK3S-69016 displayed the most favorable binding free energy with a ΔG value of -51.55 kcal/mol, followed by the IDO1- STOCK2S-34127 complex, IDO1- STOCK2S-94986 complex, and IDO1-U41 complex with ΔG values of -47.90, -43.31, and -42.51 kcal/mol, respectively. The complex with STOCK3S-69016 also showed the lowest standard deviation at 2.51 kcal/mol, within the range of -56.90 to -45.98 kcal/mol, indicating that variability in ΔG values was relatively limited. In contrast, the IDO1-STOCK2S-94986 complex

appeared to be the most unstable, exhibiting a standard deviation value of 5.16 kcal/mol within the range of -54.75 to -23.16 kcal/mol. This instability of the binding affinity in the IDO1-STOCK2S-94986 complex was visually represented in grey, indicating the most fluctuated binding free energy among the other complexes, as illustrated in Figure 4.8. Based on these results, it can be concluded that MM-GBSA ΔG values align with the results of molecular docking prior to MD simulations.

In summary, all the complexes displayed favorable outcomes, which encompassed changes in structural conformation and stability, variations in residue fluctuations, good compactness, the formation of salt bridges, and favorable binding free energy as represented by RMSD, RMSF, RoG values, salt bridge interaction, and MM-GBSA ΔG values.

In the last evaluation, toxicity predictions using various parameters were conducted. This predictive analysis plays a crucial role in assisting researchers in identifying and prioritizing compounds that exhibit both safety and efficacy for human use. As noted by Vo et.al. (2020), it is estimated that more than 30% of drug candidates are rejected due to toxicity concerns (251,252). The integration of *in silico* computational methods for toxicity prediction offers a cost-effective and rapid means of obtaining data, potentially expediting drug development in the absence of expensive, time-consuming and labor-intensive animal testing (*in vivo*) or cell studies (*in vitro*) (253). This study employed ProTox-II and TEST, both AI-based tools, to assess the toxicity of chemicals and considered a combination of parameters from two different tools encompassing predicted toxicity class, organ toxicity (hepatotoxicity), and various toxicity end points including carcinogenicity, immunotoxicity, mutagenicity, cytotoxicity, *Daphnia magna* LC₅₀ (48hr), predicted oral LD₅₀, and bioconcentration factor. The top three compounds were identified as relatively safe with a predicted toxicity class of 5, corresponding to LD₅₀ value in the range between 2000 and 5000 mg/kg (254). Compounds STOCK3S-69016, and STOCK2S-94986 showed potential activity as hepatotoxic agent, while STOCK2S-34127 exhibited potential activity as carcinogenic agent, indicating its potential to cause cancer. STOCK2S-94986 was predicted to have immunotoxic effects, with possible adverse effects on the immune system. Assessments using an aquatic organism, specifically *Daphnia magna*, was also conducted to evaluate the toxicity of the candidate compounds in an aquatic

environment (221,222). All compounds demonstrated moderate concern towards *Daphnia magna* within the concentration range of 0.1 to 10 mg/L (221,255). On the other hand, all compounds also had very low BCF values, making them less likely to bioaccumulate in aquatic organisms (223). However, organ toxicity should be validated both *in vitro* and *in vivo* to ensure the accurate assessment of the toxic effects of these compounds. In this study Tox21 assay end point predictions were also conducted. Tox21 itself is an abbreviation from the toxicology in the twenty-first century program. This program is a collaboration between the National Institutes of Health, the Environmental Protection Agency, and the FDA, aims to improve toxicity evaluation methods (253,256). In recent years, there has been notable advancement in creating robust AI models for predicting toxicity, particularly utilizing the Tox21 dataset. One of them accommodated by ProTox-II web server. There are two pathways to take into account: the nuclear receptor signaling pathways and the stress response pathways. In the nuclear receptor signaling pathways, all the compounds displayed inactivity across all seven target-pathways encompassing the aryl hydrocarbon receptor (AhR), androgen receptor (AndR), androgen receptor ligand binding domain (AR-LBD), aromatase, estrogen receptor alpha (ER), estrogen receptor ligand binding domain (ER-LBD), and peroxisome proliferator activated receptor gamma (PPAR-Gamma). Similar with the previous signaling pathway, the stress response pathways also exhibited inactive in all five pathways encompassing the nuclear factor (erythroid-derived 2)-like 2/antioxidant responsive element (nrf2/ARE), heat shock factor response element (HSE), mitochondrial membrane potential (MMP), phosphoprotein (tumor suppressor) p53, and ATPase family AAA domain-containing protein 5 (ATAD5). Both pathways were shown inactive in all compounds. This assessment and predictive analysis suggest that all the compounds yielded favorable outcomes across multiple parameters (Table 4.7).

6. CONCLUSION AND RECOMMENDATION

6.1. Conclusion

In summary, three compounds were identified as potential and elective apo-IDO1 inhibitors through virtual screening of a commercial ligand database. Below are several key findings of this study.

1. From a total of 550,557 compounds, about 394,609 compounds were met the criteria and reference values of drug-likeness parameters.
2. Using a combination of parallel ligand-based approaches from both shape similarity and pharmacophore modelling screening, the study successfully eliminated compounds, leaving 71,241 compounds.
3. The molecular docking method was validated with the RMSD values below 2.0 Å, and PDB ID 6wjy was selected due to the best result in enrichment study.
4. In molecular docking study, the top-scoring 500 compounds were successfully screened, and their MM-GBSA ΔG were calculated and ranked accordingly. The study resulted in the identification of the top 10 compounds with structural diversity after fingerprint similarity evaluation.
5. STOCK2S-34127, STOCK3S-69016, and STOCK2S-94986 were evaluated for conformational changes and atomic behavior through MD simulations, resulting in favorable stability, compactness, identification of several unstable residues, and the formation of salt bridges. Additionally, STOCK3S-69016 displayed the most favorable binding free energy with ΔG value of -51.55 kcal/mol.
6. The three hits were predicted to show low oral toxicity, moderate toxicity to *Daphnia magna*, low bioaccumulation in aquatic environments, and be inactive in both nuclear receptor signaling and stress response pathways of toxicity.

6.2. Recommendation

The identified virtual hits hold promise as a starting point to identify potential candidates as adjunct therapeutics to immune checkpoint inhibitors for cancer. These candidates are presumed to possess potent apo-IDO1 inhibition, along with qualities such as safety, good pharmacokinetics, and the ability to spare off-targets. However, further studies, including *in vitro* and *in vivo* experiments, are necessary to confirm their activity, selectivity, and potential as preclinical candidates for apo-IDO1 inhibitors.

7. REFERENCES

1. Basak D, Arrighi S, Darwiche Y, Deb S. Comparison of Anticancer Drug Toxicities: Paradigm Shift in Adverse Effect Profile. *Life*. 2021 Dec 29;12(1):48.
2. Rivera E, Gomez H. Chemotherapy resistance in metastatic breast cancer: the evolving role of ixabepilone. *Breast Cancer Research* [Internet]. 2010 Oct [cited 2023 Jun 6];12(S2). Available from: <https://breast-cancer-research.biomedcentral.com/articles/10.1186/bcr2573>
3. Bell DJ, Kerr DJ. Pharmacokinetic considerations in the use of anticancer drugs during pregnancy: challenges and new developments. *Expert Opinion on Drug Metabolism & Toxicology*. 2015 Sep 2;11(9):1341–4.
4. Abbott M, Ustoyev Y. Cancer and the Immune System: The History and Background of Immunotherapy. *Seminars in Oncology Nursing*. 2019 Oct;35(5):150923.
5. Buqué A, Bloy N, Aranda F, Castoldi F, Eggermont A, Cremer I, et al. Trial Watch: Immunomodulatory monoclonal antibodies for oncological indications. *OncoImmunology*. 2015 Apr 3;4(4):e1008814.
6. Canada H. Drug Product Database: Access the database [Internet]. 2010 [cited 2023 Jun 22]. Available from: <https://www.canada.ca/en/health-canada/services/drugs-health-products/drug-products/drug-product-database.html>
7. Hodi FS, Chiarion-Sileni V, Gonzalez R, Grob JJ, Rutkowski P, Cowey CL, et al. Nivolumab plus ipilimumab or nivolumab alone versus ipilimumab alone in advanced melanoma (CheckMate 067): 4-year outcomes of a multicentre, randomised, phase 3 trial. *The Lancet Oncology*. 2018 Nov;19(11):1480–92.
8. Kareva I, Hahnfeldt P. The Emerging “Hallmarks” of Metabolic Reprogramming and Immune Evasion: Distinct or Linked? *Cancer Research*. 2013 May 1;73(9):2737–42.
9. Li J, Eu JQ, Kong LR, Wang L, Lim YC, Goh BC, et al. Targeting Metabolism in Cancer Cells and the Tumour Microenvironment for Cancer Therapy. *Molecules*. 2020 Oct 20;25(20):4831.
10. Chang CH, Qiu J, O’Sullivan D, Buck MD, Noguchi T, Curtis JD, et al. Metabolic competition in the tumor microenvironment is a driver of cancer progression. *Cell*. 2015 Sep 10;162(6):1229–41.
11. Esfahani K, Roudaia L, Buhlaiga N, Del Rincon SV, Papneja N, Miller WH. A Review of Cancer Immunotherapy: From the Past, to the Present, to the Future. *Current Oncology*. 2020 Apr 1;27(12):87–97.

12. Stone TW, Stoy N, Darlington LG. An expanding range of targets for kynurenine metabolites of tryptophan. *Trends in Pharmacological Sciences*. 2013 Feb;34(2):136–43.
13. de Almeida VM, Santos-Filho OA. Identification of Potential Allosteric Site Binders of Indoleamine 2,3-Dioxygenase 1 from Plants: A Virtual and Molecular Dynamics Investigation. *Pharmaceuticals*. 2022 Sep 2;15(9):1099.
14. Munn DH, Sharma MD, Baban B, Harding HP, Zhang Y, Ron D, et al. GCN2 Kinase in T Cells Mediates Proliferative Arrest and Anergy Induction in Response to Indoleamine 2,3-Dioxygenase. *Immunity*. 2005 May;22(5):633–42.
15. Eleftheriadis T, Pissas G, Antoniadis G, Liakopoulos V, Tsogka K, Sounidaki M, et al. Differential effects of the two amino acid sensing systems, the GCN2 kinase and the mTOR complex 1, on primary human alloreactive CD4+ T-cells. *International Journal of Molecular Medicine*. 2016 May;37(5):1412–20.
16. Metz R, Rust S, DuHadaway JB, Mautino MR, Munn DH, Vahanian NN, et al. IDO inhibits a tryptophan sufficiency signal that stimulates mTOR: A novel IDO effector pathway targeted by D-1-methyl-tryptophan. *OncoImmunology*. 2012 Dec;1(9):1460–8.
17. Powell JD, Pollizzi KN, Heikamp EB, Horton MR. Regulation of Immune Responses by mTOR. *Annual Review of Immunology*. 2012 Apr 23;30(1):39–68.
18. Munn DH, Mellor AL. Indoleamine 2,3 dioxygenase and metabolic control of immune responses. *Trends in Immunology*. 2013 Mar;34(3):137–43.
19. Zhang G, Xing J, Wang Y, Wang L, Ye Y, Lu D, et al. Discovery of Novel Inhibitors of Indoleamine 2,3-Dioxygenase 1 Through Structure-Based Virtual Screening. *Frontiers in Pharmacology* [Internet]. 2018 Mar 29 [cited 2022 Sep 27];9. Available from: <http://journal.frontiersin.org/article/10.3389/fphar.2018.00277/full>
20. Liu X, Shin N, Koblisch HK, Yang G, Wang Q, Wang K, et al. Selective inhibition of IDO1 effectively regulates mediators of antitumor immunity. *Blood*. 2010 Apr 29;115(17):3520–30.
21. Yue EW, Sparks R, Polam P, Modi D, Douty B, Wayland B, et al. INCB24360 (Epacadostat), a Highly Potent and Selective Indoleamine-2,3-dioxygenase 1 (IDO1) Inhibitor for Immuno-oncology. *ACS Medicinal Chemistry Letters*. 2017 May 11;8(5):486–91.
22. Wang N, Zhang J, Li Q, Xu H, Chen G, Li Z, et al. Discovery of potent indoleamine 2,3-dioxygenase (IDO) inhibitor from alkaloids in *Picrasma quassioides* by virtual screening and in vitro evaluation. *Fitoterapia*. 2019 Mar;133:137–45.

23. Röhrig UF, Reynaud A, Majjigapu SR, Vogel P, Pojer F, Zoete V. Inhibition Mechanisms of Indoleamine 2,3-Dioxygenase 1 (IDO1). *J Med Chem*. 2019 Oct 10;62(19):8784–95.
24. Crosignani S, Bingham P, Bottemanne P, Cannelle H, Cauwenberghs S, Cordonnier M, et al. Discovery of a Novel and Selective Indoleamine 2,3-Dioxygenase (IDO-1) Inhibitor 3-(5-Fluoro-1 *H* -indol-3-yl)pyrrolidine-2,5-dione (EOS200271/PF-06840003) and Its Characterization as a Potential Clinical Candidate. *Journal of Medicinal Chemistry*. 2017 Dec 14;60(23):9617–29.
25. Pham KN, Yeh SR. Mapping the Binding Trajectory of a Suicide Inhibitor in Human Indoleamine 2,3-Dioxygenase 1. *Journal of the American Chemical Society*. 2018 Nov 7;140(44):14538–41.
26. Prendergast GC, Malachowski WP, DuHadaway JB, Muller AJ. Discovery of IDO1 Inhibitors: From Bench to Bedside. *Cancer Research*. 2017 Dec 15;77(24):6795–811.
27. Nelp MT, Kates PA, Hunt JT, Newitt JA, Balog A, Maley D, et al. Immune-modulating enzyme indoleamine 2,3-dioxygenase is effectively inhibited by targeting its apo-form. *Proceedings of the National Academy of Sciences*. 2018 Mar 27;115(13):3249–54.
28. Shoichet BK. Virtual screening of chemical libraries. *Nature*. 2004 Dec;432(7019):862–5.
29. Sari S. Molecular Modelling and Computer-Aided Drug Design: The Skill Set Every Scientist in Drug Research Needs and Can Easily Get. *Hacettepe University Journal of the Faculty of Pharmacy*. 2020 Jan 1;40:34–47.
30. Zoete V, Daina A, Bovigny C, Michielin O. SwissSimilarity: A Web Tool for Low to Ultra High Throughput Ligand-Based Virtual Screening. *J Chem Inf Model*. 2016 Aug 22;56(8):1399–404.
31. Zhao H. Scaffold selection and scaffold hopping in lead generation: a medicinal chemistry perspective. *Drug Discovery Today*. 2007 Feb 1;12(3):149–55.
32. Callis TB, Garrett TR, Montgomery AP, Danon JJ, Kassiou M. Recent Scaffold Hopping Applications in Central Nervous System Drug Discovery. *J Med Chem*. 2022 Oct 27;65(20):13483–504.
33. Ramírez D, Caballero J. Is It Reliable to Take the Molecular Docking Top Scoring Position as the Best Solution without Considering Available Structural Data? *Molecules*. 2018 Apr 28;23(5):1038.
34. Genheden S, Ryde U. The MM/PBSA and MM/GBSA methods to estimate ligand-binding affinities. *Expert Opinion on Drug Discovery*. 2015 May 4;10(5):449–61.

35. Kitchen DB, Decornez H, Furr JR, Bajorath J. Docking and scoring in virtual screening for drug discovery: methods and applications. *Nat Rev Drug Discov*. 2004 Nov;3(11):935–49.
36. Wang L, Wu Y, Deng Y, Kim B, Pierce L, Krilov G, et al. Accurate and Reliable Prediction of Relative Ligand Binding Potency in Prospective Drug Discovery by Way of a Modern Free-Energy Calculation Protocol and Force Field. *J Am Chem Soc*. 2015 Feb 25;137(7):2695–703.
37. Ichim CV. Revisiting immunosurveillance and immunostimulation: Implications for cancer immunotherapy. *Journal of Translational Medicine*. 2005 Feb 8;3(1):8.
38. Coley WB. CONTRIBUTION TO THE KNOWLEDGE OF SARCOMA. *Annals of Surgery*. 1891 Dec;14:199.
39. McCarthy EF. The Toxins of William B. Coley and the Treatment of Bone and Soft-Tissue Sarcomas. *Iowa Orthop J*. 2006;26:154–8.
40. Burnet M. Cancer—A Biological Approach: III. Viruses Associated with Neoplastic Conditions. IV. Practical Applications. *Br Med J*. 1957 Apr 13;1(5023):841–7.
41. Alhunaidi O, Zlotta AR. The use of intravesical BCG in urothelial carcinoma of the bladder [Internet]. 2019 [cited 2023 Jul 11]. Available from: <http://ecancer.org/en/journal/article/905-the-use-of-intravesical-bcg-in-urothelial-carcinoma-of-the-bladder>
42. Stanley M. Tumour virus vaccines: hepatitis B virus and human papillomavirus. *Philosophical Transactions of the Royal Society B: Biological Sciences*. 2017 Sep 11;372(1732):20160268.
43. Morgan DA, Ruscetti FW, Gallo R. Selective in Vitro Growth of T Lymphocytes from Normal Human Bone Marrows. *Science*. 1976 Sep 10;193(4257):1007–8.
44. Klapper JA, Downey SG, Smith FO, Yang JC, Hughes MS, Kammula US, et al. High-dose interleukin-2 for the treatment of metastatic renal cell carcinoma. *Cancer*. 2008;113(2):293–301.
45. Ishida Y, Agata Y, Shibahara K, Honjo T. Induced expression of PD-1, a novel member of the immunoglobulin gene superfamily, upon programmed cell death. *The EMBO Journal*. 1992 Nov;11(11):3887–95.
46. Khan M, Maker AV, Jain S. The Evolution of Cancer Immunotherapy. *Vaccines*. 2021 Jun 8;9(6):614.
47. Pierpont TM, Limper CB, Richards KL. Past, Present, and Future of Rituximab—The World’s First Oncology Monoclonal Antibody Therapy. *Frontiers in Oncology* [Internet]. 2018 [cited 2023 Jul 11];8. Available from: <https://www.frontiersin.org/articles/10.3389/fonc.2018.00163>

48. Chang JC. HER2 Inhibition: From Discovery to Clinical Practice. *Clinical Cancer Research*. 2007 Jan 2;13(1):1–3.
49. Lv S, Wang Y, Sun T, Wan D, Sheng L, Li W, et al. Overall Survival Benefit from Trastuzumab-Based Treatment in HER2-Positive Metastatic Breast Cancer: A Retrospective Analysis. *Oncology Research and Treatment*. 2018 Jun 15;41(7–8):450–5.
50. Conry RM, Westbrook B, McKee S, Norwood TG. Talimogene laherparepvec: First in class oncolytic virotherapy. *Human Vaccines & Immunotherapeutics*. 2018 Apr 3;14(4):839–46.
51. Leach DR, Krummel MF, Allison JP. Enhancement of Antitumor Immunity by CTLA-4 Blockade. *Science*. 1996 Mar 22;271(5256):1734–6.
52. Tarhini A, Lo E, Minor DR. Releasing the Brake on the Immune System: Ipilimumab in Melanoma and Other Tumors. *Cancer Biotherapy and Radiopharmaceuticals*. 2010 Dec;25(6):601–13.
53. Sedykh SE, Prinz VV, Buneva VN, Nevinsky GA. Bispecific antibodies: design, therapy, perspectives. *DDDT*. 2018 Jan 22;12:195–208.
54. Seimetz D, Heller K, Richter J. Approval of First CAR-Ts: Have we Solved all Hurdles for ATMPs? *Cell Med*. 2019 Jan 1;11:2155179018822781.
55. Chen DS, Mellman I. Oncology Meets Immunology: The Cancer-Immunity Cycle. *Immunity*. 2013 Jul;39(1):1–10.
56. Motz GT, Coukos G. Deciphering and Reversing Tumor Immune Suppression. *Immunity*. 2013 Jul 25;39(1):61–73.
57. Gonzalez H, Hagerling C, Werb Z. Roles of the immune system in cancer: from tumor initiation to metastatic progression. *Genes & Development*. 2018 Oct 1;32(19–20):1267–84.
58. Palucka AK, Coussens LM. The Basis of Oncoimmunology. *Cell*. 2016 Mar 10;164(6):1233–47.
59. Teng MWL, Galon J, Fridman WH, Smyth MJ. From mice to humans: developments in cancer immunoediting. *J Clin Invest*. 2015 Sep 1;125(9):3338–46.
60. Böttcher JP, Bonavita E, Chakravarty P, Bles H, Cabeza-Cabrero M, Sammicheli S, et al. NK Cells Stimulate Recruitment of cDC1 into the Tumor Microenvironment Promoting Cancer Immune Control. *Cell*. 2018 Feb 22;172(5):1022–1037.e14.
61. Domínguez-Soto A, Sierra-Filardi E, Puig-Kröger A, Pérez-Maceda B, Gómez-Aguado F, Corcuera MT, et al. Dendritic Cell-Specific ICAM-3-Grabbing Nonintegrin Expression on M2-Polarized and Tumor-Associated Macrophages

- Is Macrophage-CSF Dependent and Enhanced by Tumor-Derived IL-6 and IL-10. *The Journal of Immunology*. 2011 Feb 15;186(4):2192–200.
62. Böger C, Behrens HM, Krüger S, Röcken C. The novel negative checkpoint regulator VISTA is expressed in gastric carcinoma and associated with PD-L1/PD-1: A future perspective for a combined gastric cancer therapy? *Oncoimmunology*. 2017 Feb 21;6(4):e1293215.
 63. Snyder A, Makarov V, Merghoub T, Yuan J, Zaretsky JM, Desrichard A, et al. Genetic Basis for Clinical Response to CTLA-4 Blockade in Melanoma. *New England Journal of Medicine*. 2014 Dec 4;371(23):2189–99.
 64. Topalian SL, Hodi FS, Brahmer JR, Gettinger SN, Smith DC, McDermott DF, et al. Safety, Activity, and Immune Correlates of Anti-PD-1 Antibody in Cancer. *N Engl J Med*. 2012 Jun 28;366(26):2443–54.
 65. Topalian SL, Drake CG, Pardoll DM. Immune checkpoint blockade: a common denominator approach to cancer therapy. *Cancer Cell*. 2015 Apr 13;27(4):450–61.
 66. Kumar V, Patel S, Tcyganov E, Gabrilovich DI. The nature of myeloid-derived suppressor cells in the tumor microenvironment. *Trends Immunol*. 2016 Mar;37(3):208–20.
 67. Mantovani A, Marchesi F, Malesci A, Laghi L, Allavena P. Tumor-Associated Macrophages as Treatment Targets in Oncology. *Nat Rev Clin Oncol*. 2017 Jul;14(7):399–416.
 68. Tanaka A, Sakaguchi S. Regulatory T cells in cancer immunotherapy. *Cell Res*. 2017 Jan;27(1):109–18.
 69. Li F, Zhao Y, Wei L, Li S, Liu J. Tumor-infiltrating Treg, MDSC, and IDO expression associated with outcomes of neoadjuvant chemotherapy of breast cancer. *Cancer Biol Ther*. 2018 May 8;19(8):695–705.
 70. Maria NI, van Helden-Meeuwsen CG, Brkic Z, Paulissen SMJ, Steenwijk EC, Dalm VA, et al. Association of Increased Treg Cell Levels With Elevated Indoleamine 2,3-Dioxygenase Activity and an Imbalanced Kynurenine Pathway in Interferon-Positive Primary Sjögren's Syndrome: ELEVATED TREG CELLS AND IDO ACTIVITY IN IFN-POSITIVE PRIMARY SS. *Arthritis & Rheumatology*. 2016 Jul;68(7):1688–99.
 71. Prendergast GC, Malachowski WJ, Mondal A, Scherle P, Muller AJ. Indoleamine 2,3-Dioxygenase and Its Therapeutic Inhibition in Cancer. In: *International Review of Cell and Molecular Biology* [Internet]. Elsevier; 2018 [cited 2023 Jan 12]. p. 175–203. Available from: <https://linkinghub.elsevier.com/retrieve/pii/S1937644817300795>
 72. Bilir C, Sarisozen C. Indoleamine 2,3-dioxygenase (IDO): Only an enzyme or a checkpoint controller? *Journal of Oncological Sciences*. 2017 Jul;3(2):52–6.

73. Gerriets VA, Rathmell JC. Metabolic pathways in T cell fate and function. *Trends in Immunology*. 2012 Apr 1;33(4):168–73.
74. Jones RG, Thompson CB. Revving the Engine: Signal Transduction Fuels T Cell Activation. *Immunity*. 2007 Aug 24;27(2):173–8.
75. Pallotta MT, Rossini S, Suvieri C, Coletti A, Orabona C, Macchiarulo A, et al. Indoleamine 2,3-dioxygenase 1 (IDO1): an up-to-date overview of an eclectic immunoregulatory enzyme. *FEBS J*. 2022 Oct;289(20):6099–118.
76. Röhrig UF, Michielin O, Zoete V. Structure and Plasticity of Indoleamine 2,3-Dioxygenase 1 (IDO1). *J Med Chem*. 2021 Dec 23;64(24):17690–705.
77. Lewis-Ballester A, Pham KN, Batabyal D, Karkashon S, Bonanno JB, Poulos TL, et al. Structural insights into substrate and inhibitor binding sites in human indoleamine 2,3-dioxygenase 1. *Nature Communications* [Internet]. 2017 Dec [cited 2022 Oct 3];8(1). Available from: <http://www.nature.com/articles/s41467-017-01725-8>
78. Nelp MT, Zheng V, Davis KM, Stiefel WKJ, Groves JT. Potent Activation of Indoleamine 2,3-Dioxygenase by Polysulfides. *J Am Chem Soc*. 2019 Sep 25;141(38):15288–300.
79. Cheong JE, Ekkati A, Sun L. A patent review of IDO1 inhibitors for cancer. *Expert Opinion on Therapeutic Patents*. 2018 Apr 3;28(4):317–30.
80. Labadie BW, Bao R, Luke JJ. Reimagining IDO Pathway Inhibition in Cancer Immunotherapy via Downstream Focus on the Tryptophan–Kynurenine–Aryl Hydrocarbon Axis. *Clinical Cancer Research*. 2019 Mar 1;25(5):1462–71.
81. Tang K, Wu YH, Song Y, Yu B. Indoleamine 2,3-dioxygenase 1 (IDO1) inhibitors in clinical trials for cancer immunotherapy. *J Hematol Oncol*. 2021 Dec;14(1):68.
82. Iversen TZ, Engell-Noerregaard L, Ellebaek E, Andersen R, Larsen SK, Bjoern J, et al. Long-lasting disease stabilization in the absence of toxicity in metastatic lung cancer patients vaccinated with an epitope derived from indoleamine 2,3 dioxygenase. *Clinical Cancer Research*. 2014;20(1):221–32.
83. Kjeldsen JW, Iversen TZ, Engell-Noerregaard L, Mellempgaard A, Andersen MH, Svane IM. Durable clinical responses and long-term follow-up of stage III-IV non-small-cell lung cancer (NSCLC) patients treated with IDO peptide vaccine in a phase i study-a brief research report. *Frontiers in Immunology*. 2018;9(SEP).
84. Kjeldsen JW, Lorentzen CL, Martinenaite E, Ellebaek E, Donia M, Holmstroem RB, et al. A phase 1/2 trial of an immune-modulatory vaccine against IDO/PD-L1 in combination with nivolumab in metastatic melanoma. *Nat Med*. 2021 Dec;27(12):2212–23.

85. Hou DY, Muller AJ, Sharma MD, DuHadaway J, Banerjee T, Johnson M, et al. Inhibition of Indoleamine 2,3-Dioxygenase in Dendritic Cells by Stereoisomers of 1-Methyl-Tryptophan Correlates with Antitumor Responses. *Cancer Research*. 2007 Jan 18;67(2):792–801.
86. Fox E, Oliver T, Rowe M, Thomas S, Zakharia Y, Gilman PB, et al. Indoximod: An Immunometabolic Adjuvant That Empowers T Cell Activity in Cancer. *Front Oncol*. 2018 Sep 11;8:370.
87. Munn DH, Sharma MD, Johnson TS, Rodriguez P. IDO, PTEN-expressing Tregs and control of antigen-presentation in the murine tumor microenvironment. *Cancer Immunol Immunother*. 2017 Aug 1;66(8):1049–58.
88. Munn DH, Bronte V. Immune suppressive mechanisms in the tumor microenvironment. *Current Opinion in Immunology*. 2016 Apr 1;39:1–6.
89. Munn DH, Mellor AL. IDO in the Tumor Microenvironment: Inflammation, Counter-Regulation, and Tolerance. *Trends in Immunology*. 2016 Mar 1;37(3):193–207.
90. Zakharia Y, McWilliams RR, Rixe O, Drabick J, Shaheen MF, Grossmann KF, et al. Phase II trial of the IDO pathway inhibitor indoximod plus pembrolizumab for the treatment of patients with advanced melanoma. *J Immunother Cancer*. 2021 Jun 1;9(6):e002057.
91. Long GV, Dummer R, Hamid O, Gajewski TF, Caglevic C, Dalle S, et al. Epcadostat plus pembrolizumab versus placebo plus pembrolizumab in patients with unresectable or metastatic melanoma (ECHO-301/KEYNOTE-252): a phase 3, randomised, double-blind study. *The Lancet Oncology*. 2019 Aug 1;20(8):1083–97.
92. Jochems C, Fantini M, Fernando RI, Kwilas AR, Donahue RN, Lepone LM, et al. The IDO1 selective inhibitor epcadostat enhances dendritic cell immunogenicity and lytic ability of tumor antigen-specific T cells. *Oncotarget*. 2016 May 12;7(25):37762–72.
93. Sono M, Cady SG. Enzyme kinetic and spectroscopic studies of inhibitor and effector interactions with indoleamine 2,3-dioxygenase. 1. Norharman and 4-phenylimidazole binding to the enzyme as inhibitors and heme ligands. *Biochemistry*. 1989 Jun 27;28(13):5392–9.
94. Mautino MR, Link CJ, Vahanian NN, Adams JT, Allen CV, Sharma MD, et al. Abstract 5023: Synergistic antitumor effects of combinatorial immune checkpoint inhibition with anti-PD-1/PD-L antibodies and the IDO pathway inhibitors NLG-919 and indoximod in the context of active immunotherapy. *Cancer Research*. 2014 Oct 1;74(19_Supplement):5023.
95. Nayak-Kapoor A, Hao Z, Sadek R, Dobbins R, Marshall L, Vahanian NN, et al. Phase Ia study of the indoleamine 2,3-dioxygenase 1 (IDO1) inhibitor navoximod

- (GDC-0919) in patients with recurrent advanced solid tumors. *Journal for ImmunoTherapy of Cancer*. 2018;6(1).
96. Tu W, Yang F, Xu G, Chi J, Liu Z, Peng W, et al. Discovery of Imidazoisoindole Derivatives as Highly Potent and Orally Active Indoleamine-2,3-dioxygenase Inhibitors. *ACS Med Chem Lett*. 2019 Jun 13;10(6):949–53.
 97. Parr BT, Pastor R, Sellers BD, Pei Z, Jaipuri FA, Castanedo GM, et al. Implementation of the CYP Index for the Design of Selective Tryptophan-2,3-dioxygenase Inhibitors. *ACS Med Chem Lett*. 2020 Apr 9;11(4):541–9.
 98. Cheong JE, Sun L. Targeting the IDO1/TDO2–KYN–AhR Pathway for Cancer Immunotherapy – Challenges and Opportunities. *Trends in Pharmacological Sciences*. 2018 Mar;39(3):307–25.
 99. Gomes B, Driessens G, Bartlett D, Cai D, Cauwenberghs S, Crosignani S, et al. Characterization of the Selective Indoleamine 2,3-Dioxygenase-1 (IDO1) Catalytic Inhibitor EOS200271/PF-06840003 Supports IDO1 as a Critical Resistance Mechanism to PD-(L)1 Blockade Therapy. *Molecular Cancer Therapeutics*. 2018 Dec 3;17(12):2530–42.
 100. Huynh J, Cho MT, Monjazez AM, Tam KW, Singh A, Naderi S, et al. Phase I/II trial of BMS-986205 and nivolumab as first line therapy in hepatocellular carcinoma. *JCO*. 2022 Jun;40(16_suppl):e16200–e16200.
 101. Ortiz-Meoz RF, Wang L, Matico R, Rutkowska-Klute A, De la Rosa M, Bedard S, et al. Characterization of Apo-Form Selective Inhibition of Indoleamine 2,3-Dioxygenase**. *ChemBioChem*. 2021;22(3):516–22.
 102. Chen S, Tan J, Zhang A. The ups, downs and new trends of IDO1 inhibitors. *Bioorganic Chemistry*. 2021 May;110:104815.
 103. White C, McGowan MA, Zhou H, Sciammetta N, Fradera X, Lim J, et al. Strategic Incorporation of Polarity in Heme-Displacing Inhibitors of Indoleamine-2,3-dioxygenase-1 (IDO1). *ACS Med Chem Lett*. 2020 Apr 9;11(4):550–7.
 104. Kazmierski WM, Xia B, Miller J, De la Rosa M, Favre D, Dunham RM, et al. DNA-Encoded Library Technology-Based Discovery, Lead Optimization, and Prodrug Strategy toward Structurally Unique Indoleamine 2,3-Dioxygenase-1 (IDO1) Inhibitors. *J Med Chem*. 2020 Apr 9;63(7):3552–62.
 105. De Sousa Luis JA, Barros RPC, De Sousa NF, Muratov E, Scotti L, Scotti MT. Virtual Screening of Natural Products Database. *MRMC*. 2021 Nov;21(18):2657–730.
 106. Lipinski CA, Lombardo F, Dominy BW, Feeney PJ. Experimental and computational approaches to estimate solubility and permeability in drug discovery and development settings. *Advanced Drug Delivery Reviews*. 2001;24.

107. Oprea TI. Current trends in lead discovery: Are we looking for the appropriate properties? *Mol Divers*. 2000 Dec 1;5(4):199–208.
108. Cortes C, Vapnik V. Support-Vector Networks. *Machine Learning*. 1995;20(3):273–97.
109. Byvatov E, Fechner U, Sadowski J, Schneider G. Comparison of Support Vector Machine and Artificial Neural Network Systems for Drug/Nondrug Classification. *Journal of Chemical Information and Computer Sciences*. 2003;43(6):1882–9.
110. Gillet VJ, Willett P, Bradshaw J. Identification of biological activity profiles using substructural analysis and genetic algorithms. *Journal of Chemical Information and Computer Sciences*. 1998;38(2):165–79.
111. Young SS, Hawkins DM. Using Recursive Partitioning to Analyze a Large Sar Data Set. *SAR and QSAR in Environmental Research*. 1998 Jan;8(3–4):183–93.
112. Tian S, Wang J, Li Y, Li D, Xu L, Hou T. The application of in silico drug-likeness predictions in pharmaceutical research. *Advanced Drug Delivery Reviews*. 2015 Jun 23;86:2–10.
113. Duan J, Dixon SL, Lowrie JF, Sherman W. Analysis and comparison of 2D fingerprints: Insights into database screening performance using eight fingerprint methods. *Journal of Molecular Graphics and Modelling*. 2010 Sep 1;29(2):157–70.
114. Jørgensen AMM, Pedersen JT. Structural Diversity of Small Molecule Libraries. *J Chem Inf Comput Sci*. 2001 Mar 1;41(2):338–45.
115. Cross S, Baroni M, Carosati E, Benedetti P, Clementi S. FLAP: GRID Molecular Interaction Fields in Virtual Screening. Validation using the DUD Data Set. *J Chem Inf Model*. 2010 Aug 23;50(8):1442–50.
116. Hawkins PCD, Skillman AG, Nicholls A. Comparison of Shape-Matching and Docking as Virtual Screening Tools. *J Med Chem*. 2007 Jan 1;50(1):74–82.
117. Sastry GM, Dixon SL, Sherman W. Rapid Shape-Based Ligand Alignment and Virtual Screening Method Based on Atom/Feature-Pair Similarities and Volume Overlap Scoring. *J Chem Inf Model*. 2011 Oct 24;51(10):2455–66.
118. Abrahamian E, Fox PC, Nærum L, Christensen IT, Thøgersen H, Clark RD. Efficient Generation, Storage, and Manipulation of Fully Flexible Pharmacophore Multiplets and Their Use in 3-D Similarity Searching. *J Chem Inf Comput Sci*. 2003 Mar 1;43(2):458–68.
119. Kumar A, Zhang KYJ. Advances in the Development of Shape Similarity Methods and Their Application in Drug Discovery. *Front Chem*. 2018 Jul 25;6:315.

120. Rogers DJ, Tanimoto TT. A Computer Program for Classifying Plants. *Science*. 1960 Oct 21;132(3434):1115–8.
121. Ballester PJ, Finn PW, Richards WG. Ultrafast shape recognition: Evaluating a new ligand-based virtual screening technology. *Journal of Molecular Graphics and Modelling*. 2009 Apr 1;27(7):836–45.
122. Ballester PJ, Westwood I, Laurieri N, Sim E, Richards WG. Prospective virtual screening with Ultrafast Shape Recognition: the identification of novel inhibitors of arylamine N-acetyltransferases. *Journal of The Royal Society Interface*. 2009 Jul 8;7(43):335–42.
123. Hu B, Kuang ZK, Feng SY, Wang D, He SB, Kong DX. Three-Dimensional Biologically Relevant Spectrum (BRS-3D): Shape Similarity Profile Based on PDB Ligands as Molecular Descriptors. *Molecules*. 2016 Nov;21(11):1554.
124. Hu G, Kuang G, Xiao W, Li W, Liu G, Tang Y. Performance Evaluation of 2D Fingerprint and 3D Shape Similarity Methods in Virtual Screening. *J Chem Inf Model*. 2012 May 25;52(5):1103–13.
125. Nagarajan K, Zauhar R, Welsh WJ. Enrichment of Ligands for the Serotonin Receptor Using the Shape Signatures Approach. *J Chem Inf Model*. 2005 Jan 1;45(1):49–57.
126. Grant JA, Pickup BT. A Gaussian Description of Molecular Shape. *J Phys Chem*. 1995 Mar 1;99(11):3503–10.
127. Rush TS, Grant JA, Mosyak L, Nicholls A. A Shape-Based 3-D Scaffold Hopping Method and Its Application to a Bacterial Protein–Protein Interaction. *J Med Chem*. 2005 Mar 1;48(5):1489–95.
128. Haque IS, Pande VS. PAPER—Accelerating parallel evaluations of ROCS. *Journal of Computational Chemistry*. 2010;31(1):117–32.
129. Vaz de Lima LAC, Nascimento AS. MolShaCS: A free and open source tool for ligand similarity identification based on Gaussian descriptors. *European Journal of Medicinal Chemistry*. 2013 Jan 1;59:296–303.
130. Yan X, Li J, Liu Z, Zheng M, Ge H, Xu J. Enhancing Molecular Shape Comparison by Weighted Gaussian Functions. *J Chem Inf Model*. 2013 Aug 26;53(8):1967–78.
131. Yang SY. Pharmacophore modeling and applications in drug discovery: challenges and recent advances. *Drug Discovery Today*. 2010 Jun 1;15(11):444–50.
132. Guner OF. History and Evolution of the Pharmacophore Concept in Computer-Aided Drug Design. *Current Topics in Medicinal Chemistry*. 2(12):1321–32.

133. Kaserer T, Beck K, Akram M, Odermatt A, Schuster D. Pharmacophore Models and Pharmacophore-Based Virtual Screening: Concepts and Applications Exemplified on Hydroxysteroid Dehydrogenases. *Molecules*. 2015 Dec 19;20(12):22799–832.
134. Seidel T, Schuetz DA, Garon A, Langer T. The Pharmacophore Concept and Its Applications in Computer-Aided Drug Design. In: Kinghorn AD, Falk H, Gibbons S, Kobayashi J, Asakawa Y, Liu JK, editors. *Progress in the Chemistry of Organic Natural Products 110: Cheminformatics in Natural Product Research* [Internet]. Cham: Springer International Publishing; 2019 [cited 2023 Oct 25]. p. 99–141. (*Progress in the Chemistry of Organic Natural Products*). Available from: https://doi.org/10.1007/978-3-030-14632-0_4
135. Wermuth CG, Ganellin CR, Lindberg P, Mitscher LA. Glossary of terms used in medicinal chemistry (IUPAC Recommendations 1998). *Pure and Applied Chemistry*. 1998 Jan 1;70(5):1129–43.
136. Giordano D, Biancaniello C, Argenio MA, Facchiano A. Drug Design by Pharmacophore and Virtual Screening Approach. *Pharmaceuticals*. 2022 May 23;15(5):646.
137. Lionta E, Spyrou G, Vassilatis DK, Cournia Z. Structure-Based Virtual Screening for Drug Discovery: Principles, Applications and Recent Advances. *Curr Top Med Chem*. 2014 Aug;14(16):1923–38.
138. Taylor RD, Jewsbury PJ, Essex JW. A review of protein-small molecule docking methods. *J Comput Aided Mol Des*. 2002 Mar 1;16(3):151–66.
139. Torres PHM, Sodero ACR, Jofily P, Silva-Jr FP. Key Topics in Molecular Docking for Drug Design. *International Journal of Molecular Sciences*. 2019 Jan;20(18):4574.
140. Hollingsworth SA, Dror RO. Molecular Dynamics Simulation for All. *Neuron*. 2018 Sep;99(6):1129–43.
141. Akdemir A, Rucktooa P, Jongejan A, Elk R van, Bertrand S, Sixma TK, et al. Acetylcholine binding protein (AChBP) as template for hierarchical in silico screening procedures to identify structurally novel ligands for the nicotinic receptors. *Bioorganic & Medicinal Chemistry*. 2011 Oct 15;19(20):6107–19.
142. Gangwal RP, Damre MV, Das NR, Dhoke GV, Bhadauriya A, Varikoti RA, et al. Structure based virtual screening to identify selective phosphodiesterase 4B inhibitors. *Journal of Molecular Graphics and Modelling*. 2015 Apr 1;57:89–98.
143. Agrafiotis DK, Gibbs AC, Zhu F, Izrailev S, Martin E. Conformational Sampling of Bioactive Molecules: A Comparative Study. *J Chem Inf Model*. 2007 May 1;47(3):1067–86.
144. Yuriev E, Agostino M, Ramsland PA. Challenges and advances in computational docking: 2009 in review. *Journal of Molecular Recognition*. 2011;24(2):149–64.

145. Sousa SF, Fernandes PA, Ramos MJ. Protein–ligand docking: Current status and future challenges. *Proteins: Structure, Function, and Bioinformatics*. 2006;65(1):15–26.
146. Zsoldos Z, Reid D, Simon A, Sadjad SB, Johnson AP. eHiTS: A new fast, exhaustive flexible ligand docking system. *Journal of Molecular Graphics and Modelling*. 2007 Jul 1;26(1):198–212.
147. Ewing TJA, Makino S, Skillman AG, Kuntz ID. DOCK 4.0: Search strategies for automated molecular docking of flexible molecule databases. *J Comput Aided Mol Des*. 2001 May 1;15(5):411–28.
148. Friesner RA, Banks JL, Murphy RB, Halgren TA, Klicic JJ, Mainz DT, et al. Glide: A New Approach for Rapid, Accurate Docking and Scoring. 1. Method and Assessment of Docking Accuracy. *J Med Chem*. 2004 Mar 1;47(7):1739–49.
149. McGann M. FRED and HYBRID docking performance on standardized datasets. *J Comput Aided Mol Des*. 2012 Aug 1;26(8):897–906.
150. Rarey M, Kramer B, Lengauer T, Klebe G. A Fast Flexible Docking Method using an Incremental Construction Algorithm. *Journal of Molecular Biology*. 1996 Aug 23;261(3):470–89.
151. Gorelik B, Goldblum A. High quality binding modes in docking ligands to proteins. *Proteins: Structure, Function, and Bioinformatics*. 2008;71(3):1373–86.
152. Morris GM, Goodsell DS, Huey R, Olson AJ. Distributed automated docking of flexible ligands to proteins: Parallel applications of AutoDock 2.4. *J Computer-Aided Mol Des*. 1996 Aug 1;10(4):293–304.
153. Korb O, Stütze T, Exner TE. Empirical Scoring Functions for Advanced Protein–Ligand Docking with PLANTS. *J Chem Inf Model*. 2009 Jan 26;49(1):84–96.
154. Corbeil CR, Williams CI, Labute P. Variability in docking success rates due to dataset preparation. *J Comput Aided Mol Des*. 2012 Jun;26(6):775–86.
155. Venkatachalam CM, Jiang X, Oldfield T, Waldman M. LigandFit: a novel method for the shape-directed rapid docking of ligands to protein active sites. *Journal of Molecular Graphics and Modelling*. 2003 Jan 1;21(4):289–307.
156. Ferreira L, dos Santos R, Oliva G, Andricopulo A. Molecular Docking and Structure-Based Drug Design Strategies. *Molecules*. 2015 Jul 22;20(7):13384–421.
157. Huang SY, Grinter SZ, Zou X. Scoring functions and their evaluation methods for protein–ligand docking: recent advances and future directions. *Phys Chem Chem Phys*. 2010 Oct 7;12(40):12899–908.

158. Englebienne P, Moitessier N. Docking Ligands into Flexible and Solvated Macromolecules. 5. Force-Field-Based Prediction of Binding Affinities of Ligands to Proteins. *J Chem Inf Model*. 2009 Nov 23;49(11):2564–71.
159. Murray CW, Auton TR, Eldridge MD. Empirical scoring functions. II. The testing of an empirical scoring function for the prediction of ligand-receptor binding affinities and the use of Bayesian regression to improve the quality of the model. *J Comput Aided Mol Des*. 1998 Sep 1;12(5):503–19.
160. Huang SY, Zou X. An iterative knowledge-based scoring function to predict protein–ligand interactions: I. Derivation of interaction potentials. *Journal of Computational Chemistry*. 2006;27(15):1866–75.
161. Gohlke H, Hendlich M, Klebe G. Knowledge-based scoring function to predict protein-ligand interactions. Edited by R. Huber. *Journal of Molecular Biology*. 2000 Jan 14;295(2):337–56.
162. Charifson PS, Corkery JJ, Murcko MA, Walters WP. Consensus Scoring: A Method for Obtaining Improved Hit Rates from Docking Databases of Three-Dimensional Structures into Proteins. *J Med Chem*. 1999 Dec 1;42(25):5100–9.
163. DeWitte RS, Shakhnovich EI. SMOG: de Novo Design Method Based on Simple, Fast, and Accurate Free Energy Estimates. 1. Methodology and Supporting Evidence. *J Am Chem Soc*. 1996 Jan 1;118(47):11733–44.
164. Eldridge MD, Murray CW, Auton TR, Paolini GV, Mee RP. Empirical scoring functions: I. The development of a fast empirical scoring function to estimate the binding affinity of ligands in receptor complexes. *J Comput Aided Mol Des*. 1997 Sep 1;11(5):425–45.
165. Rognan D, Lauemøller SL, Holm A, Buus S, Tschinke V. Predicting Binding Affinities of Protein Ligands from Three-Dimensional Models: Application to Peptide Binding to Class I Major Histocompatibility Proteins. *J Med Chem*. 1999 Nov 1;42(22):4650–8.
166. Muegge I, Martin YC, Hajduk PJ, Fesik SW. Evaluation of PMF Scoring in Docking Weak Ligands to the FK506 Binding Protein. *J Med Chem*. 1999 Jul 1;42(14):2498–503.
167. Abagyan R, Totrov M, Kuznetsov D. ICM—A new method for protein modeling and design: Applications to docking and structure prediction from the distorted native conformation. *Journal of Computational Chemistry*. 1994;15(5):488–506.
168. Böhm HJ. The development of a simple empirical scoring function to estimate the binding constant for a protein-ligand complex of known three-dimensional structure. *J Computer-Aided Mol Des*. 1994 Jun 1;8(3):243–56.
169. Fan H, Schneidman-Duhovny D, Irwin JJ, Dong G, Shoichet BK, Sali A. Statistical Potential for Modeling and Ranking of Protein–Ligand Interactions. *J Chem Inf Model*. 2011 Dec 27;51(12):3078–92.

170. Bernardi TRC, Rudack T, Ribeiro JV, Barragan A, Lihan M, Shahoei R, et al. QwikMD - Easy Molecular Dynamics with NAMD and VMD.
171. Yadav MK, Ahmad S, Raza K, Kumar S, Eswaran M, Pasha KM M. Predictive modeling and therapeutic repurposing of natural compounds against the receptor-binding domain of SARS-CoV-2. *Journal of Biomolecular Structure and Dynamics*. 2023 Mar 24;41(5):1527–39.
172. Vieira IHP, Botelho EB, de Souza Gomes TJ, Kist R, Caceres RA, Zanchi FB. Visual dynamics: a WEB application for molecular dynamics simulation using GROMACS. *BMC Bioinformatics* [Internet]. 2023 Mar 22 [cited 2023 Jun 22];24(1). Available from: <https://bmcbioinformatics.biomedcentral.com/articles/10.1186/s12859-023-05234-y>
173. Kuzmanic A, Pritchard RB, Hansen DF, Gervasio FL. Importance of the Force Field Choice in Capturing Functionally Relevant Dynamics in the von Willebrand Factor. *J Phys Chem Lett*. 2019 Apr 18;10(8):1928–34.
174. Pang YP. FF12MC: A revised AMBER forcefield and new protein simulation protocol. *Proteins: Structure, Function, and Bioinformatics*. 2016;84(10):1490–516.
175. Huang J, Rauscher S, Nawrocki G, Ran T, Feig M, de Groot BL, et al. CHARMM36m: an improved force field for folded and intrinsically disordered proteins. *Nat Methods*. 2017 Jan;14(1):71–3.
176. Klauda JB, Venable RM, Freites JA, O'Connor JW, Tobias DJ, Mondragon-Ramirez C, et al. Update of the CHARMM All-Atom Additive Force Field for Lipids: Validation on Six Lipid Types. *J Phys Chem B*. 2010 Jun 17;114(23):7830–43.
177. Lu C, Wu C, Ghoreishi D, Chen W, Wang L, Damm W, et al. OPLS4: Improving Force Field Accuracy on Challenging Regimes of Chemical Space. *J Chem Theory Comput*. 2021 Jul 13;17(7):4291–300.
178. Wang J, Wolf RM, Caldwell JW, Kollman PA, Case DA. Development and testing of a general amber force field. *Journal of Computational Chemistry*. 2004;25(9):1157–74.
179. Vanommeslaeghe K, MacKerell AD Jr. Automation of the CHARMM General Force Field (CGenFF) I: Bond Perception and Atom Typing. *J Chem Inf Model*. 2012 Dec 21;52(12):3144–54.
180. Owen MC, Tóth L, Jojárt B, Komáromi I, Csizmadia IG, Viskolcz B. The Effect of Newly Developed OPLS-AA Alanyl Radical Parameters on Peptide Secondary Structure. *J Chem Theory Comput*. 2012 Aug 14;8(8):2569–80.

181. Nian B, Xu YJ, Liu Y. Molecular dynamics simulation for mechanism revelation of the safety and nutrition of lipids and derivatives in food: State of the art. *Food Research International*. 2021 Jul 1;145:110399.
182. Mishra SK, Koča J. Assessing the Performance of MM/PBSA, MM/GBSA, and QM-MM/GBSA Approaches on Protein/Carbohydrate Complexes: Effect of Implicit Solvent Models, QM Methods, and Entropic Contributions. *J Phys Chem B*. 2018 Aug 30;122(34):8113–21.
183. Godschalk F, Genheden S, Söderhjelm P, Ryde U. Comparison of MM/GBSA calculations based on explicit and implicit solvent simulations. *Phys Chem Chem Phys*. 2013 May 1;15(20):7731–9.
184. Mulakala C, Viswanadhan VN. Could MM-GBSA be accurate enough for calculation of absolute protein/ligand binding free energies? *Journal of Molecular Graphics and Modelling*. 2013 Nov 1;46:41–51.
185. Wang Z, Sun H, Shen C, Hu X, Gao J, Li D, et al. Combined strategies in structure-based virtual screening. *Phys Chem Chem Phys*. 2020 Feb 12;22(6):3149–59.
186. Vázquez J, López M, Gibert E, Herrero E, Luque FJ. Merging Ligand-Based and Structure-Based Methods in Drug Discovery: An Overview of Combined Virtual Screening Approaches. *Molecules*. 2020 Oct 15;25(20):4723.
187. Drwal MN, Griffith R. Combination of ligand- and structure-based methods in virtual screening. *Drug Discovery Today: Technologies*. 2013 Sep 1;10(3):e395–401.
188. Khan SU, Ahemad N, Chuah LH, Naidu R, Htar TT. Sequential ligand- and structure-based virtual screening approach for the identification of potential G protein-coupled estrogen receptor-1 (GPER-1) modulators. *RSC Adv*. 2019 Jan 18;9(5):2525–38.
189. Dawood HM, Ibrahim RS, Shawky E, Hammada HM, Metwally AM. Integrated in silico-in vitro strategy for screening of some traditional Egyptian plants for human aromatase inhibitors. *Journal of Ethnopharmacology*. 2018 Oct 5;224:359–72.
190. Svensson F, Karlén A, Sköld C. Virtual Screening Data Fusion Using Both Structure- and Ligand-Based Methods. *J Chem Inf Model*. 2012 Jan 23;52(1):225–32.
191. Wang R, Wang S. How Does Consensus Scoring Work for Virtual Library Screening? An Idealized Computer Experiment. *J Chem Inf Comput Sci*. 2001 Sep 1;41(5):1422–6.
192. Costa G, Rocca R, Corona A, Grandi N, Moraca F, Romeo I, et al. Novel natural non-nucleoside inhibitors of HIV-1 reverse transcriptase identified by shape- and

- structure-based virtual screening techniques. *European Journal of Medicinal Chemistry*. 2019 Jan;161:1–10.
193. Vucicevic J, Srdic-Rajic T, Pieroni M, Laurila JMM, Perovic V, Tassini S, et al. A combined ligand- and structure-based approach for the identification of rilmenidine-derived compounds which synergize the antitumor effects of doxorubicin. *Bioorganic & Medicinal Chemistry*. 2016 Jul;24(14):3174–83.
 194. Wilson GL, Lill MA. Integrating structure-based and ligand-based approaches for computational drug design. *Future Medicinal Chemistry*. 2011 Apr;3(6):735–50.
 195. Marialke J, Tietze S, Apostolakis J. Similarity Based Docking. *J Chem Inf Model*. 2008 Jan 1;48(1):186–96.
 196. Coletti A, Greco FA, Dolcianni D, Camaioni E, Sardella R, Pallotta MT, et al. Advances in indoleamine 2,3-dioxygenase 1 medicinal chemistry. *Med Chem Commun*. 2017;8(7):1378–92.
 197. Zhang H, Liu W, Liu Z, Ju Y, Xu M, Zhang Y, et al. Discovery of indoleamine 2,3-dioxygenase inhibitors using machine learning based virtual screening. *MedChemComm*. 2018;9(6):937–45.
 198. Xu X, Ren J, Ma Y, Liu H, Rong Q, Feng Y, et al. Discovery of cyanopyridine scaffold as novel indoleamine-2,3-dioxygenase 1 (IDO1) inhibitors through virtual screening and preliminary hit optimisation. *Journal of Enzyme Inhibition and Medicinal Chemistry*. 2019 Jan 1;34(1):250–63.
 199. Zhou Y, Peng J, Li P, Du H, Li Y, Li Y, et al. Discovery of novel indoleamine 2,3-dioxygenase 1 (IDO1) inhibitors by virtual screening. *Computational Biology and Chemistry*. 2019 Feb;78:306–16.
 200. Serafini M, Torre E, Aprile S, Grosso ED, Gesù A, Griglio A, et al. Discovery of Highly Potent Benzimidazole Derivatives as Indoleamine 2,3-Dioxygenase-1 (IDO1) Inhibitors: From Structure-Based Virtual Screening to *in Vivo* Pharmacodynamic Activity. *Journal of Medicinal Chemistry*. 2020 Mar 26;63(6):3047–65.
 201. Shelley JC, Chollet A, Frye LL, Greenwood JR, Timlin MR, Uchimaya M. Epik: a software program for pK_a prediction and protonation state generation for drug-like molecules. *J Comput Aided Mol Des*. 2007 Dec 1;21(12):681–91.
 202. Pu Q, Zhang H, Guo L, Cheng M, Doty AC, Ferguson H, et al. Discovery of Potent and Orally Available Bicyclo[1.1.1]pentane-Derived Indoleamine-2,3-dioxygenase 1 (IDO1) Inhibitors. *ACS Med Chem Lett*. 2020 Aug 13;11(8):1548–54.
 203. Li D, Deng Y, Achab A, Bharathan I, Hopkins BA, Yu W, et al. Carbamate and N-Pyrimidine Mitigate Amide Hydrolysis: Structure-Based Drug Design of

- Tetrahydroquinoline IDO1 Inhibitors. *ACS Med Chem Lett.* 2021 Mar 11;12(3):389–96.
204. Hamilton MM, Mseeh F, McAfoos TJ, Leonard PG, Reyna NJ, Harris AL, et al. Discovery of IACS-9779 and IACS-70465 as Potent Inhibitors Targeting Indoleamine 2,3-Dioxygenase 1 (IDO1) Apoenzyme. *J Med Chem.* 2021 Aug 12;64(15):11302–29.
205. Li D, Sloman DL, Achab A, Zhou H, McGowan MA, White C, et al. Oxetane Promise Delivered: Discovery of Long-Acting IDO1 Inhibitors Suitable for Q3W Oral or Parenteral Dosing. *J Med Chem.* 2022 Apr 28;65(8):6001–16.
206. Koshland DE. Application of a Theory of Enzyme Specificity to Protein Synthesis*. *Proceedings of the National Academy of Sciences.* 1958 Feb;44(2):98–104.
207. Shang J, Dai X, Li Y, Pistolozzi M, Wang L. HybridSim-VS: a web server for large-scale ligand-based virtual screening using hybrid similarity recognition techniques. *Bioinformatics.* 2017 Nov 1;33(21):3480–1.
208. Salim N, Holliday J, Willett P. Combination of Fingerprint-Based Similarity Coefficients Using Data Fusion. *J Chem Inf Comput Sci.* 2003 Mar 1;43(2):435–42.
209. Berman HM, Westbrook J, Feng Z, Gilliland G, Bhat TN, Weissig H, et al. The Protein Data Bank. *Nucleic Acids Res.* 2000 Jan 1;28(1):235–42.
210. Mysinger MM, Carchia M, Irwin JohnJ, Shoichet BK. Directory of Useful Decoys, Enhanced (DUD-E): Better Ligands and Decoys for Better Benchmarking. *J Med Chem.* 2012 Jul 26;55(14):6582–94.
211. Davies C, Dötsch L, Ciulla MG, Hennes E, Yoshida K, Gasper R, et al. Identification of a Novel Pseudo-Natural Product Type IV IDO1 Inhibitor Chemotype. *Angewandte Chemie International Edition.* 2022;61(40):e202209374.
212. Pham KN, Lewis-Ballester A, Yeh SR. Structural Basis of Inhibitor Selectivity in Human Indoleamine 2,3-Dioxygenase 1 and Tryptophan Dioxygenase. *J Am Chem Soc.* 2019 Nov 27;141(47):18771–9.
213. Liu W, Zou Y, Li K, Zhong H, Yu L, Ge S, et al. Apo-Form Selective Inhibition of IDO for Tumor Immunotherapy. *The Journal of Immunology.* 2022 Jul 1;209(1):180–91.
214. Hopkins B, Zhang H, Bharathan I, Li D, Pu Q, Zhou H, et al. Utilization of Metabolite Identification and Structural Data to Guide Design of Low-Dose IDO1 Inhibitors. *ACS Med Chem Lett.* 2021 Sep 9;12(9):1435–40.

215. Phillips JC, Hardy DJ, Maia JDC, Stone JE, Ribeiro JV, Bernardi RC, et al. Scalable molecular dynamics on CPU and GPU architectures with NAMD. *The Journal of Chemical Physics*. 2020 Jul 28;153(4):044130.
216. Humphrey W, Dalke A, Schulten K. VMD: Visual molecular dynamics. *Journal of Molecular Graphics*. 1996 Feb;14(1):33–8.
217. Jo S, Kim T, Iyer VG, Im W. CHARMM-GUI: A web-based graphical user interface for CHARMM. *Journal of Computational Chemistry*. 2008;29(11):1859–65.
218. Li J, Abel R, Zhu K, Cao Y, Zhao S, Friesner RA. The VSGB 2.0 model: A next generation energy model for high resolution protein structure modeling. *Proteins: Structure, Function, and Bioinformatics*. 2011;79(10):2794–812.
219. Bai Q, Tan S, Xu T, Liu H, Huang J, Yao X. MolAICal: a soft tool for 3D drug design of protein targets by artificial intelligence and classical algorithm. *Briefings in Bioinformatics*. 2021 May 1;22(3):bbaa161.
220. Wu X, Xu L, Li E, Dong G. Application of molecular dynamics simulation in biomedicine. *Chem Biol Drug Des*. 2022 May;99(5):789–800.
221. Adema DMM. *Daphnia magna* as a test animal in acute and chronic toxicity tests. *Hydrobiologia*. 1978 Jun 1;59(2):125–34.
222. Ankley GT, Villeneuve DL. The fathead minnow in aquatic toxicology: Past, present and future. *Aquatic Toxicology*. 2006 Jun 10;78(1):91–102.
223. Arnot JA, Gobas FA. A review of bioconcentration factor (BCF) and bioaccumulation factor (BAF) assessments for organic chemicals in aquatic organisms. *Environ Rev*. 2006 Dec;14(4):257–97.
224. Veber DF, Johnson SR, Cheng HY, Smith BR, Ward KW, Kopple KD. Molecular Properties That Influence the Oral Bioavailability of Drug Candidates. *J Med Chem*. 2002 Jun 1;45(12):2615–23.
225. Muegge I, Heald SL, Brittelli D. Simple Selection Criteria for Drug-like Chemical Matter. *J Med Chem*. 2001 Jun 1;44(12):1841–6.
226. Ghose AK, Viswanadhan VN, Wendoloski JJ. A Knowledge-Based Approach in Designing Combinatorial or Medicinal Chemistry Libraries for Drug Discovery. 1. A Qualitative and Quantitative Characterization of Known Drug Databases. *J Comb Chem*. 1999 Jan 12;1(1):55–68.
227. Egan WJ, Merz Kenneth M, Baldwin JJ. Prediction of Drug Absorption Using Multivariate Statistics. *J Med Chem*. 2000 Oct 1;43(21):3867–77.
228. Hill M, Pereira V, Chauveau C, Zagani R, Remy S, Tesson L, et al. Heme oxygenase-1 inhibits rat and human breast cancer cell proliferation: mutual cross

- inhibition with indoleamine 2,3-dioxygenase. *FASEB J.* 2005 Dec;19(14):1957–68.
229. Kralj S, Jukič M, Bren U. Molecular Filters in Medicinal Chemistry. *Encyclopedia.* 2023 Jun;3(2):501–11.
230. Lumley JA. Compound Selection and Filtering in Library Design. *QSAR & Combinatorial Science.* 2005;24(9):1066–75.
231. Zhu F, Logan G, Reynisson J. Wine Compounds as a Source for HTS Screening Collections. A Feasibility Study. *Molecular Informatics.* 2012;31(11–12):847–55.
232. Baell JB, Holloway GA. New Substructure Filters for Removal of Pan Assay Interference Compounds (PAINS) from Screening Libraries and for Their Exclusion in Bioassays. *Journal of Medicinal Chemistry.* 2010 Apr 8;53(7):2719–40.
233. Grant JA, Gallardo MA, Pickup BT. A fast method of molecular shape comparison: A simple application of a Gaussian description of molecular shape. *Journal of Computational Chemistry.* 1996;17(14):1653–66.
234. Bernèche S, Roux B. Energetics of ion conduction through the K⁺ channel. *Nature.* 2001 Nov;414(6859):73–7.
235. Khafizov K, Perez C, Koshy C, Quick M, Fendler K, Ziegler C, et al. Investigation of the sodium-binding sites in the sodium-coupled betaine transporter BetP. *Proceedings of the National Academy of Sciences.* 2012 Oct 30;109(44):E3035–44.
236. Li J, Shaikh SA, Enkavi G, Wen PC, Huang Z, Tajkhorshid E. Transient formation of water-conducting states in membrane transporters. *Proceedings of the National Academy of Sciences.* 2013 May 7;110(19):7696–701.
237. Spahn V, Del Vecchio G, Labuz D, Rodriguez-Gaztelumendi A, Massaly N, Temp J, et al. A nontoxic pain killer designed by modeling of pathological receptor conformations. *Science.* 2017 Mar 3;355(6328):966–9.
238. Perez A, Morrone JA, Simmerling C, Dill KA. Advances in free-energy-based simulations of protein folding and ligand binding. *Curr Opin Struct Biol.* 2016 Feb;36:25–31.
239. Dror RO, Green HF, Valant C, Borhani DW, Valcourt JR, Pan AC, et al. Structural basis for modulation of a G-protein-coupled receptor by allosteric drugs. *Nature.* 2013 Nov 14;503(7475):295–9.
240. Wacker D, Wang S, McCorvy JD, Betz RM, Venkatakrishnan AJ, Levit A, et al. Crystal Structure of an LSD-Bound Human Serotonin Receptor. *Cell.* 2017 Jan 26;168(3):377–389.e12.

241. Liu X, Zhang Y, Duan H, Luo Q, Liu W, Liang L, et al. Inhibition Mechanism of Indoleamine 2, 3-Dioxygenase 1 (IDO1) by Amidoxime Derivatives and Its Revelation in Drug Design: Comparative Molecular Dynamics Simulations. *Front Mol Biosci.* 2020 Jan 28;6:164.
242. Iurcu-Mustata G, Van Belle D, Wintjens R, Prévost M, Rooman M. Role of salt bridges in homeodomains investigated by structural analyses and molecular dynamics simulations. *Biopolymers.* 2001;59(3):145–59.
243. Bosshard HR, Marti DN, Jelesarov I. Protein stabilization by salt bridges: concepts, experimental approaches and clarification of some misunderstandings. *Journal of Molecular Recognition.* 2004;17(1):1–16.
244. Mbaye MN, Hou Q, Basu S, Teheux F, Pucci F, Rooman M. A comprehensive computational study of amino acid interactions in membrane proteins. *Sci Rep.* 2019 Aug 19;9(1):12043.
245. Meuzelaar H, Vreede J, Woutersen S. Influence of Glu/Arg, Asp/Arg, and Glu/Lys Salt Bridges on α -Helical Stability and Folding Kinetics. *Biophysical Journal.* 2016 Jun;110(11):2328–41.
246. Christ CD, Mark AE, van Gunsteren WF. Basic ingredients of free energy calculations: A review. *Journal of Computational Chemistry.* 2010;31(8):1569–82.
247. Wang E, Sun H, Wang J, Wang Z, Liu H, Zhang JZH, et al. End-Point Binding Free Energy Calculation with MM/PBSA and MM/GBSA: Strategies and Applications in Drug Design. *Chem Rev.* 2019 Aug 28;119(16):9478–508.
248. Li Y, Shen J, Sun X, Li W, Liu G, Tang Y. Accuracy assessment of protein-based docking programs against RNA targets. *J Chem Inf Model.* 2010 Jun 28;50(6):1134–46.
249. Wang Z, Sun H, Yao X, Li D, Xu L, Li Y, et al. Comprehensive evaluation of ten docking programs on a diverse set of protein–ligand complexes: the prediction accuracy of sampling power and scoring power. *Phys Chem Chem Phys.* 2016 May 4;18(18):12964–75.
250. Kollman PA, Massova I, Reyes C, Kuhn B, Huo S, Chong L, et al. Calculating Structures and Free Energies of Complex Molecules: Combining Molecular Mechanics and Continuum Models. *Acc Chem Res.* 2000 Dec 1;33(12):889–97.
251. Hua Y, Shi Y, Cui X, Li X. In silico prediction of chemical-induced hematotoxicity with machine learning and deep learning methods. *Mol Divers.* 2021 Aug 1;25(3):1585–96.
252. Vo AH, Van Vleet TR, Gupta RR, Liguori MJ, Rao MS. An Overview of Machine Learning and Big Data for Drug Toxicity Evaluation. *Chem Res Toxicol.* 2020 Jan 21;33(1):20–37.

253. Tran TTV, Surya Wibowo A, Tayara H, Chong KT. Artificial Intelligence in Drug Toxicity Prediction: Recent Advances, Challenges, and Future Perspectives. *J Chem Inf Model*. 2023 May 8;63(9):2628–43.
254. Banerjee P, Eckert AO, Schrey AK, Preissner R. ProTox-II: a webserver for the prediction of toxicity of chemicals. *Nucleic Acids Research*. 2018 Jul 2;46(W1):W257–63.
255. Wang NX, Liu YY, Wei ZB, Yang LY, Miao AJ. Waterborne and Dietborne Toxicity of Inorganic Arsenic to the Freshwater Zooplankton *Daphnia magna*. *Environ Sci Technol*. 2018 Aug 7;52(15):8912–9.
256. Huang R, Sakamuru S, Martin MT, Reif DM, Judson RS, Houck KA, et al. Profiling of the Tox21 10K compound library for agonists and antagonists of the estrogen receptor alpha signaling pathway. *Sci Rep*. 2014 Jul 11;4(1):5664.

8. APPENDIX

APPENDIX-1 Turnitin originality report

Discovery New Indoleamine 2,3-Dioxygenase 1 (Ido1)
Inhibitors Through Virtual Screening

ORJİNALLİK RAPORU

% 27	% 16	% 25	% 7
BENZERLİK ENDEKSİ	İNTERNET KAYNAKLARI	YAYINLAR	ÖĞRENCİ ÖDEVLERİ

BİRİNCİL KAYNAKLAR

1	Ferreira, Leonardo, Ricardo dos Santos, Glaucius Oliva, and Adriano Andricopulo. "Molecular Docking and Structure-Based Drug Design Strategies", <i>Molecules</i> , 2015. Yayın	% 3
2	Shulun Chen, Jing Tan, Ao Zhang. "The ups, downs and new trends of IDO1 inhibitors", <i>Bioorganic Chemistry</i> , 2021 Yayın	% 2
3	www.frontiersin.org İnternet Kaynağı	% 2
4	www.ncbi.nlm.nih.gov İnternet Kaynağı	% 2
5	Jae Eun Cheong, Lijun Sun. "Targeting the IDO1/TDO2-KYN-AhR Pathway for Cancer Immunotherapy – Challenges and Opportunities", <i>Trends in Pharmacological Sciences</i> , 2018 Yayın	% 2

APPENDIX-2 Digital Turnitin Originality Report



Digital Receipt

This receipt acknowledges that Turnitin received your paper. Below you will find the receipt information regarding your submission.

The first page of your submissions is displayed below.

Submission author: Naufa Hanif
Assignment title: Discovery New Indoleamine 2,3-Dioxygenase 1 (Ido1) Inhibit...
Submission title: Discovery New Indoleamine 2,3-Dioxygenase 1 (Ido1) Inhibit...
File name: Thesis-Naufa-corr-afterdefense-turnitin.docx
File size: 9.26M
Page count: 81
Word count: 19,136
Character count: 114,216
Submission date: 19-Jan-2024 08:18PM (UTC+0300)
Submission ID: 2274004261



APPENDIX-3 NAMD script**RMSD calculation script**

```

mol new step3_input.psf type psf
mol addfile step5_production.dcd type dcd first 0 last -1 step 1 waitfor all

# wrap a trajectory to avoid RMSD calculation errors

pbc wrap -centersel "protein" -center com -compound residue -all

## Align to first frame

# the frame being compared

set reference [atomselect top "protein and backbone" frame 0]

# the frame to be compared
set compare [atomselect top "protein and backbone"]

#get the number of frames of the trajectory

set num_steps [molinfo top get numframes]

# get the correct num as the trajectory start from zero

set outfile [open rmsd.dat w]

for {set frame 0} {$frame < $num_steps} {incr frame} {
    # get the correct frame
    $compare frame $frame
    # compute the 4*4 matrix transformation that takes one set of
coordinates onto the other
    set trans_mat [measure fit $compare $reference]

    # do the alignment
    $compare move $trans_mat
    # compute the RMSD
    set rmsd [measure rmsd $compare $reference ]
    # print the RMSD
    puts $outfile "$frame  $rmsd"
}
close $outfile

```

RMSF calculation script

```

set num [expr {$num_steps - 1}]
# RMSF calculation
set outfile [open rmsf.dat w]
set sel [atomselect top "protein and name CA"]
set rmsf [measure rmsf $sel first 0 last $num step 1]
for {set i 0} {$i < [$sel num]} {incr i} {
  puts $outfile "[expr {$i+1}] [lindex $rmsf $i]"
}
close $outfile

```

Salt bridge formation script

```

# Salt bridges
file mkdir saltbridges
package require saltbr

saltbr -sel [atomselect top protein] -frames all -log saltbridges.log -outdir
./saltbridges

```

SASA calculation script

```

## SASA
# selection
set sel [atomselect top "protein"]
set n [molinfo top get numframes]
set output [open "SASA.dat" w]
# sasa calculation loop
for {set i 0} {$i < $n} {incr i} {
  molinfo top set frame $i
  set sasa [measure sasa 1.4 $sel -restrict $sel]
  puts "\t\t progress: $i/$n"
  puts $output "$i $sasa"
}
puts "\t\t progress: $n/$n"
puts "Done."
puts "output file: SASA.dat"
close $output

```

Radius of gyration (RoG) calculation script

For calculating center of mass

```

proc center_of_mass {selection} {
  # some error checking
  if {[ $selection num] <= 0} {
    error "center_of_mass: needs a selection with atoms"
  }
  # set the center of mass to 0
  set com [veczero]
  # set the total mass to 0
  set mass 0
  # [ $selection get {x y z}] returns the coordinates {x y z}
  # [ $selection get {mass}] returns the masses
  # so the following says "for each pair of {coordinates} and masses,
  # do the computation ..."
  foreach coord [ $selection get {x y z}] m [ $selection get mass] {
    # sum of the masses
    set mass [expr $mass + $m]
    # sum up the product of mass and coordinate
    set com [vecadd $com [vecscale $m $coord]]
  }
  # and scale by the inverse of the number of atoms
  if { $mass == 0} {
    error "center_of_mass: total mass is zero"
  }
  # The "1.0" can't be "1", since otherwise integer division is done
  return [vecscale [expr 1.0/$mass] $com]
}

```

For calculating radius of gyration

```

proc gyr_radius {sel} {
  # make sure this is a proper selection and has atoms
  if {[ $sel num] <= 0} {
    error "gyr_radius: must have at least one atom in selection"
  }
  # gyration is sqrt( sum((r(i) - r(center_of_mass))^2) / N)
  set com [center_of_mass $sel]
  set sum 0
  foreach coord [ $sel get {x y z}] {
    set sum [vecadd $sum [veclength2 [vecsub $coord $com]]]
  }
  return [expr sqrt($sum / ([ $sel num] + 0.0))]
}

```

For loop trajectories

```
# load necessary tcl functions (Ref : http://www.ks.uiuc.edu/Research/vmd/vmd-1.7.1/ug/node182.html )
```

```
source gyr_radius.tcl
```

```
source center_of_mass.tcl
```

```
set outfile [open rg.dat w]
```

```
puts $outfile "i rad_of_gyr"
```

```
set nf [molinfo top get numframes]
```

```
set i 0
```

```
set prot [atomselect top "protein"]
```

```
while { $i < $nf } {
```

```
    $prot frame $i
```

```
    $prot update
```

```
    set i [expr { $i + 1 }]
```

```
    set rog [gyr_radius $prot]
```

```
    puts $outfile "$i $rog"
```

```
}
```

```
close $outfile
```

```
exit
```

9. CURRICULUM VITAE

NAUFA HANIF

Researcher, Pharmacist

Nationality : Indonesia
 Email : naufa.hanif@mail.ugm.ac.id
 Date of birth : March, 26th 1996
 Place of birth : Semarang, Central Java, Indonesia
 Gender : Male
 ORCID ID : 0000-0003-4937-8904
 Scopus Author ID : 57226449824
 Web of Science Researcher ID : ABA-2456-2021
 LinkedIn profile : naufa-hanif
 ResearchGate profile : Naufa Hanif
 Loop profile : 1788430
 SciProfiles : 2745654
 Scopus H-Index : 3
 WoS H-Index : 2
 GS H-Index : 4

EDUCATION

Sep 2021 - present - **Master of Pharmacy**
 Department of Pharmaceutical Chemistry Graduate School of Health Sciences, Hacettepe University, Türkiye
 Marter's thesis title: "*Discovery new indoleamine 2,3-dioxygenase 1 (IDO1) inhibitors through virtual screening*"
 Supervisor: Asst. Prof. Suat Sari
 GPA: 3.07 (78.30)

Feb 2019 - Feb 2020 - **Pharmacist-Licensed Program**
 Faculty of Pharmacy, Universitas Gadjah Mada, Indonesia
 Had intern in the three different workplace : Pharmacy (Apotek UGM), Public Health Center (Puskesmas Tegalrejo), Industry (PT. Pfizer Indonesia)
 GPA: 3.86 (96.50)

Aug 2014 - Jan 2019 - **Bachelor of Pharmacy**
 Faculty of Pharmacy, Universitas Gadjah Mada, Indonesia
 Area of interest: Science and Technology Pharmacy
 Undergraduate thesis title: "*Antioxidant and Anti-senescence Activity Of Ethanolic Extract of Caesalpinia sappan L. Toward 4T1 Breast Cancer Cells*"
 Supervisor: Prof. Edy Meiyanto and Dr.rer.nat Adam Hermawan
 GPA: 3.25 (81.25)

SKILLS and EXPERTISES

1. Virtual Screening (both ligand-based and structure-based)
2. Molecular Dynamic Simulations,
3. Thin Layer Chromatography,
4. Cytotoxicity test (MTT assay),
5. ROS measurement by DCFDA-staining Flowcytometry

RESEARCH EXPERIENCE and SCIENTIFIC PUBLICATION (2019-2023)

1. Azzahra, S., **Hanif, N.**, Hermawan, A., 2022. MDM2 is a Potential Target Gene of Glycyrrhizic Acid for Circumventing Breast Cancer Resistance to Tamoxifen: Integrative Bioinformatics Analysis. *Asian Pacific Journal of Cancer Prevention* 23, 2341–2350. <https://doi.org/10.31557/APJCP.2022.23.7.2341>
2. **Hanif, N.**, Hermawan, A., Meiyanto, E., 2019. *Caesalpinia sappan* L. Ethanolic Extract Decrease Intracellular ROS Level and Senescence of 4T1 Breast Cancer Cells. *Indonesian Journal of Cancer Chemoprevention* 10, 16. <https://doi.org/10.14499/indonesianjancanchemoprev10iss1pp16-23>
3. Hermawan, A., Putri, H., **Hanif, N.**, Fatimah, N., Prasetyo, H.H., 2022a. Identification of potential target genes of honokiol in overcoming breast cancer resistance to tamoxifen. *Front. Oncol.* 12, 1019025. <https://doi.org/10.3389/fonc.2022.1019025>
4. Hermawan, A., Putri, H., **Hanif, N.**, Ikawati, M., 2021. Integrative Bioinformatics Study of Tangeretin Potential Targets for Preventing Metastatic Breast Cancer. *Evidence-Based Complementary and Alternative Medicine* 2021, 1–15. <https://doi.org/10.1155/2021/2234554>
5. Hermawan, A., Wulandari, F., **Hanif, N.**, Utomo, R.Y., Jenie, R.I., Ikawati, M., Tafrihani, A.S., 2022b. Identification of potential targets of the curcumin analog CCA-1.1 for glioblastoma treatment: integrated computational analysis and in vitro study. *Scientific Reports* 12. <https://doi.org/10.1038/s41598-022-18348-9>
6. Ibadurrahman, W., **Hanif, N.**, Hermawan, A., 2022. Functional network analysis of p85 and PI3K as potential gene targets and mechanism of oleanolic acid in overcoming breast cancer resistance to tamoxifen. *Journal of Genetic Engineering and Biotechnology* 20. <https://doi.org/10.1186/s43141-022-00341-4>
7. Skolastika, S., **Hanif, N.**, Ikawati, M., Hermawan, A., 2022. Comprehensive Computational Analysis of Honokiol Targets for Cell Cycle Inhibition and Immunotherapy in Metastatic Breast Cancer Stem Cells. *Evidence-Based Complementary and Alternative Medicine* 2022, 1–18. <https://doi.org/10.1155/2022/4172531>
8. Yuda, G.P.W.C., **Hanif, N.**, Hermawan, A., 2023. Computational Screening Using a Combination of Ligand-Based Machine Learning and Molecular Docking Methods for the Repurposing of Antivirals Targeting the SARS-CoV-2 Main Protease. *DARU J Pharm Sci.* <https://doi.org/10.1007/s40199-023-00484-w>

JOURNAL EDITORIAL BOARD

Reviewer in International Journal

1. BMC Complementary Medicine and Therapies [Impact Factor (IF): 3.9 (2022); Quartile: **Q1**; SCImago Journal Rank (SJR): 0.69]
2. BMC Medical Genomics [IF: 2.7 (2022); Quartile: **Q2**; SJR: 0.89]
3. Clinical Proteomics [IF: 3.8 (2022); Quartile: **Q2**; SJR: 0.94]
4. Frontiers in Oncology [IF: 4.7 (2022); Quartile: **Q2**; SJR: 1.14]
5. Investigational New Drugs [IF: 3.4 (2022); Quartile: **Q1**; SJR: 0.94]
6. Journal of Cancer Research and Clinical Oncology [IF: 3.6 (2022); Quartile: **Q1**; SJR: 1.02]
7. Journal of Orthopaedic Surgery and Research [IF: 2.6 (2022); Quartile: **Q2**; SJR: 0.74]
8. Naunyn-Schmiedeberg's Archives of Pharmacology [IF: 3.6 (2022); Quartile: **Q2**; SJR: 0.66]
9. Scientific Reports [IF: 4.6 (2022); Quartile: **Q1**; SJR: 0.97]

Reviewer in National Journal

1. Medical Sains
2. Pharmacy Reports

PROFESSIONAL EXPERIENCES

- Jan – Jun 2021 • **Department of Pharmacy, Faculty of Medicine and Health Science, Universitas Muhammadiyah Yogyakarta** | approx. 5 months
Worked as lecturer assistant of several subjects, such as analytical chemistry (HPLC, ELISA, spectrophotometry UV-Vis), pharmaceutical technology (tablet, suspension, emulsion and their evaluation), organic chemistry (aspirin synthesis) and medicinal chemistry that mainly discuss about computational drug design and molecular docking (as coordinator).
- Aug 2020 – Jan 2021 • **Citrus House** | approx. 1 semester
As general manager, I manage all of the activity. There are 6 division (administration, raw material, production, artistic-public relation, analysis, and infrastructure) that all of them controlled and supervised by me.
- Jun – Aug 2020 • **PT. UNISIA Polifarma** | 3 months
Worked as a professional pharmacist. Self-medication, counseling, prescription service, stock opname, online service are several activity that i did in there.
- Aug, Sep, Dec 2019 and Mar – May 2020 • **UGM Pharmacy (Apotek UGM)** | approx. 5 months
Learned so much important and useful things during do my internship in UGM Pharmacy. Started from managerial aspects (procurement, ordering, purchasing, etc) until health services (self-medication, counseling, monitoring of drug therapy, etc).
- Oct – Nov 2019 • **PT. Pfizer Indonesia** | 2 months
As a apothecary student, I do my internship in Pfizer, one of the world's biopharmaceutical companies in the Department of Production. I learned how to produce drugs with high quality both manufacturing and packaging.
- Aug – Dec 2019 • **Laboratory of Medicinal Chemistry, Department of Pharmaceutical Chemistry, Faculty of Pharmacy, Universitas Gadjah Mada, Yogyakarta** | 1 semester
Worked as laboratory teaching assistant of medicinal chemistry II that mainly discuss about computational drug design and molecular docking.
- Feb – Jun 2018 • **Laboratory of Bioanalysis and Clinical Chemistry, Department of Pharmaceutical Chemistry, Faculty of Pharmacy, Universitas Gadjah Mada, Yogyakarta** | 1 semester
Selected as assistant coordinator that responsible to arrange schedule of other assistant shift and handled the subject of boron analysis in cell by Inductively Coupled Plasma (ICP).
- **Laboratory of Biochemistry, Department of Pharmaceutical Chemistry, Faculty of Pharmacy, Universitas Gadjah Mada, Yogyakarta** | 1 semester
As laboratory leaching assistant delivered some materials such as how to use any chemical equipment, separate protein by SDS-PAGE, also determine amino acid sequence in polypeptides.
- Sep – Dec 2017 • **Laboratory of Biopharmaceutics, Department of Pharmaceutical, Faculty of Pharmacy, Universitas Gadjah Mada, Yogyakarta** | 1 semester
Assisted at least 5 materials, one of them is how to operate WinSAAM (a program to look interactive biological modelling).
- Feb – Jun 2016 and 2017 • **Laboratory of Physical Pharmacy, Department of Pharmaceutical, Faculty of Pharmacy, Universitas Gadjah Mada, Yogyakarta** | 2 semester
Worked for 2 semesters and delivered some materials, like buffer capacity; particle sizes; flow viscosity and natural properties (rheology).